2015

Understanding the Role of Transmembrane and Juxtamembrane Domains in Plexin and Neuropilin Signaling

Rachael Elizabeth Barton
Lehigh University

Understanding the Role of Transmembrane and Juxtamembrane Domains in Plexin and Neuropilin Signaling

by

Rachael Elizabeth Barton

Presented to the Graduate and Research Committee
of Lehigh University
in Candidacy for the Degree of
Doctor of Philosophy
in Chemical and Biomolecular Engineering

Lehigh University
May 2015

Certificate of Approval

Approved and recommended for acceptance as a dissertation in partial fulfillment of the requirements of the degree of Doctor of Philosophy

_____
Date

_____
Bryan W. Berger, Ph.D.
Dissertation Advisor

_____
Accepted Date

Committee Members:

_____
Angela Brown, Ph.D.
Committee Member

_____
Hugo S. Caram, Ph.D.
Committee Member

_____
M. Kathryn Iovine, Ph.D.
Committee Member

_____
Kelly M. Schultz, Ph.D.
Committee Member

Copyright Permissions

The material presented in Chapters 2 and 4 has been previously published and can be found under the citations listed at the beginning of these chapters. Additionally, the material in Chapter 3 has been submitted for publication.

Acknowledgments

I would like to extend my heartfelt thanks to the many people that contributed to the success of my graduate education. First and foremost, I would like to thank my thesis advisor, Dr. Bryan W. Berger, for his guidance and continuous support of my academic and professional endeavors. His passion for good science and enthusiasm for exploring new scientific frontiers, while also helping me to 'look past the trees and see the forest', helped to cultivate my skills as a researcher. I have sincerely appreciated the effort he invested into making my graduate experience meaningful, from ensuring that I could pursue my personal own professional goals, such as gaining teaching and mentorship experience while at Lehigh University, to establishing interdisciplinary collaborations to excel my research. His constant willingness to help has been valued.

I would also like to extend my gratitude to Dr. M. Kathryn Iovine for assistance in the lab, the classroom, and as a mentor. With her help, I have expanded my technical skillset beyond that of a traditional chemical engineer. Her realistic approaches to research helped me gain a plethora of knowledge not just in molecular biology, but also in research fundamentals, such as how to prioritize experiments.

I would like to thank my committee members, Dr. Angela Brown, Dr. Hugo S. Caram, and Dr. Kelly M. Schultz, for the time and advice they have given me not only as it pertained to research, but also with respect to career and life choices. I have appreciated their candid efforts toward helping me reach my professional goals both during my doctoral dissertation as well as post-graduation.

I also would like to thank the professors under which I had the opportunity to serve as a teaching assistant, Dr. Kemal Tuzla, Dr. Susan F. Perry, and Dr. Lori Herz, as well as the professors who helped provide me with mentorship opportunities, Dr. Neal Simon and Dr. Vassie C. Ware. I am grateful for these educational experiences, in which I had the opportunity to be both a teacher and a student.

I am also grateful to Joyita Bhadra for being a wonderful mentorship partner both in and out of BDSI and offering both emotional and technical support throughout my graduate education. Thank you also to all the undergraduate students we have mentored throughout the last five years for your eagerness to

learn, willingness to help, and patience while I learned with you. Special thanks in particular to students I have individually and directly mentored, in particular Theresa Collins, Danica Palacio, Alyssa Driscoll, Samuel Flores, Durlav Mudbhari, Josh Parris, Ivan Basurto, Nathanael Sallada, and Paige Dyrek.

I would like to thank the Berger lab members (Logan C. MacDonald, Pin-Chuan Su, Benjamaporn Wonganu, Sajedehalsadat Yazdanparast Tafti, Zhou Yang, Leah Spangler, and Christopher Curran) and Iovine lab members (Rebecca Bowman, Diane Jones, Jayalakshmi Govindan, Rajeswari Banerji, and Quynh Ton) for their technical and/or emotional support throughout the past five years. Thank you also to Paul Bader, Maria Brace, John Caffrey, Lee Graham, Janine Jekels, Barbara Kessler, Cindy Lohman, Tracey Lopez, and Vicki Ruggiero for technical and administrative assistance.

I am grateful to Lehigh University for providing me with a Presidential Fellowship to begin my doctoral studies and the Department of Chemical and Biomolecular Engineering for acceptance and support. I am also grateful for funding provided by the Howard Hughes Medical Institute Biosystems Dynamics Summer Institute, the Pennsylvania Research in Advanced Manufacturing Program, the NIH, and the NSF that made my doctoral work possible.

Finally, thank you to the many friends and family members, especially my parents, Kelly and Catherine Barton, and siblings, Samantha, John, Heather, Meghan, Catherine, and Maxwell, for your love, friendship, understanding, and encouragement. My success and happiness would not have been possible without you.

Table of Contents

List of Figures x

List of Tables xviii

Abstract 1

Chapter 1. Introduction to Neuropilns and Plexins, Transmembrane Receptors Involved in Development and Disease 3

1.1 Introduction 3
1.2 Current Understanding of Plexin and Neuropilin Structure-Function Relationships 4
1.3 Determination of Plexin and Neuropilin Homodimer Interfaces 10
1.4 References 11

Chapter 2. A Cytosolic Juxtamembrane Interface Modulates Plexin A3 Oligomerization and Signal Transduction 20

2.1 Introduction 21
2.2 Materials and Methods 24
2.2.1 Plasmids 25
2.2.2 AraTM Assay 25
2.2.3 $BRET^2$ Assay 26
2.2.4 Zebrafish Housing and Husbandry 28
2.2.5 Zebrafish RNA Injections 30
2.3 Results 31
2.3.1 A Juxtamembrane Helix Promotes Oligomerization of PlxnA3 31
2.3.2 A Juxtamembrane Heptad Repeat Influences PlxnA3 Function in Zebrafish Motor Neuron Development 36
2.4 Discussion 38
2.5 References 40

Chapter 3. Interplay of Specific Trans- and Juxtamembrane Interface in PlexinA3 Dimerization and Signal Transduction 45

3.1 Introduction 46
3.2 Materials and Methods 49
3.2.1 Modelling 49
3.2.2 Plasmids 49
3.2.3 AraTM Assay 50
3.2.4 Zebrafish Care and Embryo Injections 50
3.3 Results 52
3.3.1 Transmembrane Glycines Modulate PlxnA3 Homodimerization 52
3.3.2 TM and JM Interfaces Independently Regulate PlxnA3 Homodimerization 54
3.3.3 Glycines in the Transmembrane Domain Modulate PlxnA3 Function in a Zebrafish Axonal Guidance Assay 56
3.4 Discussion 57
3.5 References 61

Chapter 4. Cysteines in the Neuropilin-2 MAM Domain Modulate Receptor Homooligomerization and Signal Transduction 66

4.1 Introduction 67
4.2 Materials and Methods 71
4.2.1 Plasmids 71
4.2.2 Mammalian Cell Culture 72
4.2.3 BRET^2 Assay 72
4.2.4 NRP2a Overexpression in Zebrafish 74
4.2.5 Semaphorin Binding 74
4.3 Results 75
4.3.1 Specific Cysteines in the MAM Domain Influence NRP2a Homooligomerization 75
4.3.2 Mutations to the NRP2a MAM Domain Influence Overexpression Phenotypes in Zebrafish Vascular Patterning 77
4.3.3 Mutations to the NRP2a MAM Domain Influence Sema3F Binding 79
4.4 Discussion 80
4.5 References 82

Chapter 5. Concluding Remarks and Future Work 89

5.1 The Role of Dimerization, Oligomerization, and Ligand-Binding on Plexin Function 91
5.1.1 Materials and Methods 94
5.1.1.1 Plasmids 94
5.1.1.2 Expression and Purification 94
5.2 The Role of Off-Interface Transmembrane and Juxtamembrane Residues on Plexin A3 Dimerization 95
5.3 Structural Stability of the Plexin A3 Transmembrane Domain and Cooperative Effects on Dimerization and Function 99
5.3.1 Materials and Methods 106
5.3.1.1 Plasmids and Peptides 106
5.3.1.2 Expression and Purification of ompF-TM + JM 106
5.3.1.3 BRET^2 Assay 107
5.4 Cooperative Effects of the Neuropilin-2a MAM Domain with Other Intramolecular Domains 108
5.4.1 Materials and Methods 116
5.4.1.1 Plasmids 116
5.4.1.2 AraTM Assay 117
5.4.1.3 NativePAGE Western Blots 117
5.5 Behavior of the Neuropilin-2a MAM Domain in Solution 118
5.5.1 Materials and Methods 133
5.5.1.1 Plasmids 133
5.5.1.2 Expression and Purification of Nrp2a MAM and MBP-MAM Constructs 133
5.5.1.3 NativePAGE Gels 134
5.5.1.4 Cross-linking 135
5.5.1.5 Size Exclusion Chromatography 136
5.5.1.6 Tryptophan Fluorescence Measurements 136
5.5.1.7 Circular Dichroism 136
5.5.1.8 Homology Modeling and Docking 137
5.6 Heteromeric Interaction Interfaces of Neuropilins and Plexins 137
5.6.1 Materials and Methods 148
5.6.1.1 Plasmids 148
5.6.1.2 DN-AraTM Measurements 149

5.7 Final Remarks 149
5.8 References 150

Appendix A. Understanding Biosurfactant Sequence and Structural Features for Enhanced Targeted Drug Delivery 157

A1.1 Materials and Methods 163
A1.1.1 Plasmids 163
A1.1.2 Expression and Purification 163
A1.1.3 Emulsion Studies 163
A1.2 References 164

Vita 165

List of Figures

Figure 1.1. Clustering drives plexin-neuropilin-semaphorin activity. This clustering is modulated in part by transmembrane and juxtamembrane interactions. 5

Figure 1.2. Motifs in PLXN TM and JM domains may affect dimerization. (A) A richness in small amino acids in the TM domain and a heptad repeat in the JM domain are conserved across species and PLXNA family members and likely affect PLXN dimerization. (B) Residues in the JM heptad repeat lie on the same interface of the *Mus musculus* PLXNA3 crystal structure (PDB #3IG3). (C) A crystal structure of the *Danio rerio* PLXNC1 CYTO domain dimerized via a N-terminal GCN4 coiled-coil fusion (PDB #4M8M) suggests residues homologous to the *Danio rerio* PLXNA3 JM heptad repeat lie at the interface of the dimer. 9

Figure 2.1. Clustering drives plexin activation. (A) Cartoon illustration indicating the relationship between plexin oligomeric state and function. (B) A cytosolic juxtamembrane heptad repeat in PlxnA3 is conserved across species and may regulate this phenomenon. (C) A crystal structure of the *Mus musculus* PLXNA3 cytosolic domain (PDB # 3IG3) with residues comprising a heptad repeat highlighted in green. 22

Figure 2.2. Expression and orientation of PlxnA3 TMCY AraTM constructs. (A) Anti-MBP western blot (1:10000 dilution, NEB) of PlxnA3 TMCY AraTM constructs. (B) Maltose complementation test of PlxnA3 TMCY AraTM constructs. (C) Spheroplast assay on the WT PlxnA3 TMCY AraTM construct. Ladder markings are in kDa. The expected molecular weight of PlxnA3 TMCY AraTM constructs is 67 kDa. 26

Figure 2.3. AraTM results for a three-replicate round of PlxnA3 TM + JM AraTM measurements. (A) Non-normalized average slope of fluorescence *vs.* absorbance, with error bars indicating standard error determined from three replicates. (B) Average slope of fluorescence *vs.* absorbance represented as a percent change in slope from WT, with error bars indicating standard error of the mutant construct plus standard error of the WT construct. Red bars marked with '*' indicate non-overlapping mean +/- SEM with the WT protein in each graph. 27

Figure 2.4. Expression of proteins in the BRET2 assay. (A) Anti-GFP (1:1000 dilution, Clontech) western blot confirming expression of PlxnA3-GFP2 in the BRET2 assay. The expected molecular weights are 176 kDa and 27 kDa for PlxnA3-GFP2 and GFP2, respectively. (B) Anti-RLuc (1:2500 dilution, Millipore) western blot confirming expression of PlxnA3-RLuc in the BRET2 assay. The expected molecular weights are 185 kDa and 36 kDa for PlxnA3-RLuc and RLuc, respectively. (C) Anti-FLAG staining of COS-7 cells expressing FLAG-tagged Nrp2a. No fluorescence was observed in mock-transfected cells. The scale bar in the bottom left frame is the same for all images. (D) Dot blot confirming alkaline phosphatase activity in media from cells transfected with alkaline phosphatase-tagged SEMA3F. (E) Confirmation of alkaline-phosphatase-tagged SEMA3F binding to COS-7 cells expressing Nrp2a and PlxnA3. 29

Figure 2.5. Residues in the PlxnA3 JM heptad repeat promote homomeric interactions in the AraTM assay. Residues on the JM heptad repeat interface influence TM + JM oligomerization, as determined via site-directed mutagenesis. Error bars indicate standard error as determined from a minimum of eleven replicates collected over the course of three experiments. 32

Figure 2.6. Random mutagenesis yielded additional mutants on the predicted JM interface that alter PlxnA3 homomeric interactions. (A) AraTM results for EP-PCR mutants, where error bars indicate standard error as determined from four replicates. (B) The crystal structure of the *Mus musculus* PLXNA3 cytosolic juxtamembrane domain from PDB # 3IG3 indicates the EP-PCR mutants (orange) lie on the same interface as hydrophobic residues involved in the juxtamembrane heptad repeat (green). 33

Figure 2.7. $BRET^2$ results indicate alterations to the PlxnA3 JM heptad repeat influence homooligomerization. (A) PlxnA3 homooligomerization in the context of the receptor with the extracellular, TM, and JM domains (residues 1-1314) in a mammalian membrane indicate residues in the JM heptad repeat influence homomeric interactions. (B) The presence of the Nrp2a co-receptor and SEMA3F ligand do not alter homooligomerization of the WT PlxnA3 receptor at the concentrations examined. (C) The presence of the Nrp2a co-receptor and SEMA3F ligand corrects the disruption to PlxnA3 homooligomerization caused by mutation M1281F to that of the WT receptor, whereas mutant M1281L still exhibits significant enhancement to homooligomerization compared to WT. Error bars indicate standard error as determined from a minimum of 21 replicates collected over the course of three experiments.35

Figure 2.8. Knockdown of *plxna3* results in aberrant motor neuron patterns. The motor neurons of 24 hour post fertilization *sidetracked* zebrafish embryos (top) exhibit ectopic motor neuron exit points from the motor cord (arrows) compared to WT embryos (bottom). Asterisks indicate endogenous motor neuron exit points. Embryos are oriented anterior (left) to posterior (right)..... 37

Figure 3.1. Plexin transmembrane and juxtamembrane domains contribute to receptor clustering and activation. (A) Extracellular binding of a semaphorin ligand (Sema) to plexin (Plxn) and neuropilin (Nrp) leads to receptor clustering and activation. (B) A small amino acid-rich region in the transmembrane domain and a cytosolic juxtamembrane heptad repeat are conserved across class A plexins and postulated to modulate homooligomerization. (C) Primary sequence analysis of the glycine-rich *Danio rerio* PlexinA3 transmembrane domain reveals two interfaces capable of participating in small-x_3-small packing motifs. Structural representation of the PlexinA3 transmembrane domain was generated using the asymmetric *E_z-3D* Potential Finder..... 48

Figure 3.2. PlxnA3 TMCY constructs express in similar levels and the correct orientation (AraTM assay). (A) Anti-MBP (1:10,000 dilution, NEB) western blots of Plexin A3 TMCY mutants. Expected molecular weight ~67 kDa. (B) Maltose complementation results (day 8) confirming orientation of Plexin A3 TMCY constructs. Each row represents a separate plate. 51

Figure 3.3. (A) Disruption of small-x_3-small interfaces in the PlexinA3 TM domain via point mutations enhance TM-JM dimerization in the AraTM assay. Similarly, extension of the small-x_3-small interfaces via introduction of glycines disrupt TM-JM dimerization. (B)

Double and triple mutations disrupting the PlexinA3 TM small-x_3-small interfaces enhance dimerization of the TM-JM in the AraTM assay. Error bars indicate standard error as determined from twelve replicates collected over a minimum of three experiments. 53

Figure 3.4. Mutations to the PlexinA3 JM domain dominate dimerization tendencies of the TM-JM in the AraTM assay. Error bars indicate standard error as determined from twelve replicates collected over a minimum of three experiments. 55

Figure 3.5. Embryos with the *sidetracked* phenotype exhibit ectopic motor neuron exit points (arrows). Endogenous motor neuron exit points are marked with an asterisk. Embryos were 24 hours post fertilization at the time of fixation and are oriented (left-to-right) anterior-to-posterior. 56

Figure 3.6. Model for competitive TM and JM interactions in regulation of PlexinA3 signal transduction. 59

Figure 4.1. NRP2a is a transmembrane receptor. (A) NRP2a consists of two CUB domains, two factor V/VIII domains, a MAM domain, a single-spanning transmembrane region, and a short cytosolic tail. NRP homooligomerization may play a role in NRP-plexin-sema and NRP-VEGFR-VEGF signal transduction by promoting aggregation. (B) Primary sequence of the *Danio rerio* NRP2a MAM domain. The MAM domain contains four conserved cysteines that impact homooligomerization in other MAM domain family members. 68

Figure 4.2. NRP2 BRET2 constructs are expressed in COS-7 cells upon transfection. Ladder markings are in kDa. Anti-RLuc (top), anti-tubulin (top), and anti-GFP (bottom) western blots of cultures co-transfected with NRP2-RLuc and NRP2-GFP fusion constructs. R = NRP2-RLuc fusion (140 kDa), T = tubulin (55 kDa), G = NRP2-GFP fusion (130 kDa). 73

Figure 4.3. Cysteines in the NRP2a MAM domain of influence receptor homooligomerization in a mammalian membrane, as determined by BRET2. Results were collected from at least three separate transfections of each condition and error bars represent standard error. 76

Figure 4.4. WT NRP2a overexpression causes ISV branching in 48 hours post fertilization zebrafish embryos. 78

Figure 4.5. Mutant C711S reduces binding of Sema3F to the full-length NRP2a receptor. (A) Representative images of hook-Sema3F-bound cells. (B) Mutant C711S disrupts Sema3F-binding. Cells were transfected with water, WT, or mutant NRP2a constructs and treated with 50x-concentrated hook-Sema3F. Twenty random fields of view for each condition per round (three rounds total) were examined at an exposure time consistent within the round and the total number of Sema3F-bound cells were counted. Error bars indicate standard error. 80

Figure 5.1. Mechanisms of transmembrane protein activation. (A) Traditionally, membrane protein activation is thought to occur through translational or rotational motion. (B) Activation of the plexin transmembrane receptor may rely upon a variation of horizontal translation that results in high local concentration due to clustering caused by a network of dimers and trimers. 92

Figure 5.2. The Danio rerio PlxnA3 JM was successfully expressed and purified as a thrombin-cleavable MBP fusion. Ladder markings are in kDa. Expected molecular weights are 48.8 kDa, 42.7 kDa, and 6.1 kDa for the MBP-JM, MBP, and JM, respectively. 94

Figure 5.3. Off-interface residues in the TM and JM may modulate receptor dimerization. (A) Sequence of the *Danio rerio* PlxnA3 TM (purple) and JM (green) domains. Two small-x3-small interfaces in the TM domain and a heptad repeat in the JM domain (red font) modulate TM + JM dimerization (Chapters 2 & 3). Additional off-interface residues, such as G1249 and A1255 in the TM domain, or R1276 and L1279 in the JM domain, may modulate dimerization. Another small-x3-small interface in-frame with G1246 + G1250 (A1258 + A1262) may also modulate dimerization. (B) Helical wheel diagram of the PlxnA3 JM domain with the heptad repeat at the core of the dimer interface (Chapter 2). (C) Helical wheel diagram of the PlxnA3 JM domain with an alternative leucine (L1279) at the dimer core and predicted disruptive electrostatic interactions (K1275 + R1276) de-stabilizing the interaction. Helical wheel diagrams and salt bridge prediction were generated using DrawCoil 1.0. 96

Figure 5.4. Off-interface residues TM and JM residues contribute to dimerization. (A) Off-interface residues in the TM (purple) and JM (green) modulate TM + JM dimerization in the AraTM assay. JM mutations (M1281F and M1281L, Chapter 3) dominate in mutations to both the TM and JM domains (blue). Error bars indicate standard error as determined from a minimum of twelve replicates collected over the course of three experiments. (B) Anti-MBP (1:10,000 dilution, NEB) western blots confirming expression of PlxnA3 TM + JM mutants. Expected molecular weight ~67 kDa. Portions of these western blots appeared in Chapters 2 (right) and 3 (left). (C) Maltose complementation tests on PlxnA3 TM + JM constructs. Each column represents a separate plate. Portions of the plates (the WT or pAraCy controls) may have appeared in Chapters 2 and 3. 97

Figure 5.5. Mutations to both TM and JM domains (blue) are non-additive from TM mutations alone (purple) and JM mutations alone (green). Values originally appeared in Chapters 2 and 3 and Section 5.2 and are re-plotted here for clarification. 100

Figure 5.6. CD spectra of the *Danio* rerio PlxnA3 TM domain (A) at various concentrations in FOS-Choline-15, (B) at various temperatures (0.3 mg/mL in FOS-Choline-15), (C) with TFE in (0.3 mg/mL in FOS-Choline-15), and (D) at 0.3 mg/mL in FOS-Choline-15 micelles or DMPC/DHPC bicelles. 102

Figure 5.7. The *Danio rerio* PlxnA3 TM + JM was successfully expressed and purified as a thrombin-cleavable ompF fusion. Ladder markings are in kDa. Expected molecular weights are 26.8 kDa, 17.4 kDa, and 9.4 kDa for the ompF-TM + JM, ompF, and TM + JM, respectively. 102

Figure 5.8. Select mutations to the Plexin A3 TM domain influence homooligomerization with a full extracellular domain intact (A) BRET2 results. Error bars indicate standard error determined from a minimum of forty-six replicates collected over the course of six experiments. Expression of PlxnA3 BRET2 constructs. (B) Anti-RLuc (1:1,000 dilution, Millipore) western blot of PlxnA3 BRET2 transfections. Expected molecular weight ~185 kDa (R). (C) Anti-GFP (1:1,000 dilution, Clontech) and anti-tubulin (1:1,000 dilution,

Abcam) western blot of PlxnA3 BRET2 transfections. Expected molecular weights ~176 kDa (PlxnA3-GFP2, G) and ~50 kDa (tubulin, T). 104

Figure 5.9. *Danio rerio* Nrp1 and Nrp2a transmembrane sequences. Nrp1 exhibits two small-x3-small motifs (red). An alanine insertion in the Nrp2a transmembrane sequence yields an additional small-x3-small motif (blue). 108

Figure 5.10. Mutations to the Nrp2a MAM and TM domains alter MAM-TM-CYTO homodimerization in the AraTM assay. (A) Specific residues in the Nrp2a MAM (blue) and TM (purple) domains modulate homodimerization of the MAM-TM-CYTO domains, as determined using the AraTM assay. Results were collected over the course of at least three experiments and error bars indicate standard error. (B) An anti-MBP western blot on samples from a spheroplast protection assay reveals WT Nrp2a MAM-TM-CYTO is correctly oriented in the cell membrane. WC = whole cell lysate, P = periplasm, SP = spheroplast, S = supernatant, PK = Proteinase K, NP40 = Nonidet P-40. Ladder markings are in kDa, Nrp2a MAM-TM-CYTO is ~ 92 kDa. (C) Anti-MBP western blot of AraTM constructs, as expressed by SB1676 cells in AraTM measurements. (D) Mutant constructs orient themselves correctly in the cell membrane, as determined by a maltose complementation test (growth on a plate with maltose as the sole sugar source signifies correct orientation). 109

Figure 5.11. A comparison of Nrp2a MAM-TM-CYTO constructs in AraTM and full-length constructs in BRET2 suggest mutations to the TM domain (G872L) disrupt homodimerization in both assays, suggesting the switch from dimer-disrupting (AraTM) to dimer-enhancing (BRET2) was specific to MAM domain mutations. Error bars indicate standard error. Mutations are those presented in Chapter 4 and Figure 5.10, re-plotted for comparative purposes. 111

Figure 5.12. A NativePAGE western blot of Nrp2a-GFP2 constructs suggest the full-length receptor homo-oligomerizes, and MAM mutant C711S promotes homomeric aggregation. Ladder markings in kDa, expected molecular weight of monomeric WT NRP2-GFP2 is 130 kDa. Apparent molecular weights are marked as M (monomer), D (dimer), and T4 (tetramer). 112

Figure 5.13. Cooperative effects between the MAM domain and other domains may define oligomeric state and conformation of the full-length receptor. (A) In the context of MAM-TM-CYTO (*AraTM assay*), mutations to select cysteines disrupt dimerization. MAM-driven dimerization (via disulfide bonds, *circle pairs*, or another driving force, *green triangle*) may compete with TM-driven dimerization (*arrows*). An intact C711 and C794, no lone cysteines, and shielding of other driving forces (e.g., *burial of the green triangle by intact C711 and C794 disulfide bonds*) allow for native TM interactions. (B) In the full-length receptor (*BRET2 assay*), select cysteine mutations enhance dimerization. Residues C711 and C794 may cooperate with another extracellular domain, defining the overall shape (e.g., *semi-ovals* vs. *squares*). A requirement to satisfy disulfide bonds (*C643S and C711S*) or better shape complementarity (*C711S + C794S*) may bring receptor cytosolic domains closer together. The requirement to satisfy disulfide bonds, combined with an overall change in receptor shape, may also disrupt ligand binding (*C711S, Chapter 4*). 113

Figure 5.14. Constructs to investigate via BRET2 to elucidate putative cooperative partners of the MAM domain. Extracellular domain constructs could also be evaluated by small angle x-ray scattering if oligomerization studies imply domain cooperativity. 115

Figure 5.15. NativePAGE on MBP-MAM. (A) NativePAGE gels on purified MAM-MBP mutants illustrates mutations of cysteines C711 and C794 in the MAM domain influence the equilibrium of oligomeric states. (B) In the presence of the reducing agent β-mercaptoethanol, a band at the apparent dimer molecular weight persists. Ladder markings in kDa, expected molecular weight of monomeric WT MAM-MBP is 62.5 kDa. D marks apparent molecular weight of a dimer, H marks higher-order oligomer. 119

Figure 5.16. The NRP2a MAM domain exists in monomeric and dimeric states when analyzed by SDS-PAGE, in the presence or absence of reducing agent (DTT) and chemical cross-linker (BS3). Addition of reducing agent reduces the ratio of dimer to monomer for the WT MAM domain as well as mutations C643S and C636S + C643S. Similar monomer/dimer ratios exist in the presence or absence of reducing agent in MAM domains where the disulfide bond involving C711 has been disrupted (C711S and C711S + C794S). Ladder markings in kDa, monomeric WT NRP2a MAM domain is 23 kDa. M marks monomer, D marks dimer. 122

Figure 5.17. The Nrp2a MAM domain exists as monomer and oligomer in PBS, as determined by size-exclusion chromatography. (A) Chromatograms for Nrp2a MAM domain constructs. (B) Ratios of absorbance intensity of oligomer to monomer for Nrp2a MAM domain constructs. Comparisons to WT suggest mutation C711S promotes oligomer formation. 124

Figure 5.18. Tryptophan fluorescence studies on the Nrp2a MAM domain suggest mutant C711S exposes alternate interfaces compared to WT. (A) Shifts in barycentric mean fluorescence values from free tryptophan suggest the isolated Nrp2a MAM domain tertiary and/or quaternary structures allow for tryptophan burial. Mutants C711S and C711S + C794S exhibit different folding from WT. Error bars indicate standard deviation from three spectral acquisitions. (B) Trends in fluorescence intensity suggest disulfide bonds play a role in tryptophan burial in the WT and C711S Nrp2a MAM domains, with disulfide bonds allowing WT to bury more tryptophan and causing C711S to expose more tryptophan. 126

Figure 5.19. Circular dichroism spectra of Nrp2a MAM domains in PBS. WT and mutant constructs exhibit β-sheet characteristics, in the absence (A) or presence (B) of TCEP..... 127

Figure 5.20. Homomeric Nrp2a interactions likely occur via a cysteine-rich interface in the MAM domain. (A) A model of the Nrp2a MAM domain, based on a crystal structure of the PTPμ MAM domain, supports the theory of a cysteine-rich interface that stabilizes dimerization, as the four cysteines lie on the same interface. (B) Our model suggests not all cysteine pairs of the NRP2 MAM domain (left) are close enough to form intramolecular disulfide bonds, in contrast to the MAM domain of PTPμ (right). 129

Figure 5.21. (A) Model of a Nrp2a MAM dimer in which C711 and C794 are in close-enough proximity to interact. Mutations M713W and N782Q were predicted to introduce steric hindrances to dimerization. Mutations M674W, R697E, and R750E, off-interface residues, were predicted to have no effect on dimeric interactions. (B) As determined via AraTM, changing amino acids on the predicted homomeric interface resulted in disruption (M713W

and N782Q), whereas a predicted off-interface mutation (M674W) did not. Mutations to predicted off-interface charged residues (R697E and R750E) also disrupted dimerization. Values and error bars are as described in Figure 3A. (C) Anti-MBP western blot (1:1,000, NEB) and (D) maltose complementation tests of Nrp2a MAM-TM-CYTO constructs confirm expression and orientation of the AraTM constructs. (E) NativePAGE gel on MAM mutants. None of the mutations examined in the model increased the amount of higher-order oligomers introduced by C711S and C794S. Mutation N782Q did introduce bands at lower molecular weight than dimer, supporting our model for the dimer interface. Ladder markings in kDa, expected molecular weight of monomeric WT MAM-MBP is 62.5 kDa. M marks apparent monomer, D marks apparent dimer, H marks higher-order oligomer. 131

Figure 5.22. Primary sequence comparison of human neuropilins. (A) Alignment of human membrane-anchored neuropilin MAM-TM-CYTO sequences. TM-CYTO domains are indicated by red font, whereas MAM-TM-CYTO domains are both black and red font. Bolded residues are those predicted to be in the membrane environment. (B) The primary sequence of all NRP TM domains exhibit at least one small-x3-small motif. Different colors indicate different small-x3-small motifs. 139

Figure 5.23. DNAraTM measurements of human NRP2 homodimerization and NRP1-NRP2 heterodimerization. (A) DNAraTM measurements for NRP2 TM-CYTO-AraC homodimerization, NRP2 MAM-TM-CYTO-AraC homodimerization, and NRP2 MAM-TM-CYTO-AraC heterodimerization with NRP1 MAM-TM-CYTO-AraC*. Results represent average values of a minimum of 15 samples collected over the course of three experiments. Error bars indicate standard error. (B) An anti-HA (1:1,000, Cell Signaling) western blot indicates NRP2 TM-CYTO-AraC constructs may express better than NRP2 MAM-TM-CYTO-AraC constructs. (C) NRP2 MAM-TM-CYTO-AraC constructs express in equivalent levels independent of NRP1 MAM-TM-CYTO-AraC* co-expression, as indicated by an anti-HA (1:1,000, Cell Signaling) western blot. (D) NRP1 MAM-TM-CYTO-AraC* is expressed in all heterodimer conditions tested in the DNAraTM assay, as indicated by an anti-myc (1:1,000, Cell Signaling) western blot. Expected molecular weights are roughly 75 kDa for TM-CYTO-AraC constructs and 90 kDa for MAM-TM-CYTO-AraC and MAM-TM-CYTO-AraC* constructs. 141

Figure 5.24. NRP1 and NRP2a(22) MAM-TM-CYTO-AraC* constructs heterodimerize with NRP1, NRP2a(22), and NRP2b(0) MAM-TM-CYTO-AraC constructs in the DNAraTM assay, as indicated by decreased level of GFP expression for a given culture density upon co-expression of MAM-TM-CYTO-AraC* with the MAM-TM-CYTO constructs. Values represent average slopes of fluorescence *vs.* absorbance collected from a minimum of 22 replicates collected over the course of six experiments. Error bars indicate standard error.. 142

Figure 5.25. NRP1 MAM-TM-CYTO-AraC heterodimerization with NRP1 MAM-TM-CYTO-AraC* competition. Results represent the average value from a minimum of 22 samples collected over the course of six experiments. Error bars indicate standard error. 143

Figure 5.26. NRP2a(22) MAM-TM-CYTO-AraC heterodimerization with NRP1 MAM-TM-CYTO-AraC* competition. Results represent the average value from a minimum of 22 samples collected over the course of six experiments. Error bars indicate standard error. ... 144

Figure 5.27. NRP2b(0) MAM-TM-CYTO-AraC heterodimerization with NRP1 MAM-TM-CYTO-AraC* competition. Results represent the average value from a minimum of 22 samples collected over the course of six experiments. Error bars indicate standard error. ... 144

Figure 5.28. NRP2a(22) MAM-TM-CYTO-AraC heterodimerization with NRP2a(22) MAM-TM-CYTO-AraC* competition. Results represent the average value from a minimum of 22 samples collected over the course of six experiments. Error bars indicate standard error. ... 145

Figure 5.29. NRP1 MAM-TM-CYTO-AraC heterodimerization with NRP2a(22) MAM-TM-CYTO-AraC* competition. Results represent the average value from a minimum of 22 samples collected over the course of six experiments. Error bars indicate standard error. ... 147

Figure 5.30. NRP2b(0) MAM-TM-CYTO-AraC heterodimerization with NRP2a(22) MAM-TM-CYTO-AraC* competition. Results represent the average value from a minimum of 22 samples collected over the course of six experiments. Error bars indicate standard error. ... 147

Figure 5.31. Anti-myc (1:1,000, Cell Signaling) western blot confirming expression of (A) NRP1 and (B) NRP2a(22) MAM-TM-CYTO-AraC* DNAraTM constructs. Expected molecular weights of WT constructs are 91 kDa and 92.5 kDa for NRP1 and NRP2a(22), respectively. Ladder markings are in kDa. 149

Figure A1. Structure of HFBII, a naturally-occurring peptide biosurfactant (PDB # 1R2M). Tertiary structure is maintained by disulfide bonds (cyan), and amphiphilicity is a result of a patch of aliphatic side chains (orange). 158

Figure A2. OmpF-HFBII.2 can be expressed using a bacterial expression system. (A) Coomassie-stained SDS-PAGE gel and (B) anti-His (1:1,000, Cell Signaling) western blot confirming expression and cleavage of ompF-HFBII.2. The poly-histidine tag is on the ompF fragment of the the fused protein; bands present on the Coomassie-stained gel and absent on the western blot may be HFBII.2-only (green boxes: monomeric HFBII.2; yellow box: oligomeric HFBII.2 without ompF). The addition of 1% β-mercaptoethanol reduces, but does not eliminate, oligomerization. Expected monomeric molecular weights are 7.4 kDa, 17.4 kDa, and 24.8 kDa for HFBII.2, ompF, and ompF-HFBII.2, respectively..... 159

Figure A3. MALDI-TOF spectra of thrombin-cleaved ompF-HFBII.2 subjected to reverse phase chromatography with an (A) acetonitrile or (B) isopropanol gradient. Expected m/z for HFBII.2 is 7.4. 161

Figure A4. A preliminary macroscopic emulsion study suggests the presence of HFBII.2 affects oil emulsification. Enhanced emulsification is indicated by the persistence of a middle (white) layer, whereas the appearance of three layers (a clear layer on the top and bottom) indicates poor emulsification. 162

List of Tables

Table 2.1. Percentage of Embryos Exhibiting s*idetracked* Phenotype 38

Table 3.1. Percentage of Homozygous *sidetracked* Embryos Exhibiting Phenotype 57

Table 4.1. Percentage of fli1-GFP embryos exhibiting ISV branching 78

Table 5.1. Percentage of Embryos Exhibiting *sidetracked* Phenotype 103

Table 5.2. Neuropilin Cloning Domains in the DNAraTM Assay. 148

Abstract

Neuropilins (nrps) and plexins (plxns) are transmembrane (TM) proteins that form co-receptor complexes to guide neuronal, vascular, lymphatic, and bone development as well as cancer metastasis. While it is understood that nrp serves as the extracellular ligand-binding receptor and plxn as the signal-transducing portion of the complex, little is understood about the mechanism of activation of the signal transduction cascade beyond ligand binding. Understanding the mechanisms of plxn and nrp activation may provide insight necessary for rational design of novel cancer therapeutics.

Co-receptor clustering is believed to induce activation. Previous studies suggest deletion of the plxn extracellular domain leads to a constitutively active plxn, but lack of membrane-anchorage of the cytosolic domain yields inactivity, implying a role for the plxn TM and juxtamembrane (JM) domains in clustering and subsequent activation. We demonstrate that a heptad repeat in the cytosolic JM domain modulates *Danio rerio* PlxnA3 homodimerization of the TM + JM domains in a bacterial membrane via the AraTM homodimer assay and of the TM + JM domains with a full extracellular domain intact via a bioluminescence resonance energy transfer ($BRET^2$) assay. A specific mutation (M1281L) that enhances homodimerization in the $BRET^2$ assay in the presence of a Nrp2a co-receptor and semaphorin-3F ligand also fails to rescue motor neuron patterning in PlxnA3-knockout zebrafish embryos, in contrast to the wild-type protein. We also demonstrate via these same techniques that a glycine-rich segment of the PlxnA3 TM domain modulates receptor homodimerization, competing with the dimerization motif of the JM domain. Specifically, mutations to small-x_3-small motifs in the PlxnA3 TM domain enhance dimerization of the TM + JM domains in the AraTM assay. Mutations to both the TM and JM dimerization motifs demonstrate, in the context of the TM + JM system, the heptad repeat in the JM dominates TM + JM dimerization. Mutations to the small-x_3-small TM

dimerization motifs exhibit reduced functionality in the zebrafish embryo axonal guidance assay. Collectively, these results demonstrate that enhanced PlxnA3 dimerization does not correlate with enhanced function. The TM-driven dimerization serves to weaken the JM dimer, likely allowing switchability between co-receptors as well as active and inactive states.

The nrp MAM domain is also believed to contribute to the observed clustering phenomenon with the intact, full-length plxn receptor. We show that cysteines in the *Danio rerio* Nrp2a MAM domain, in particular residue C711, modulate Nrp2 homodimerization, as determined via the $BRET^2$ assay. Mutation of residue C711 also disrupts ligand binding. While zebrafish embryos injected with wild-type *nrp2a* RNA exhibit ectopic vascular branching, significantly fewer embryos injected with *nrp2a* RNA with the C711S mutation exhibit this overexpression phenotype.

Collectively, this work provides insight into the dimerization mechanisms important for nrp and plxn activity. The structure-function correlations determined may assist in rational design of targeted therapeutics to alter nrp and plxn activity.

Chapter 1

Introduction to Neuropilins and Plexins, Transmembrane Receptors Involved in Development and Disease

1.1 Introduction

Neuropilins (nrps) and plexins (plxns) are two families of Type I transmembrane (TM) receptors involved in neuronal, vascular, and lymphatic development as well as zebrafish fin regeneration. Semaphorins (semas) are their ligand binding partners (1-14). At least nine plxns in four different classes (A-D), two nrps (1 and 2) comprised of at least ten different isoforms, and twenty semas in eight classes (classes 1-8) are known to date, with classifications grouped based on homology (3,4,15-20). Class A plxns are known to interact with the secreted dimeric class 3 semas, and in this system, nrps are necessary co-receptors (1-3,10,21). In the plxn-nrp-sema signaling complex, semas serve as the guidance cue, directing the plxn-nrp-expressing cell towards or away from the sema source. Nrps act as the glue that joins sema and plxn and dictates specificity of the plxn-sema association. Plxns serve as the enforcers; upon association with semas and nrps, plxns initiate a signal transduction cascade to alter cell motility (1-3,8,10,15,16,21,22).

While the plxn, nrp, and sema machinery is important for development, it also has implications in disease (3,4,12,17,23-37). In particular, plxns, nrps, and semas have been implicated in influencing development of bladder, breast, endometrial, lung, ovarian, pancreatic,

and prostate cancers as well as melanomas and leukemia, with effects depending on the stage and type of cancer (3,25-27). Implications that plxns, nrps, and semas may regulate cancer progression has led to recent investigations regarding their use as anti-cancer therapeutics. Antibodies disrupting NRP1 and NRP2 signaling inhibited tumor growth and demonstrated anti-metastatic potential in mouse lung tumor models (33,35). Overexpression of SEMA3F also disrupted tumor angiogenesis in a mouse melanoma model (28). Hence, plxn-nrp-sema signaling may modulate tumor growth and metastasis. Understanding signaling mechanisms of these receptors is important from a cancer therapeutic standpoint. From understanding of plxn and nrp structure-function relationships, we may be able to rationally design drugs to promote the anti-tumor and anti-metastatic effects observed with select combinations of these receptors.

1.2 Current Understanding of Plexin and Neuropilin Structure-Function Relationships

Structurally, nrps are comprised of two extracellular CUB (complement protein C1r/C1s, Uegf, and Bmp1) domains, two coagulation factor V/VIII (FA V/VIII) domains, one MAM (meprin, A-5 protein, and protein tyrosine phosphatase μ, PTPμ) domain, a single-spanning TM region, and a short cytosolic tail (Figure 1.1) (14,18,23,31,33,38-40). In addition to interactions with plxns, nrps are known to interact with vascular endothelial growth factor receptors, integrins, and cell adhesion molecules (38,41,42). The short cytosolic domain (CYTO) for nrps has been shown to be nonessential for nrp-plxn signaling (1,39); thus, in the plxn-nrp-sema signal transduction process, plxns are thought responsible for the intracellular signaling. Nrp is necessary for extracellular ligand binding, with the sema-binding domains of class A plxns failing to bind semas in the absence of the nrp co-receptor (1-3,10,21). By imparting specificity in

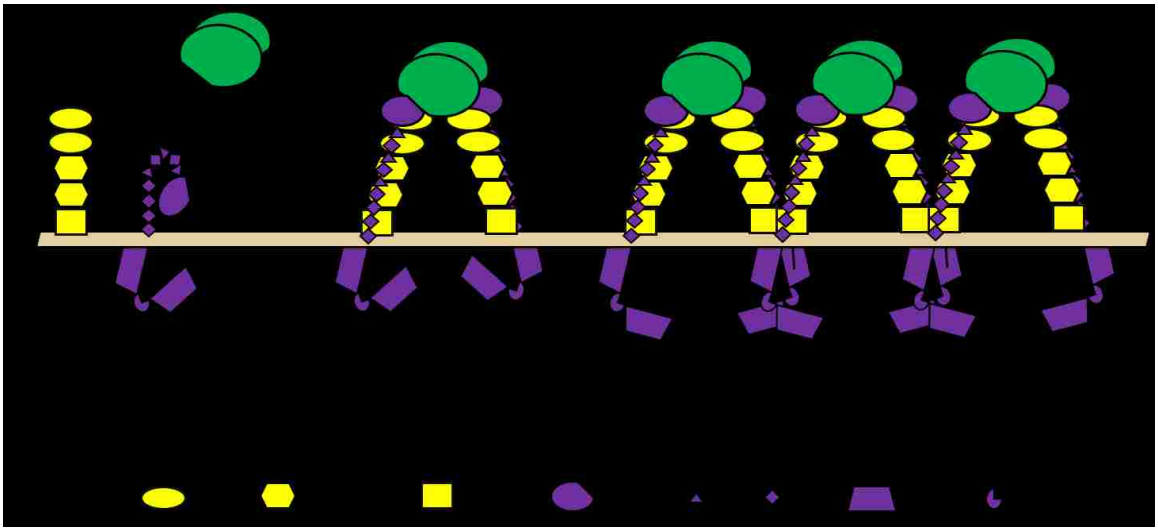

Figure 1.1. Clustering drives plexin-neuropilin-semaphorin activity. This clustering is modulated in part by transmembrane and juxtamembrane interactions.

ligand binding and co-receptor complex formation, nrp modulates the responses of class A plxns to extracellular cues (1,2,43,44).

The plxn structure consists of a sema-binding domain, three plexin-semaphorin-integrin (PSI) domains, and three immunoglobulin, plexin, and transcription factor (IPT) domains extracellularly; a single-pass TM domain; and a CYTO region homologous with RasGAPs (Ras GTPase-activating proteins) (Figure 1.1) (1,3). The sema-binding domain interacts with the sema domain of sema proteins during activation, and for PLXNA1, deletion of this domain alone or the entire extracellular domain leads to a constitutively active receptor, implying an auto-inhibition mechanism involving the sema domain and another extracellular domain (44).

The activity of the plxn CYTO portion is characterized by its GTPase-activating protein (GAP) activity (7,9,15,16,45). Structurally, the CYTO domain is comprised of an N-terminal juxtamembrane helix (JM) followed by a GAP domain with a RhoGTPase-binding domain (RBD) insert; the two halves of the GAP domain are termed C1 and C2 for the N- and C-termini,

respectively (7,9,11,46). In an inactive conformation, the C1 and C2 domains form a closed pocket thought to be inaccessible to G-proteins, preventing plxn GAP activity (7). Upon binding of sema extracellularly in conjunction with RhoGTPase (Rac1, Rnd1, or RhoD) binding to the intracellular RBD or possibly a juxtamembrane pocket, the plxn adopts a new conformation that confers GAP activity (7,9,11,46). Previous studies suggested the G-proteins R-Ras and M-Ras were the objects of this activity (16,45), though recent studies suggest Rap may be the subject of the GTP hydrolysis (11,46).

Expression of the PLXNA1 CYTO domain alone in solution does not confer collapse activity (21,44). In solution, the PLXNA1, PLXNA3, and PLXNB1 CYTO domains are monomeric or weakly dimeric or trimeric, with oligomerization affinities low enough that higher-order structures have yet to be detected by analytical ultracentrifugation (6,7,9,46). Though the PLXNA1, A2, A4, and C1 CYTO domains in solution exhibit low levels of activity in an *in vitro* RapGAP assay, forced dimerization enhances their activity, implying clustering or dimerization modulates activity (46). With the addition of a cross-linker, a membrane-anchored PLXNB1 CYTO domain also causes cellular contraction (47). While membrane-tethering of the PLXNA1 CYTO domain with a myristoylation anchor fails to elicit activity in the absence of overexpression of additional proteins, expression of the PLXNA1 TM + CYTO domains triggers cellular contraction in a COS-7 collapse assay (21,44). Collectively, these observations suggest clustering or dimerization is a key contributing factor to plxn activity, and this phenomenon is modulated in part by the TM and juxtamembrane domains (Figure 1.1). A clustered state driving plxn activity is supported by an early immunohistological observation that, upon addition of SEMA3A to chick E7 dorsal root ganglion (DRG) neurons, PLXNA1 and NRP1 associate to form regions with high local concentrations of receptors (2). As such, the mechanism governing plxn homomeric interactions has yet to be determined. Results collectively suggest the plxn TM

and juxtamembrane domains, as well as the nrp co-receptor, modulate the clustering phenomenon.

While it is known that plxn-nrp co-receptor complexes form at the cell surface, the stoichiometry of this complex is less well understood. Recently, a low-resolution crystal structure of the CUB and FA V/VIII domains of NRP1 with the four N-terminal extracellular domains of PLXNA2 bound to SEMA3A was reported, providing insight into the structure of this complex (10). The structure reveals a 2:2:2 NRP1:PLXNA2:SEMA3A stoichiometry, though neither the NRP1 nor PLXNA2 extracellular domain fragments exhibit dimerization tendencies in solution in the absence of ligand-binding (10). This is in contrast to studies on full-length NRP1 and NRP2a receptors, which run as dimers on western blots and can co-immunoprecipitate (co-IP) alternatively-tagged full-length nrp receptors (39,48-50). NRP1 dimerization is thought to be partially due to the TM domain, which shows a capacity for dimerization in the ToxLuc assay and the bacterial adenylate cyclase 2-hybrid assay (BACTH) (22,51,52). The NRP1 TM domain exhibits a ‘small-x_3-small' motif, a common TM helix-packing motif first identified with Glycophorin A (GpA) (22,51,53). In this motif, 'small' represents a small amino acid (typically glycine, alanine, or serine) and x represents any amino acid. Alignment of the small amino acids on a helical face creates a groove into which ridges created by the side chains from larger amino acids fit, and dimerization is driven by geometric packing, promotion of additional side chain interactions, hydrogen bonding and reduced entropic effects (relative to interactions of larger side chains) (53-56). Through use of the ToxLuc assay and the bacterial adenylate cyclase 2-hybrid assay (BACTH), it was demonstrated that mutations to the NRP1 TM small-x_3-small motif disrupts TM homodimerization (51,52).

Domain-binding and deletion studies, however, suggest additional homomeric interactions may be facilitated by the nrp MAM domain (39,48,49). MAM domains in protein

tyrosine phosphatases and meprins have been demonstrated to modulate homooligomerization in their respective proteins (57-59). In meprins and protein tyrosine phosphatases, intra- and intermolecular disulfide bonds shape protein structure and modulate homomeric interactions (57-60). The role of cysteine chemistry or another specific driving force in nrp MAM homooligomerization, however, is not yet understood. How these interactions affect full-length receptor clustering, and their effect on the plxn-nrp-sema signaling pathway, as well as other nrp-dependent signaling pathways, has still to be determined.

While plxn-nrp-sema associations could promote full-length plxn clustering, it does not explain the ability of PLXNA1 to induce collapse upon removal of the sema domain (in the absence of a nrp co-receptor and sema ligand) (44). Recent studies involving the PLXNA1 TM domain in the BACTH assay demonstrated this region has a weak but significant propensity to homodimerize (22,52). In particular, the PLXNA1 TM domain is rich in small amino acids (glycines and alanines). Simulation work suggests these amino acids can participate in alternative forms of small-x_3-small associations, the most common motif for TM interactions, depending on bilayer composition and the presence or absence of the TM domain of the NRP1 co-receptor (22). The JM domain of PLXNs also contains a heptad repeat that likely contributes to coiled-coil formation (Figure 1.2) (11). The coiled-coil motif is characterized by a hydrophobic core formed by a heptad repeat, with salt bridges stabilizing the interactions. In other words, for residues ABCDEFG, residues A and D are hydrophobic, and as such, lie on the same face of a helical peptide; dimerization allows the hydrophobic residues to be shielded from the solvent, and salt bridges formed by charged residues at the B, C, E, F, or G positions stabilize these interactions (61). A crystal structure of the PLXNC1 CYTO domain dimerized through a GCN4 coiled-coil motif also suggests that the JM may regulate plxn homooligomerization and subsequent signaling, though the coiled-coil portion immediately membrane-proximal was thought to be

Transmembrane (TM)
AII I VLLIAIIAVLIA
AMM L LLILAITAVLVA
AMV L LLILAITVVLVA
AMM L LLILAITAVLVA
AII I LLILIVIIIILIA
AIV I LLILVIVAVLIA
LKRLQLQMDNLESRV
LKRLQLQMDNLESRV
LKRLQLQMDNLESRV
LKRLQLQMDNLESRV
LKRLQMQMHNLESRV
LKRLQLQMDNLESRV

flexible and not involved in dictating homomeric interactions (11). Thus, recent studies have surmised that plxn TM and JM domains are involved in homooligomerization; however, research investigating these domain interactions thus far have been on the isolated domains themselves, rather than in conjunction with each other.

1.3 Determination of Plexin and Neuropilin Homodimer Interfaces

In order to determine the factors promoting clustering of nrp and plxn receptors, we have focused on the individual proteins to understand intrinsic homodimerization. As signaling requires both extracellular and intracellular events (sema-binding extracellularly, and RhoGTPase-binding intracellularly), we focused on the connecting TM and juxtamembrane domains. *Danio rerio* Nrp2a and PlxnA3 served as our model receptors for each class of protein. With PlxnA3, we demonstrate that the JM coiled-coil promotes homodimerization of the PlxnA3 TM + JM domains in the context of an *E. coli* membrane via the AraTM assay and also promotes dimerization of the TM + JM domains in the context of a mammalian cell membrane with a full extracellular domain intact in a bioluminescence resonance energy transfer ($BRET^2$) assay. A dimer-enhancing mutation, M1281L, also enhances dimerization in the $BRET^2$ assay in the presence of the Nrp2a co-receptor and SEMA3F ligand, and fails to rescue wild-type motor neuron patterning in PlxnA3-knockout embryonic zebrafish assay. Additionally, mutation to small-x_3-small interfaces in the PlxnA3 TM domain enhance dimerization of the TM + JM domains in the AraTM assay. We demonstrate that in the TM + JM system, mutations to the JM heptad repeat are dominant over mutations to the TM small-x_3-small motifs, implying TM-driven dimerization negatively regulates JM-driven dimerization. The dimer-enhancing TM mutations also disrupt PlxnA3 function, as determined using the zebrafish axonal guidance assay. Hence, enhanced PlxnA3 dimerization does not correlate with enhanced function. For Nrp2a

homooligomerization studies, our results indicate that a specific interface in the Nrp2a MAM domain, which includes a conserved cysteine (C711), plays a significant role in homooligomerization. Mutation C711S enhances homodimerization, as determined via the $BRET^2$ assay, reduces SEMA3F-binding in transiently-transfected COS-7 cells, and exhibits a decreased Nrp2a overexpression phenotype in a zebrafish embryo vascular patterning assay. Collectively, our results provide insights into the TM and juxtamembrane interfaces modulating Nrp2a and PlxnA3 homomeric interactions and subsequent function (Figure 1.1). Such insight may assist in rational design of therapeutics targeting the plxn-nrp-sema signaling cascade. These therapeutics may subsequently be used to disrupt tumor growth and the metastatic process.

1.4 References

1. Tamagnone, L., Artigiani, S., Chen, H., He, Z., Ming, G. I., Song, H., Chedotal, A., Winberg, M. L., Goodman, C. S., Poo, M., Tessier-Lavigne, M., and Comoglio, P. M. (1999) Plexins are a large family of receptors for transmembrane, secreted, and GPI-anchored semaphorins in vertebrates. *Cell* **99**, 71-80
2. Takahashi, T., Fournier, A., Nakamura, F., Wang, L. H., Murakami, Y., Kalb, R. G., Fujisawa, H., and Strittmatter, S. M. (1999) Plexin-neuropilin-1 complexes form functional semaphorin-3A receptors. *Cell* **99**, 59-69
3. Kruger, R. P., Aurandt, J., and Guan, K. L. (2005) Semaphorins command cells to move. *Nat Rev Mol Cell Biol* **6**, 789-800
4. Wong, O. G., Nitkunan, T., Oinuma, I., Zhou, C., Blanc, V., Brown, R. S., Bott, S. R., Nariculam, J., Box, G., Munson, P., Constantinou, J., Feneley, M. R., Klocker, H., Eccles, S. A., Negishi, M., Freeman, A., Masters, J. R., and Williamson, M. (2007) Plexin-B1 mutations in prostate cancer. *Proc Natl Acad Sci U S A* **104**, 19040-19045

5. Tong, Y., Chugha, P., Hota, P. K., Alviani, R. S., Li, M., Tempel, W., Shen, L., Park, H. W., and Buck, M. (2007) Binding of Rac1, Rnd1, and RhoD to a novel Rho GTPase interaction motif destabilizes dimerization of the plexin-B1 effector domain. *J Biol Chem* **282**, 37215-37224

6. Tong, Y., Hota, P. K., Penachioni, J. Y., Hamaneh, M. B., Kim, S., Alviani, R. S., Shen, L., He, H., Tempel, W., Tamagnone, L., Park, H. W., and Buck, M. (2009) Structure and function of the intracellular region of the plexin-b1 transmembrane receptor. *J Biol Chem* **284**, 35962-35972

7. He, H., Yang, T., Terman, J. R., and Zhang, X. (2009) Crystal structure of the plexin A3 intracellular region reveals an autoinhibited conformation through active site sequestration. *Proc Natl Acad Sci U S A* **106**, 15610-15615

8. Janssen, B. J., Robinson, R. A., Perez-Branguli, F., Bell, C. H., Mitchell, K. J., Siebold, C., and Jones, E. Y. (2010) Structural basis of semaphorin-plexin signalling. *Nature* **467**, 1118-1122

9. Bell, C. H., Aricescu, A. R., Jones, E. Y., and Siebold, C. (2011) A dual binding mode for RhoGTPases in plexin signalling. *PLoS Biol* **9**, e1001134

10. Janssen, B. J., Malinauskas, T., Weir, G. A., Cader, M. Z., Siebold, C., and Jones, E. Y. (2012) Neuropilins lock secreted semaphorins onto plexins in a ternary signaling complex. *Nat Struct Mol Biol* **19**, 1293-1299

11. Wang, Y., Pascoe, H. G., Brautigam, C. A., He, H., and Zhang, X. (2013) Structural basis for activation and non-canonical catalysis of the Rap GTPase activating protein domain of plexin. *Elife* **2**, e01279

12. Roney, K., Holl, E., and Ting, J. (2013) Immune plexins and semaphorins: old proteins, new immune functions. *Protein Cell* **4**, 17-26

13. Ton, Q. V., and Kathryn Iovine, M. (2012) Semaphorin3d mediates Cx43-dependent phenotypes during fin regeneration. *Dev Biol* **366**, 195-203

14. Zachary, I. C., Frankel, P., Evans, I. M., and Pellet-Many, C. (2009) The role of neuropilins in cell signalling. *Biochem Soc Trans* **37**, 1171-1178

15. Rohm, B., Rahim, B., Kleiber, B., Hovatta, I., and Puschel, A. W. (2000) The semaphorin 3A receptor may directly regulate the activity of small GTPases. *FEBS Lett* **486**, 68-72

16. Negishi, M., Oinuma, I., and Katoh, H. (2005) Plexins: axon guidance and signal transduction. *Cell Mol Life Sci* **62**, 1363-1371

17. Balakrishnan, A., Penachioni, J. Y., Lamba, S., Bleeker, F. E., Zanon, C., Rodolfo, M., Vallacchi, V., Scarpa, A., Felicioni, L., Buck, M., Marchetti, A., Comoglio, P. M., Bardelli, A., and Tamagnone, L. (2009) Molecular profiling of the "plexinome" in melanoma and pancreatic cancer. *Hum Mutat* **30**, 1167-1174

18. Rossignol, M., Gagnon, M. L., and Klagsbrun, M. (2000) Genomic organization of human neuropilin-1 and neuropilin-2 genes: identification and distribution of splice variants and soluble isoforms. *Genomics* **70**, 211-222

19. Cackowski, F. C., Xu, L., Hu, B., and Cheng, S. Y. (2004) Identification of two novel alternatively spliced Neuropilin-1 isoforms. *Genomics* **84**, 82-94

20. Gagnon, M. L., Bielenberg, D. R., Gechtman, Z., Miao, H. Q., Takashima, S., Soker, S., and Klagsbrun, M. (2000) Identification of a natural soluble neuropilin-1 that binds vascular endothelial growth factor: In vivo expression and antitumor activity. *Proc Natl Acad Sci U S A* **97**, 2573-2578

21. Zanata, S. M., Hovatta, I., Rohm, B., and Puschel, A. W. (2002) Antagonistic effects of Rnd1 and RhoD GTPases regulate receptor activity in Semaphorin 3A-induced cytoskeletal collapse. *J Neurosci* **22**, 471-477

22. Aci-Seche, S., Sawma, P., Hubert, P., Sturgis, J. N., Bagnard, D., Jacob, L., Genest, M., and Garnier, N. (2014) Transmembrane recognition of the semaphorin co-receptors neuropilin 1 and plexin A1: coarse-grained simulations. *PLoS One* **9**, e97779

23. Ellis, L. M. (2006) The role of neuropilins in cancer. *Mol Cancer Ther* **5**, 1099-1107

24. Stanton, M. J., Dutta, S., Zhang, H., Polavaram, N. S., Leontovich, A. A., Honscheid, P., Sinicrope, F. A., Tindall, D. J., Muders, M. H., and Datta, K. (2013) Autophagy control by the VEGF-C/NRP-2 axis in cancer and its implication for treatment resistance. *Cancer Res* **73**, 160-171

25. Pellet-Many, C., Frankel, P., Jia, H., and Zachary, I. (2008) Neuropilins: structure, function and role in disease. *Biochem J* **411**, 211-226

26. Staton, C. A., Shaw, L. A., Valluru, M., Hoh, L., Koay, I., Cross, S. S., Reed, M. W., and Brown, N. J. (2011) Expression of class 3 semaphorins and their receptors in human breast neoplasia. *Histopathology* **59**, 274-282

27. Capparuccia, L., and Tamagnone, L. (2009) Semaphorin signaling in cancer cells and in cells of the tumor microenvironment--two sides of a coin. *J Cell Sci* **122**, 1723-1736

28. Bielenberg, D. R., Hida, Y., Shimizu, A., Kaipainen, A., Kreuter, M., Kim, C. C., and Klagsbrun, M. (2004) Semaphorin 3F, a chemorepulsant for endothelial cells, induces a poorly vascularized, encapsulated, nonmetastatic tumor phenotype. *J Clin Invest* **114**, 1260-1271

29. Goel, H. L., Chang, C., Pursell, B., Leav, I., Lyle, S., Xi, H. S., Hsieh, C. C., Adisetiyo, H., Roy-Burman, P., Coleman, I. M., Nelson, P. S., Vessella, R. L., Davis, R. J., Plymate, S. R., and Mercurio, A. M. (2012) VEGF/neuropilin-2 regulation of Bmi-1 and consequent repression of IGF-IR define a novel mechanism of aggressive prostate cancer. *Cancer Discov* **2**, 906-921

30. Yasuoka, H., Kodama, R., Tsujimoto, M., Yoshidome, K., Akamatsu, H., Nakahara, M., Inagaki, M., Sanke, T., and Nakamura, Y. (2009) Neuropilin-2 expression in breast cancer: correlation with lymph node metastasis, poor prognosis, and regulation of CXCR4 expression. *BMC Cancer* **9**, 220

31. Bagri, A., Tessier-Lavigne, M., and Watts, R. J. (2009) Neuropilins in tumor biology. *Clin Cancer Res* **15**, 1860-1864

32. Harsha, H. C., Kandasamy, K., Ranganathan, P., Rani, S., Ramabadran, S., Gollapudi, S., Balakrishnan, L., Dwivedi, S. B., Telikicherla, D., Selvan, L. D., Goel, R., Mathivanan, S., Marimuthu, A., Kashyap, M., Vizza, R. F., Mayer, R. J., Decaprio, J. A., Srivastava, S., Hanash, S. M., Hruban, R. H., and Pandey, A. (2009) A compendium of potential biomarkers of pancreatic cancer. *PLoS Med* **6**, e1000046

33. Caunt, M., Mak, J., Liang, W. C., Stawicki, S., Pan, Q., Tong, R. K., Kowalski, J., Ho, C., Reslan, H. B., Ross, J., Berry, L., Kasman, I., Zlot, C., Cheng, Z., Le Couter, J., Filvaroff, E. H., Plowman, G., Peale, F., French, D., Carano, R., Koch, A. W., Wu, Y., Watts, R. J., Tessier-Lavigne, M., and Bagri, A. (2008) Blocking neuropilin-2 function inhibits tumor cell metastasis. *Cancer Cell* **13**, 331-342

34. Narazaki, M., Segarra, M., and Tosato, G. (2008) Neuropilin-2: a new molecular target for antiangiogenic and antitumor strategies. *J Natl Cancer Inst* **100**, 81-83

35. Pan, Q., Chanthery, Y., Liang, W. C., Stawicki, S., Mak, J., Rathore, N., Tong, R. K., Kowalski, J., Yee, S. F., Pacheco, G., Ross, S., Cheng, Z., Le Couter, J., Plowman, G., Peale, F., Koch, A. W., Wu, Y., Bagri, A., Tessier-Lavigne, M., and Watts, R. J. (2007) Blocking neuropilin-1 function has an additive effect with anti-VEGF to inhibit tumor growth. *Cancer Cell* **11**, 53-67

36. Drenberg, C. D., Livingston, S., Chen, R., Kruk, P. A., and Nicosia, S. V. (2009) Expression of Semaphorin 3F and Its Receptors in Epithelial Ovarian Cancer, Fallopian Tubes, and Secondary Mullerian Tissues. *Obstet Gynecol Int* **2009**, 730739

37. Nguyen, H., Ivanova, V. S., Kavandi, L., Rodriguez, G. C., Maxwell, G. L., and Syed, V. (2011) Progesterone and 1,25-dihydroxyvitamin D(3) inhibit endometrial cancer cell growth by upregulating semaphorin 3B and semaphorin 3F. *Mol Cancer Res* **9**, 1479-1492

38. Fukasawa, M., Matsushita, A., and Korc, M. (2007) Neuropilin-1 interacts with integrin beta1 and modulates pancreatic cancer cell growth, survival and invasion. *Cancer Biol Ther* **6**, 1173-1180

39. Nakamura, F., Tanaka, M., Takahashi, T., Kalb, R. G., and Strittmatter, S. M. (1998) Neuropilin-1 extracellular domains mediate semaphorin D/III-induced growth cone collapse. *Neuron* **21**, 1093-1100

40. Schwarz, Q., and Ruhrberg, C. (2010) Neuropilin, you gotta let me know: should I stay or should I go? *Cell Adh Migr* **4**, 61-66

41. Falk, J., Bechara, A., Fiore, R., Nawabi, H., Zhou, H., Hoyo-Becerra, C., Bozon, M., Rougon, G., Grumet, M., Puschel, A. W., Sanes, J. R., and Castellani, V. (2005) Dual functional activity of semaphorin 3B is required for positioning the anterior commissure. *Neuron* **48**, 63-75

42. Castellani, V., Chedotal, A., Schachner, M., Faivre-Sarrailh, C., and Rougon, G. (2000) Analysis of the L1-deficient mouse phenotype reveals cross-talk between Sema3A and L1 signaling pathways in axonal guidance. *Neuron* **27**, 237-249

43. Kirkbride, K. C., Ray, B. N., and Blobe, G. C. (2005) Cell-surface co-receptors: emerging roles in signaling and human disease. *Trends Biochem Sci* **30**, 611-621

44. Takahashi, T., and Strittmatter, S. M. (2001) Plexina1 autoinhibition by the plexin sema domain. *Neuron* **29**, 429-439

45. Oinuma, I., Ishikawa, Y., Katoh, H., and Negishi, M. (2004) The Semaphorin 4D receptor Plexin-B1 is a GTPase activating protein for R-Ras. *Science* **305**, 862-865

46. Wang, Y., He, H., Srivastava, N., Vikarunnessa, S., Chen, Y. B., Jiang, J., Cowan, C. W., and Zhang, X. (2012) Plexins are GTPase-activating proteins for Rap and are activated by induced dimerization. *Sci Signal* **5**, ra6

47. Driessens, M. H., Hu, H., Nobes, C. D., Self, A., Jordens, I., Goodman, C. S., and Hall, A. (2001) Plexin-B semaphorin receptors interact directly with active Rac and regulate the actin cytoskeleton by activating Rho. *Curr Biol* **11**, 339-344

48. Chen, H., He, Z., Bagri, A., and Tessier-Lavigne, M. (1998) Semaphorin-neuropilin interactions underlying sympathetic axon responses to class III semaphorins. *Neuron* **21**, 1283-1290

49. Giger, R. J., Urquhart, E. R., Gillespie, S. K., Levengood, D. V., Ginty, D. D., and Kolodkin, A. L. (1998) Neuropilin-2 is a receptor for semaphorin IV: insight into the structural basis of receptor function and specificity. *Neuron* **21**, 1079-1092

50. Takahashi, T., Nakamura, F., Jin, Z., Kalb, R. G., and Strittmatter, S. M. (1998) Semaphorins A and E act as antagonists of neuropilin-1 and agonists of neuropilin-2 receptors. *Nat Neurosci* **1**, 487-493

51. Roth, L., Nasarre, C., Dirrig-Grosch, S., Aunis, D., Cremel, G., Hubert, P., and Bagnard, D. (2008) Transmembrane domain interactions control biological functions of neuropilin-1. *Mol Biol Cell* **19**, 646-654

52. Sawma, P., Roth, L., Blanchard, C., Bagnard, D., Cremel, G., Bouveret, E., Duneau, J. P., Sturgis, J. N., and Hubert, P. (2014) Evidence for New Homotypic and Heterotypic

Interactions between Transmembrane Helices of Proteins Involved in Receptor Tyrosine Kinase and Neuropilin Signaling. *J Mol Biol* **426**, 4099-4111

53. MacKenzie, K. R., Prestegard, J. H., and Engelman, D. M. (1997) A transmembrane helix dimer: structure and implications. *Science* **276**, 131-133

54. Russ, W. P., and Engelman, D. M. (2000) The GxxxG motif: a framework for transmembrane helix-helix association. *J Mol Biol* **296**, 911-919

55. Senes, A., Gerstein, M., and Engelman, D. M. (2000) Statistical analysis of amino acid patterns in transmembrane helices: the GxxxG motif occurs frequently and in association with beta-branched residues at neighboring positions. *J Mol Biol* **296**, 921-936

56. Mueller, B. K., Subramaniam, S., and Senes, A. (2014) A frequent, GxxxG-mediated, transmembrane association motif is optimized for the formation of interhelical Calpha-H hydrogen bonds. *Proc Natl Acad Sci U S A* **111**, E888-895

57. Cismasiu, V. B., Denes, S. A., Reilander, H., Michel, H., and Szedlacsek, S. E. (2004) The MAM (meprin/A5-protein/PTPmu) domain is a homophilic binding site promoting the lateral dimerization of receptor-like protein-tyrosine phosphatase mu. *J Biol Chem* **279**, 26922-26931

58. Marchand, P., Volkmann, M., and Bond, J. S. (1996) Cysteine mutations in the MAM domain result in monomeric meprin and alter stability and activity of the proteinase. *J Biol Chem* **271**, 24236-24241

59. Aricescu, A. R., Siebold, C., Choudhuri, K., Chang, V. T., Lu, W., Davis, S. J., van der Merwe, P. A., and Jones, E. Y. (2007) Structure of a tyrosine phosphatase adhesive interaction reveals a spacer-clamp mechanism. *Science* **317**, 1217-1220

60. Aricescu, A. R., Hon, W. C., Siebold, C., Lu, W., van der Merwe, P. A., and Jones, E. Y. (2006) Molecular analysis of receptor protein tyrosine phosphatase mu-mediated cell adhesion. *EMBO J* **25**, 701-712

61. Woolfson, D. N. (2005) The design of coiled-coil structures and assemblies. *Adv Protein Chem* **70**, 79-112

Chapter 2

A Cytosolic Juxtamembrane Interface Modulates Plexin A3 Oligomerization and Signal Transduction[2a]

[2a]*The work in this chapter has been published as "A cytosolic juxtamembrane interface modulates plexin A3 oligomerization and signal transduction" by Rachael Barton, Danica Palacio, M. Kathryn Iovine, and Bryan W. Berger in* PLOS ONE*, 2015.*

Abstract

Plexins (plxns) are transmembrane (TM) receptors involved in the guidance of vascular, lymphatic vessel, and neuron growth as well as cancer metastasis. Plxn signaling results in cytosolic GTPase-activating protein activity, and previous research implicates dimerization as important for activation of plxn signaling. Purified, soluble plxn extracellular and cytosolic domains exhibit only weak homomeric interactions, suggesting a role for the plxn TM and juxtamembrane regions in homooligomerization. In this study, we consider a heptad repeat in the *Danio rerio* PlxnA3 cytosolic juxtamembrane domain (JM) for its ability to influence PlxnA3 homooligomerization in TM-domain containing constructs. Site-directed mutagenesis in conjunction with the AraTM assay and bioluminescent energy transfer ($BRET^2$) suggest an interface involving a JM heptad repeat, in particular residue M1281, regulates PlxnA3 homomeric interactions when examined in constructs containing an ectodomain, TM and JM domain. In the presence of a neuropilin-2a co-receptor and semaphorin 3F ligand, disruption to PlxnA3 homodimerization caused by an M1281F mutation is eliminated, suggesting destabilization of the PlxnA3 homodimer in the JM is not sufficient to disrupt co-receptor complex formation. In

contrast, enhanced homodimerization of PlxnA3 caused by mutation M1281L remains even in the presence of ligand semaphorin 3F and co-receptor neuropilin-2a. Consistent with this pattern of PlxnA3 dimerization in the presence of ligand and co-receptor, destabilizing mutations to PlxnA3 homodimerization (M1281F) are able to rescue motor patterning defects in *sidetracked* zebrafish embryos, whereas mutations that enhance PlxnA3 homodimerization (M1281L) are not. Collectively, our results indicate the JM heptad repeat, in particular residue M1281, forms a switchable interface that modulates both PlxnA3 homomeric interactions and signal transduction.

2.1 Introduction

Plexins (plxns) are a family of type I transmembrane (TM) receptors involved in neuronal, vascular, and lymphatic development as well as zebrafish fin regeneration in conjunction with semaphorins (semas), their ligand binding partners (1-13). Class A plxns are known to interact with the secreted class 3 semaphorins, and in this system, neuropilins (nrps) are necessary co-receptors (1-3,10,14). In the plxn-nrp-sema signaling complex, semas serve as the guidance cue, directing the plxn-nrp-expressing cell towards or away from the sema source (1-3,10,14-17). The nrp acts to join sema and plxn, dictating specificity of the sema-plxn association and initiating a signal transduction cascade to alter cell motility (1-3,8,10,14-17). Furthermore, mutations to plxns have been reported in melanomas as well as lung, breast, pancreatic, and prostate cancers, suggesting their altered signaling may play a role in cancer development (4,18). As such, understanding plxn-dependent signaling mechanisms are important both in terms of determining their role in development and disease.

The plxn structure consists of an extracellular sema domain, three plexin-semaphorin-integrin (PSI) domains, and three immunoglobulin, plexin, and transcription factor (IPT) domains, a single-spanning transmembrane domain, and a cytosolic region (CYTO) homologous

with Ras GTPase-activating proteins (GAPs) (1,3). Deletion studies have shown that the CYTO portion of plxns confers activity provided the TM domain is intact or the CYTO domain is tethered to the membrane and cross-linked in a dimeric or clustered state (19,20), indicating plxn CYTO oligomerization is important in signal transduction. In particular, overexpression of *Mus musculus* PLXNA1 (mPLXNA1) TM + CYTO in transfected cells is enough to trigger growth cone collapse without the presence of nrp co-receptor or addition of a sema ligand (19). Similarly, fusion of human PLXNB1 (hPLXNB1) CYTO to the CD2 extracellular + TM domains with the addition of cross-linker also results in cellular contraction (20). Furthermore, inducing dimerization of the CYTO domains of mPLXNA1, mPLXNA2, mPLXNA4, and mPLXNC1 enhances RapGAP activity over their monomeric counterparts (21). Overall, these results suggest that plxn CYTO dimerization is important for sema-dependent signal transduction (Figure 2.1A).

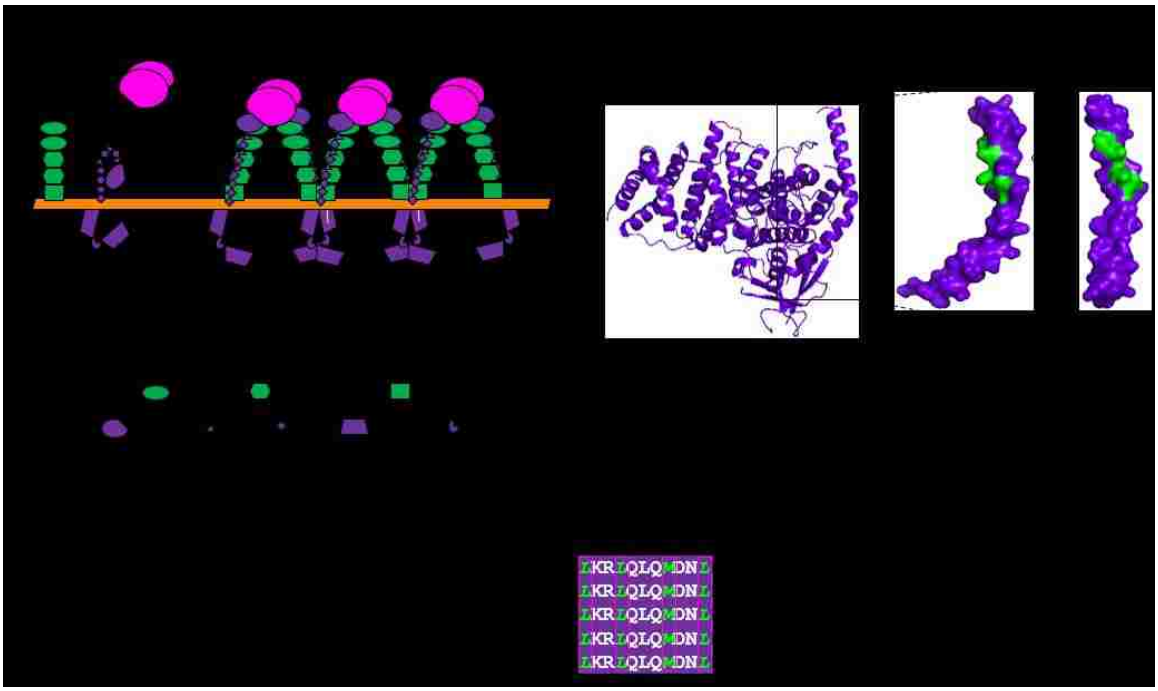

Figure 2.1. Clustering drives plexin activation. (A) Cartoon illustration indicating the relationship between plexin oligomeric state and function. (B) A cytosolic juxtamembrane heptad repeat in PlxnA3 is conserved across species and may regulate this phenomenon. (C) A crystal structure of the *Mus musculus* PLXNA3 cytosolic domain (PDB # 3IG3) with residues comprising a heptad repeat highlighted in green.

Interestingly, *in vitro* the CYTO portion of plxns are primarily monomeric, with monomer only detected by analytical ultracentrifugation for mPLXNA3 and hPLXNB1 (6,7,9). Likewise, the full-length mPLXNA2 extracellular domain also exhibits weak homomeric interactions through the extracellular membrane-proximal domains, indicating the extracellular domain may not provide a strong ligand-independent driving force for receptor homodimerization (8). A dimer of the hPLXNB1 RhoGTPase-binding domain (RBD) has been reported, though this dimer did not form in solution and crystal structures of the full-length hPLXNB1 CYTO domain suggest the contacts between loops responsible for dimerization in the RBD domain alone are replaced by intramolecular interactions (5,6). A trimeric structure for the hPLXNB1 CYTO domain has also been reported, though in solution this oligomeric state could not be confirmed, suggesting a high local concentration at the membrane may be necessary for hPLXNB1 CYTO association into dimers and trimers (9). A recent study involving the hPLXNA1 TM domain demonstrated the TM region has a weak but significant propensity to interact, putatively through alternative forms of specific GxxxG associations that depend on bilayer composition and the presence or absence of the TM domain of the hNRP1 co-receptor (15). Thus, while in some instances homomeric interactions have been identified for plxns, a unified picture of how plxn homooligomerization occurs is still an area of active research.

In this study, we consider the cytosolic juxtamembrane helix (JM) in the presence of the TM to examine its influence on the homomeric interactions of *Danio rerio* PlxnA3. Using the AraTM assay (22), we examine the TM + JM interactions in cell membranes and identify an interface containing a heptad repeat in the JM as influential to dimerization, with mutations to M1281 in the heptad repeat capable of both enhancing (M1281L) or disrupting (M1281F) PlxnA3 homodimerization. These same interactions are also observed with the full extracellular domain intact with a truncated CYTO domain in a mammalian membrane using the bioluminescence resonance energy transfer ($BRET^2$) assay. In the presence of the functionally-relevant Nrp2a co-

receptor and SEMA3F ligand (23), we find that disruption to PlxnA3 homomeric interactions via mutation M1281F can be corrected by the addition of a Nrp2a co-receptor and SEMA3F ligand such that PlxnA3 mutant M1281F homodimerizes with a signal similar to that of wild-type (WT) PlxnA3. In contrast, the PlxnA3 mutant M1281L exhibits a greater extent of homodimerization as compared to WT PlxnA3, even in the presence of Nrp2a co-receptor and SEMA3F ligand. To examine the functional effects of these mutations, we injected WT or mutant *plxna3* mRNA into the *sidetracked* (*set*) zebrafish line, which lacks membrane-anchored PlxnA3 and exhibits aberrant motor neuron patterning (24), and examined rescue of WT zebrafish motor neuron patterning. We find that alterations to PlxnA3 homomeric interactions are correlated with phenotype observed: neutral mutations in the presence of a nrp co-receptor and sema ligand (M1281F) rescue zebrafish motor neuron development, whereas mutations that result in enhanced plxn homodimerization in the presence of a nrp co-receptor and sema ligand (M1281L) do not. Collectively, our results suggest the heptad repeat interface in the JM affects PlxnA3 homooligomerization, and residue M1281 in the heptad repeat acts as a switch that modulates PlxnA3 oligomeric state and subsequent function.

2.2 Materials and Methods

This study was carried out in strict accordance with the recommendations in the Guide for the Care and Use of Laboratory Animals of the National Institutes of Health. The protocols used for this manuscript were approved by Lehigh's Institutional Animal Care and Use Committee (IACUC) (approval date 11/8/2013). Lehigh University's Animal Welfare Assurance Number is A-3877-01. All experiments were performed to minimize pain and discomfort.

2.2.1 Plasmids

A full-length WT *Danio rerio plxna3* nucleotide template (NCB Accession # AB262187.1, with a translational mutation C1090S) was provided by Dr. Michael Granato (University of Pennsylvania). This construct was subsequently cloned into pcDNA3.1/V5-His-TOPO (Invitrogen) with a C-terminal His-tag as per manufacturer's instructions. Full-length WT *Danio rerio nrp2a* (NCB Accession # BC162118, Thermo Scientific) was cloned similarly into pcDNA3.1/V5-His-TOPO with a C-terminal FLAG-tag for co-expression studies. The plasmid encoding alkaline phosphatase-tagged (AP-) *SEMA3F* was kindly provided by Dr. Roman J. Giger (University of Michigan).

For the BRET^2 assay, a truncated coding sequence for WT *plxna3* (amino acids 1-1314 of NCB Accession # BAF81998.1) was cloned into pGFP^2-N3 (BioSignal Packard) at NheI/HindIII and into pRLuc-N1 (BioSignal Packard) at XhoI/HindIII. For the AraTM assay, the coding sequence for WT *plxna3* TM + JM (amino acids 1241-1314 of NCB Accession # BAF81998.1) was cloned into pAraTM as SacI/KpnI inserts.

PlxnA3 mutants were generated using the QuikChange II Site-Directed Mutagenesis Kit (Agilent Technologies) as per manufacturer's instructions. For random mutations in pAraTM constructs, EP-PCR was performed as previously described (25).

2.2.2 AraTM Assay

AraTM measurements were performed as previously described, with the exception that cultures for AraTM measurements were grown for 16-24 hours from glycerol stocks generated from transformed cells grown in selective lysogeny broth (Lennox) medium, rather than from plates. Orientation in the membrane and level of protein expression was confirmed as previously described (Figure 2.2) (22). Results are reported in terms of the average percent change from WT

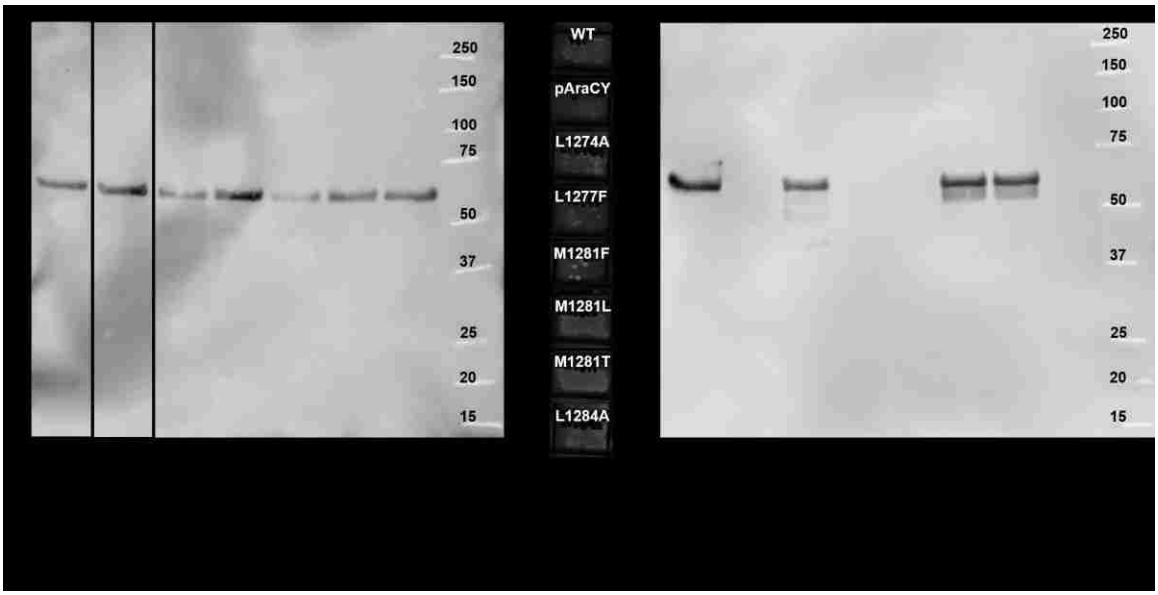

Figure 2.2. Expression and orientation of PlxnA3 TMCY AraTM constructs. (A) Anti-MBP western blot (1:10000 dilution, NEB) of PlxnA3 TMCY AraTM constructs. (B) Maltose complementation test of PlxnA3 TMCY AraTM constructs. (C) Spheroplast assay on the WT PlxnA3 TMCY AraTM construct. Ladder markings are in kDa. The expected molecular weight of PlxnA3 TMCY AraTM constructs is 67 kDa.

in slope of green fluorescent protein (GFP) fluorescence *vs.* absorbance determined from a minimum of 11 independent replicates. Standard error was determined by calculating the standard error of these samples and adding the standard error from WT to these values. Figure 2.3 illustrates a sample of non-normalized and normalized data for one round of experiments (three replicates) analyzed as previously described (22).

2.2.3 BRET^2 Assay

COS-7 cells (ATCC) were grown to 40-90% confluency and transfected at a cell density of 1 x 10^6 cells/mL in HEPES-buffered saline using 8 µg plasmid DNA per construct and the pre-set COS-7 parameters of the Bio-Rad Gene Pulser XCell. Transfections were then transferred to 2.6 mL media (for BRET^2 measurements) or 1.5 mL media (for AP-SEMA3F expression). Cultures for BRET^2 measurements were seeded in eight wells of a 96-well dish (200 µL/well) and

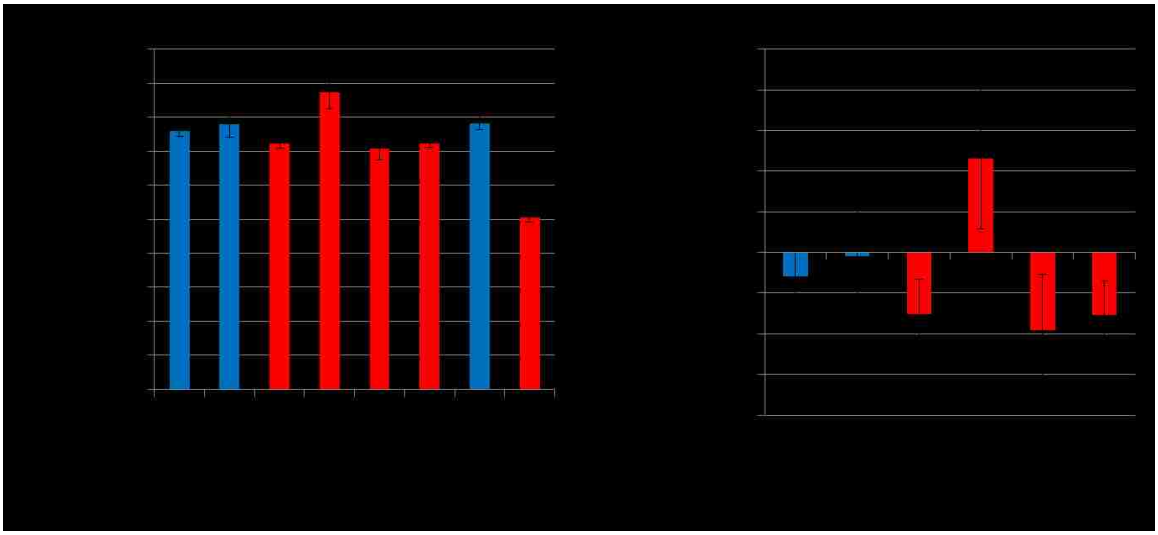

Figure 2.3. AraTM results for a three-replicate round of PlxnA3 TM + JM AraTM measurements. (A) Non-normalized average slope of fluorescence *vs.* absorbance, with error bars indicating standard error determined from three replicates. (B) Average slope of fluorescence *vs.* absorbance represented as a percent change in slope from WT, with error bars indicating standard error of the mutant construct plus standard error of the WT construct. Red bars marked with '*' indicate non-overlapping mean +/- SEM with the WT protein in each graph.

cultures for AP-SEMA3F expression consisted of six AP-SEMA3F transfections in a 100 mm dish. Proteins were allowed to grow for two days following the cultivation environment recommended by ATCC with the addition of 1% (v/v) 100X Antibiotic/Antimycotic solution (100 U/mL penicillin G, 100 µg/mL streptomycin, and 0.25 µg/mL amphotericin B) (Hyclone). Following expression, media for BRET^2 wells receiving AP-SEMA3F treatment was removed and replaced with 200 µL AP-SEMA3F expression media. Treatment occurred for a minimum of 1.5 hours at 37ºC with 5% CO_2. BRET^2 measurements proceeded as previously described using a Tecan Infinite F200 multi-well plate reader (26,27). Western blots were used to confirm similar expression levels between WT and mutant PlxnA3 BRET^2 constructs following measurements (EGFP monoclonal antibody, Clontech, and MSX Renilla Luciferase antibody, Millipore). Cell-staining confirmed expression of FLAG-tagged Nrp2a (mouse monoclonal anti-FLAG antibody, Sigma, and Alexa Fluor 546, Life Technologies), and the presence of AP-SEMA3F in the media

was confirmed by testing for AP activity via dot blot and a reaction involving 5-bromo 4-chloro 3-indolyl phosphate (Roche) and nitro blue tetrazolium (Roche) previously described (28). AP-Sema3F binding to Nrp2a- and PlxnA3-transfected cells was confirmed by testing for AP activity on parallel cultures of treated cells as previously described (Figure 2.4) (28).

For analysis, the total luminescence in each well was analyzed, and measurements were only kept for wells with total luminescence values above that of mock-transfected cells. A normalized energy transfer efficiency ratio was determined by calculating the ratio of green luminescence to magenta luminescence in a given well and dividing this value by the ratio of green luminescence to magenta luminescence for mock-transfected cells of that round of experiments. Results presented represent the average normalized energy transfer efficiency ratio determined from a minimum of three independent transfections (a total of at least 21 replicates per condition), with standard error calculated as described for the AraTM assay.

2.2.4 Zebrafish Housing and Husbandry

Zebrafish are housed in a recirculating system built by Aquatic Habitats (now Pentair). Both 3L tanks (up to 12 fish/tank) and 10 L tanks (up to 30 fish/tank) are used.

The fishroom has a 14:10 light:dark cycle and room temperature varies from 27-29°C (Westerfield, 1993 – full ref below). Water quality is automatically monitored and dosed to maintain conductivity (400-600 µS) and pH (6.95-7.30). Nitrogen levels are maintained by a biofilter. A 10 % water change occurs daily. Recirculating water is filtered sequentially through pad filters, bag filters, and a carbon canister before circulating over UV lights for sterilization. Fish are fed three times daily, once with brine shrimp (hatched from INVE artemia cysts) and twice with flake food (Aquatox AX5) supplemented with 7.5 % micropellets (Hikari), 7.5 % golden pearl (300-500 micron, Brine Shrimp direct), and 5 % cyclo-peeze (Argent).

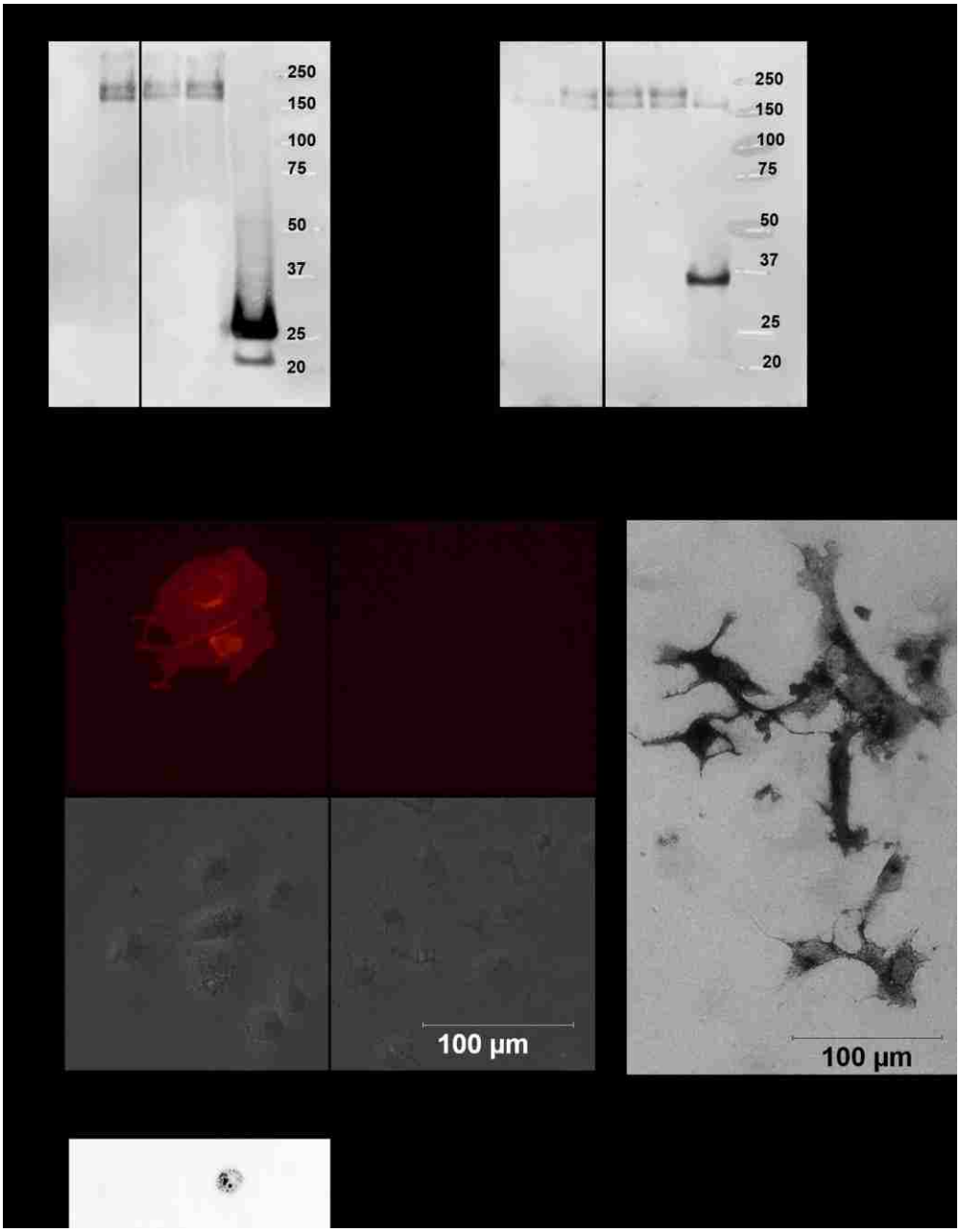

Figure 2.4. Expression of proteins in the BRET^2 assay. (A) Anti-GFP (1:1000 dilution, Clontech) western blot confirming expression of PlxnA3-GFP^2 in the BRET^2 assay. The expected molecular weights are 176 kDa and 27 kDa for PlxnA3-GFP^2 and GFP^2, respectively. (B) Anti-RLuc (1:2500 dilution, Millipore) western blot confirming expression of PlxnA3-RLuc in the BRET^2 assay. The expected molecular weights are 185 kDa and 36 kDa for PlxnA3-RLuc and RLuc, respectively. (C) Anti-FLAG staining of COS-7 cells expressing FLAG-tagged Nrp2a. No fluorescence was observed in mock-transfected cells. The scale bar in the bottom left frame is the same for all images. (D) Dot blot confirming alkaline phosphatase activity in media from cells transfected with alkaline phosphatase-tagged SEMA3F. (E) Confirmation of alkaline-phosphatase-tagged SEMA3F binding to COS-7 cells expressing Nrp2a and PlxnA3.

Heterozygous *plxna3*/+ parents were set up in breeding cages in the afternoon before gamete collection. In the morning, adult fish were lightly anesthetized with tricane methansulfonate, and embryos were obtained by collecting eggs and sperm separately prior to mixing with water. No animals were sacrificed for this study.

2.2.5 Zebrafish RNA Injections

The *set* zebrafish line and genotyping protocol were provided by Dr. Michael Granato (University of Pennsylvania) (24,29). Capped full-length *plxna3* (WT or mutant) mRNA was generated using the mMESSAGE mMACHINE T7 Transcription Kit (Ambion) according to manufacturer's instructions using the pcDNA3.1/V5-His-TOPO *plxna3* constructs linearized with XhoI. Embryos from heterozygous or homozygous *set* zebrafish intercrosses were subsequently injected with the *plxna3* mRNA at 1 µg/µL while in the single-cell stage and allowed to grow for 24 hours, at which point chorions were popped and embryos were fixed in 4% paraformaldehyde for 2 hours at room temperature or overnight at 4ºC. Methanol dehydration, collagenase treatment, and embryo staining occurred as previously described with a SV2 antibody (Developmental Studies Hybridoma Bank, University of Iowa) (24). Embryos were imaged at 20x magnification via fluorescence microscopy (Nikon Eclipse TE2000-U). In previous studies, embryos were rated as positive for the *plxna3*-knockdown (*set*) phenotype if they had two or more branched motor nerves or at least one hemisegment with two or more motor neuron exit points from the spinal cord (30). In this study, embryos were rated as positive for the *set* phenotype if they exhibited three or more clear ectopic motor neuron exit points. Following imaging, embryos were genotyped with forward primer CCCTTGCAACTGGTGTTTATA and

reverse primer AATGTGTCCTTTAGCAGTGG and a subsequent PsiI digestion that cleaved the PCR product generated from *set* DNA.

2.3 Results

2.3.1 A Juxtamembrane Helix Promotes Oligomerization of PlxnA3

The PlxnA3 JM domain contains two heptad repeats, which can result in oligomerization of α-helices driven through hydrophobic interactions by hydrophobic residues at the 'a' and 'd' positions within the heptad repeat (31-33). Leucine comprises over 30% of interfacial amino acids found in the heptad repeats of α-helical proteins (33). In the PlxnA3 JM, a heptad repeat occurs with leucines L1274, L1277, and L1284 as well as methionine M1281 (Figure 2.1B-C). While methionine is not commonly found in the core of a heptad repeat (33), previous studies have shown that methionine-containing heptad repeats can promote formation of higher-order oligomers rather than dimers in heptad-repeat containing helices (31). To determine if the heptad repeat in the JM domain influences PlxnA3 homodimerization in the context of the TM-domain-containing receptor, we utilized the AraTM assay. AraTM is a method used to characterize type I integral membrane protein dimerization in *E. coli* membranes, in which the receptor domain of interest is expressed as a fusion to a modified transcriptional activator AraC. If the receptor domains interact, they form a functional AraC dimer that activates transcription of green fluorescent protein (GFP) under control of the P_{BAD} promoter; hence, the level of GFP expression is directly proportional to dimerization (22). We expect mutations disrupting the heptad repeat through eliminating the hydrophobic leucine (L1274A, L1284A, L1277F) or introducing polar or larger side-chains instead of methionine (M1281T, M1281F) to disrupt PlxnA3 dimerization, and replacing methionine with the hydrophobic leucine (M1281L) to enhance PlxnA3 dimerization. Consistent with our prediction, we find disruption of the proposed core leucines (M1281F,

M1281T and L1284A) significantly disrupts dimerization, whereas introducing an additional leucine into the core (M1281L) enhances dimerization (Figure 2.5). Interestingly, disruptive effects are greatest for positions M1281 and L1284 in the heptad repeat, whereas mutations L1274A and L1277F have only a minor effect on dimerization. Collectively, our results indicate the heptad repeat is important for PlxnA3 TM + JM homodimerization, and specific mutations in the second heptad repeat either enhance or diminish dimerization based on their hydrophobicity.

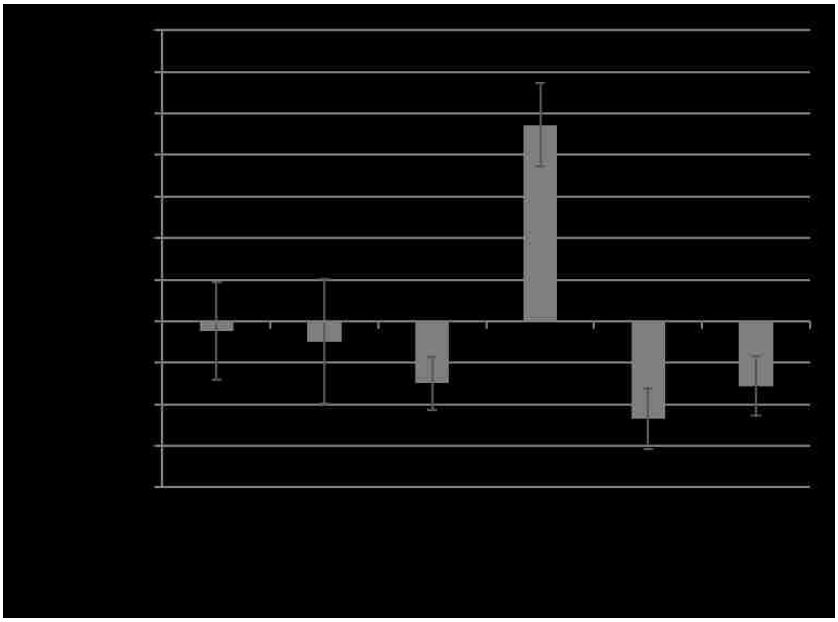

Figure 2.5. Residues in the PlxnA3 JM heptad repeat promote homomeric interactions in the AraTM assay. Residues on the JM heptad repeat interface influence TM + JM oligomerization, as determined via site-directed mutagenesis. Error bars indicate standard error as determined from a minimum of eleven replicates collected over the course of three experiments.

To further identify residues that may impact PlxnA3 TM + JM oligomerization, we performed error-prone PCR (EP-PCR) on the AraTM TM + JM construct and identified either enhancing or disruptive mutants that exhibited significant changes in GFP expression in the assay relative to WT. In particular, two mutants resulted from the EP-PCR studies which consistently enhanced homodimerization relative to wild-type: V1288F and D1302Y (Figure 2.6). Based on

the mPLXNA3 CYTO crystal structure (PDB # 3IG3) (7), both residues V1288 and D1302 lie along the same face of the JM helix as the heptad repeat (homologous residues mPLXNA3 V1268 and D1282 in PDB # 3IG3). Thus, our unbiased search using EP-PCR identified two JM mutants (V1288F and D1302Y) that also alter homodimerization. Both mutants occur on the same face of the JM helix as the heptad repeat based on the previously reported mPLXNA3 JM crystal structure (7), again consistent with a role for a specific JM interface in regulating PlxnA3 homodimerization.

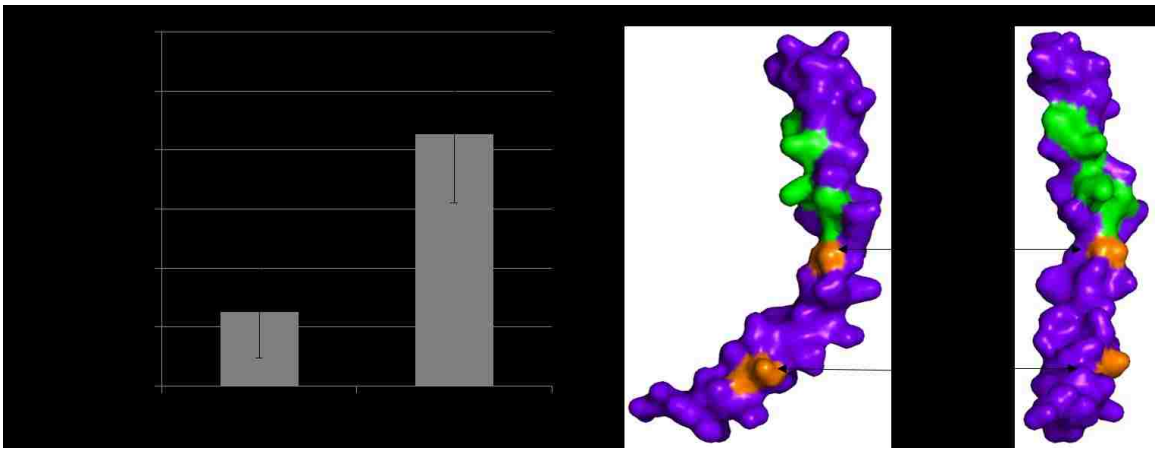

Figure 2.6. Random mutagenesis yielded additional mutants on the predicted JM interface that alter PlxnA3 homomeric interactions. (A) AraTM results for EP-PCR mutants, where error bars indicate standard error as determined from four replicates. (B) The crystal structure of the *Mus musculus* PLXNA3 cytosolic juxtamembrane domain from PDB # 3IG3 indicates the EP-PCR mutants (orange) lie on the same interface as hydrophobic residues involved in the juxtamembrane heptad repeat (green).

While we were able to identify potential mutations in the PlxnA3 TM + JM that enhance and disrupt homodimerization, it is important to confirm these effects in the context of the receptor with a full-length extracellular domain in a mammalian membrane. Thus, we introduced mutations identified in the TM + JM region in the AraTM assay and determined their effects on constructs containing the extracellular, TM and JM region (amino acids 1-1314 of NCB Accession # BAF81998.1) using the BRET^2 assay. We chose to truncate the PlxnA3 JM in the

flexible loop region following the α-helix observed in the crystal structure of PlxnA3 CYTO (PDB # 3IG3) to minimize effects of truncations on the secondary structure of the JM region. In these studies, PlxnA3 is co-expressed as an N-terminal fusion to *Renilla* luciferase (RLuc) and modified GFP (GFP^2). The RLuc-tagged PlxnA3 is capable of converting DeepBlueC to coelenteramide, which emits light at 395 nm; if a GFP^2-tagged PlxnA3 is nearby or interacting, this light excites the GFP^2 tag and light is emitted at 510 nm. The ratio of the light emitted at 510 nm to light emitted at 395 nm (the $BRET^2$ efficiency ratio) is proportional to the distance between receptors. As such, we would expect mutations disruptive to dimerization to exhibit a lower $BRET^2$ efficiency ratio than WT, and those that enhance dimerization to exhibit a higher $BRET^2$ efficiency ratio than WT (26,27). As shown in Figure 2.7A, the JM mutation M1281L enhances PlxnA3 dimerization, while mutation M1281F disrupts it. These results are in agreement with AraTM results for the PlxnA3 TM + JM (Figure 2.5), and suggest methionine M1281 acts as a switch within the JM region to regulate PlxnA3 homomeric interactions.

To better understand the role of the JM domains in PlxnA3 oligomerization in the presence of Nrp2 and SEMA3F, which are known interaction partners during neuronal development (23), we performed $BRET^2$ measurements on WT and mutant PlxnA3 constructs co-transfected with full-length Nrp2a and treated with media from AP-SEMA3F-expressing cells (34). The presence of Nrp2a and SEMA3F did not result in significant changes to homodimerization for the WT receptor, as measured by $BRET^2$ (Figure 2.7B). This suggests that if homomeric interactions of the PlxnA3 JM change upon formation of a Nrp2a-SEMA3F-PlxnA3 co-receptor complex under the investigated experimental conditions, the change does not alter net distance between neighboring PlxnA3 JM domains. However, in the presence of the Nrp2a co-receptor and SEMA3F ligand, mutant M1281F, which is disruptive for homodimerization of PlxnA3 in the absence of Nrp2a and SEMA3F (Figure 2.7A), exhibits increased levels of PlxnA3 homodimerization, with a $BRET^2$ signal similar to that of WT PlxnA3

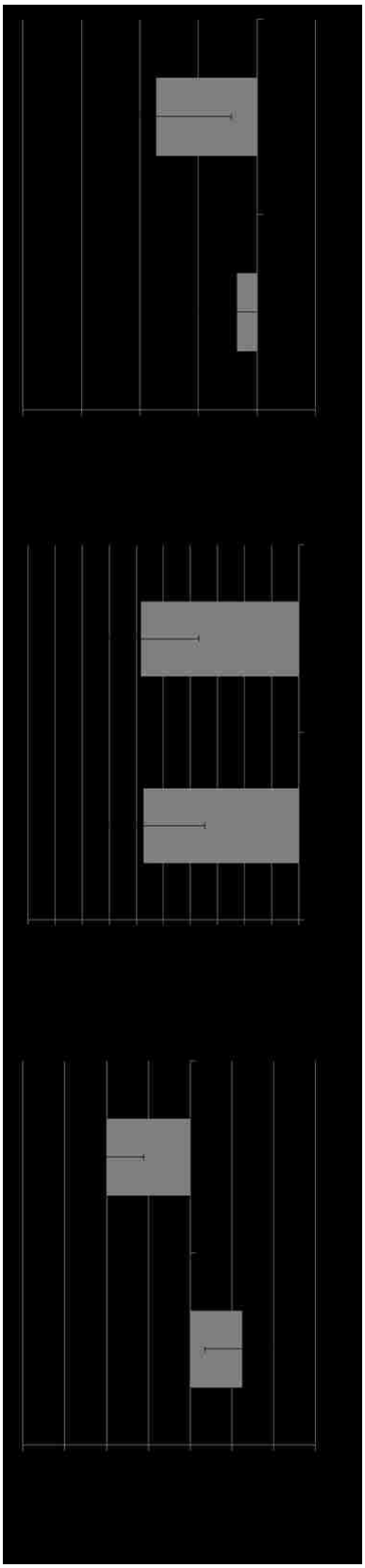

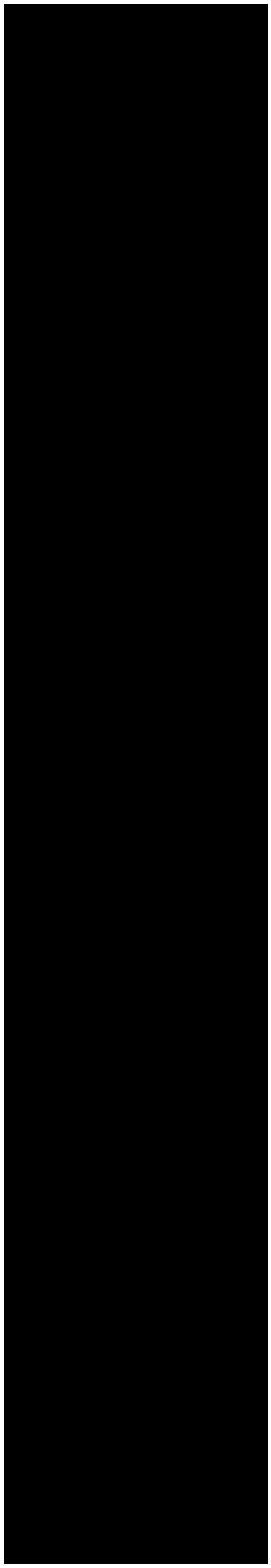

(Figure 2.7C). Therefore, we conclude co-receptor complex formation promotes PlxnA3 homodimerization independent of disruptive PlxnA3 JM domain mutations such as M1281F. However, mutant M1281L increases PlxnA3 homodimerization independent of whether Nrp2a and SEMA3F are present (Figure 2.7A). As such, PlxnA3 homodimerization is influenced by both intrinsic (the heptad repeat within the JM) as well as extrinsic (Nrp2a, SEMA3F) factors, with mutations in the JM region that enhance plxn homodimerization insensitive to the presence of Nrp2a and SEMA3F.

2.3.2 A Juxtamembrane Heptad Repeat Influences PlxnA3 Function in Zebrafish Motor Neuron Development

In zebrafish neuronal development, PlxnA3 acts as a negative guidance receptor. Expression of intact PlxnA3 guides motor axons to exit the spinal cord at midsegments and grow rostrally (24,30). The *set* zebrafish line is a transgenic line in which a mutation in the *plxna3* gene results in a truncated form of the receptor incapable of signaling. As such, motor neurons in homozygous *set* mutants exit the spinal cord at ectopic locations and branch (Figure 2.8) (24). To examine if mutations to the PlxnA3 JM affecting homodimerization also affect function, we used the *set* zebrafish line in conjunction with RNA injections of WT or mutant *plxna3* and examined embryos for ectopic exit points (24).

Our results indicate that injection of WT *plxna3* RNA at the single-cell stage of homozygous *set* zebrafish embryos rescues the phenotype of WT zebrafish (i.e. only 36% of *set* embryos injected with WT RNA exhibit ectopic exit points, compared to 80% of uninjected embryos, $p<0.005$ by Fisher's Exact Test, FET) (Table 2.1). Injection of *plxna3* mutant M1281F also rescues the motor neuron patterning of WT zebrafish embryos (i.e. only 33% of M1281F RNA-injected embryos exhibit ectopic exit points, $p<0.005$ compared to uninjected by FET). In contrast, injection of *plxna3* mutant M1281L RNA, however, failed to rescue motor neuron

patterning of the *set* embryos (i.e. 50% of *set* embryos injected with M1281L RNA exhibit ectopic exit points, p=0.07 compared to uninjected by FET). These results are consistent with PlxnA3 homodimerization results in the presence of the Nrp2a co-receptor and SEMA3F ligand, in which the disruptive mutant M1281F in the absence of Nrp2a-SEMA3F was capable of homodimerization similar to WT in the presence of Nrp2a-SEMA3F, whereas mutant M1281L exhibited a greater extent of homodimerization independent of Nrp2a-SEMA3F (Figure 2.7C). Hence, our results suggest an interface containing a heptad repeat in the PlxnA3 cytosolic juxtamembrane, and in particular residue M1281, influences PlxnA3 homooligomerization and subsequent function (Figure 2.1). Importantly, our results suggest that promoting PlxnA3 CYTO homomeric interactions, as with mutation M1281L, does not necessarily enhance function, and that a specific conformation within a given oligomeric state is necessary for PlxnA3 function; in this study, the homomeric interactions and oligomeric state formed by the WT and M1281F PlxnA3 are preferred for nrp-plxn-sema signal transduction over the dimeric M1281L PlxnA3 receptor.

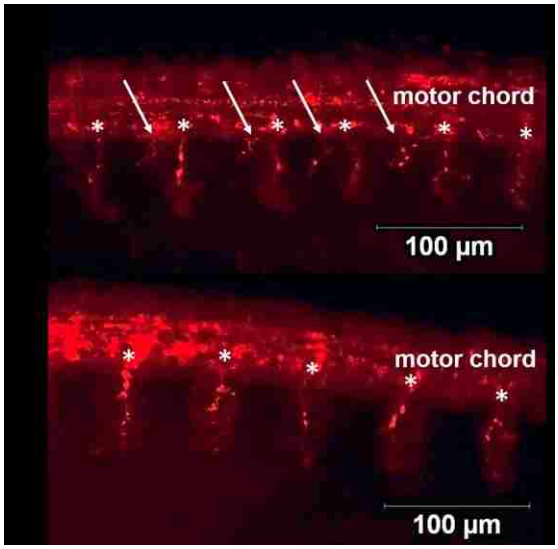

Figure 2.8. Knockdown of *plxna3* results in aberrant motor neuron patterns. The motor neurons of 24 hour post fertilization *sidetracked* zebrafish embryos (top) exhibit ectopic motor neuron exit points from the motor cord (arrows) compared to WT embryos (bottom). Asterisks indicate endogenous motor neuron exit points. Embryos are oriented anterior (left) to posterior (right).

Table 2.1. Percentage of Embryos Exhibiting s*idetracked* Phenotype[2b]

Type of Injection	Number of Embryos Examined	Percentage of Embryos Exhibiting s*idetracked* Phenotype	P-value Compared to Uninjected
Uninjected	30	80	1
WT *plxna3* RNA	22	36	0.003
M1281F *plxna3* RNA	12	33	0.009
M1281L *plxna3* RNA	12	50	0.07

[2b]*P-values were determined using Fisher's Exact Test.*

2.4 Discussion

Previous studies suggest plxn clustering is necessary for activation, though purified extracellular and cytosolic domains exhibit only weak tendencies toward homooligomerization (6,7,9,19-21). Here, we demonstrate that mutations to the JM heptad repeat interface affect PlxnA3 TM + JM homodimerization (Figures 2.5 and 2.6), with residue M1281 acting as a switch to either enhance (M1281L) or disrupt (M1281F) PlxnA3 homodimerization (Figures 2.5 and 2.7). While the addition of Nrp2a and SEMA3F did not affect WT PlxnA3 homodimerization, disruption of PlxnA3 homodimerization via mutation M1281F was corrected in the presence of both ligand and co-receptor (Figure 2.7), and was also able to rescue zebrafish motor neuron patterning in *set* embryos (Figure 2.8 and Table 2.1). In contrast, enhancement of PlxnA3 homodimerization through mutation M1281L was not influenced by the presence of Nrp2a and SEMA3F, and was unable to rescue WT zebrafish motor neuron patterning in *set* embryos (Figure 2.8 and Table 2.1). Thus, M1281 and the associated JM heptad repeat (residues 1281-1287) acts as a switch to regulate the extent of PlxnA3 homodimerization and suggest that interactions promoting weak, but specific, oligomerization of the PlxnA3 JM region are preferred for Nrp2a-PlxnA3-SEMA3F signal transduction versus interactions that enhance PlxnA3 homodimerization at the expense of flexibility in homodimerization during nrp-sema co-receptor formation. In this sense, the JM interface required for PlxnA3 signaling resembles the type of

interface required for stabilization of integrin heterodimers, in which a weak, but specific, transmembrane interface was required for switchability between active and inactive states to regulate signal transduction (35). Given that class A plxns are capable of forming multiple parings with cognate nrp co-receptors and sema ligands (for instance, PLXNA3 participates in NRP1-SEMA3A interactions as well as NRP2-SEMA3F interactions) (3), the additional flexibility in switching between monomer and homooligomeric states for plxns may reflect the necessity of maintaining the flexibility required for proper co-receptor complex formation and subsequent signal transduction.

Previous analyses of the plxn JM region also indicate that switchable interactions involving the heptad repeat region are important for signal transduction. For mPLXNA3, the crystal structure of the cytosolic domain suggests the C-terminal portion of the JM (residues subsequent to L1280 in mPLXNA3, or homologous with residue L1310 in the *Danio rerio* PlxnA3 utilized in this study) makes extensive contacts with the mPLXNA3 GAP domain and mutations to the JM region disrupt function (7). When including the TM domain of PlxnA3 in the current study, we also find that residues more proximal to the TM influence homodimerization (Figures 2.5, 2.6, and 2.7), and in particular mutations at residue M1281 can enhance or disrupt PlxnA3 homodimerization (Figures 2.5 and 2.7). The effects of the M1281 mutation on PlxnA3 function described in this study (Table 2.1) are also consistent with previous functional analyses of the analogous region in mPLXNA3 and *Drosophila* plxnA (M1261R in mPLXNA3 and M1320R in *Drosophila* plxnA), in which mutants fail to induce growth cone collapse in a PLXNA3-NRP2-SEMA3F growth cone collapse model and exhibit only partial function in a *Drosophila* axon guidance assay (7). While the effects of arginine mutations on dimerization in these studies is unknown, we do find that mutations which alter the hydrophobicity of the heptad repeat can either enhance (M1281L) or disrupt (M1281F) dimerization, and for M1281L, impair PlxnA3 signaling. Thus, our results indicate a specific oligomeric state and conformation are

required for PlxnA3 signal transduction, and the conformation of the activated state requires specific interactions in the heptad repeat of PlxnA3. Conservation of methionine within the heptad repeat of the PlxnA3 JM, and its ability to act as an oligomeric switch, may also reflect its role in creating an oligomeric interface permissive to higher order oligomers versus dimers, thereby providing the flexibility to create a specific interface for signal transduction with switchable interactions.

In summary, our AraTM and BRET^2 results suggest a specific interface of the PlxnA3 JM domain promotes oligomerization in the context of a membrane-anchored receptor. Mutation to residue M1281 in *Danio rerio* PlxnA3 in particular can enhance or disrupt PlxnA3 homooligomerization, dependent upon type of mutation made (Figures 2.5 and 2.7). Such interaction likely contributes to plxn clustering and subsequent activation (Figure 2.1). Our BRET^2 co-receptor studies suggest Nrp2a and SEMA3F serve to promote PlxnA3 homodimerization for the disruptive mutant M1281F, but not for the dimer-enhancing mutant M1281L. The altered oligomeric state of M1281L in the presence of Nrp2a and SEMA3F correlates with PlxnA3 signaling, in which injection of M1281L mRNA into *set* zebrafish embryos failed to rescue WT motor neuron patterning. As such, residue M1281 regulates PlxnA3 homomeric interactions and subsequent function, suggesting the JM region of plxn forms a specific interface required for signal transduction.

2.5 References

1. Tamagnone, L., Artigiani, S., Chen, H., He, Z., Ming, G. I., Song, H., Chedotal, A., Winberg, M. L., Goodman, C. S., Poo, M., Tessier-Lavigne, M., and Comoglio, P. M. (1999) Plexins are a large family of receptors for transmembrane, secreted, and GPI-anchored semaphorins in vertebrates. *Cell* **99**, 71-80

2. Takahashi, T., Fournier, A., Nakamura, F., Wang, L. H., Murakami, Y., Kalb, R. G., Fujisawa, H., and Strittmatter, S. M. (1999) Plexin-neuropilin-1 complexes form functional semaphorin-3A receptors. *Cell* **99**, 59-69

3. Kruger, R. P., Aurandt, J., and Guan, K. L. (2005) Semaphorins command cells to move. *Nat Rev Mol Cell Biol* **6**, 789-800

4. Wong, O. G., Nitkunan, T., Oinuma, I., Zhou, C., Blanc, V., Brown, R. S., Bott, S. R., Nariculam, J., Box, G., Munson, P., Constantinou, J., Feneley, M. R., Klocker, H., Eccles, S. A., Negishi, M., Freeman, A., Masters, J. R., and Williamson, M. (2007) Plexin-B1 mutations in prostate cancer. *Proc Natl Acad Sci U S A* **104**, 19040-19045

5. Tong, Y., Chugha, P., Hota, P. K., Alviani, R. S., Li, M., Tempel, W., Shen, L., Park, H. W., and Buck, M. (2007) Binding of Rac1, Rnd1, and RhoD to a novel Rho GTPase interaction motif destabilizes dimerization of the plexin-B1 effector domain. *J Biol Chem* **282**, 37215-37224

6. Tong, Y., Hota, P. K., Penachioni, J. Y., Hamaneh, M. B., Kim, S., Alviani, R. S., Shen, L., He, H., Tempel, W., Tamagnone, L., Park, H. W., and Buck, M. (2009) Structure and function of the intracellular region of the plexin-b1 transmembrane receptor. *J Biol Chem* **284**, 35962-35972

7. He, H., Yang, T., Terman, J. R., and Zhang, X. (2009) Crystal structure of the plexin A3 intracellular region reveals an autoinhibited conformation through active site sequestration. *Proc Natl Acad Sci U S A* **106**, 15610-15615

8. Janssen, B. J., Robinson, R. A., Perez-Branguli, F., Bell, C. H., Mitchell, K. J., Siebold, C., and Jones, E. Y. (2010) Structural basis of semaphorin-plexin signalling. *Nature* **467**, 1118-1122

9. Bell, C. H., Aricescu, A. R., Jones, E. Y., and Siebold, C. (2011) A dual binding mode for RhoGTPases in plexin signalling. *PLoS Biol* **9**, e1001134

10. Janssen, B. J., Malinauskas, T., Weir, G. A., Cader, M. Z., Siebold, C., and Jones, E. Y. (2012) Neuropilins lock secreted semaphorins onto plexins in a ternary signaling complex. *Nat Struct Mol Biol* **19**, 1293-1299

11. Wang, Y., Pascoe, H. G., Brautigam, C. A., He, H., and Zhang, X. (2013) Structural basis for activation and non-canonical catalysis of the Rap GTPase activating protein domain of plexin. *Elife* **2**, e01279

12. Roney, K., Holl, E., and Ting, J. (2013) Immune plexins and semaphorins: old proteins, new immune functions. *Protein Cell* **4**, 17-26

13. Ton, Q. V., and Kathryn Iovine, M. (2012) Semaphorin3d mediates Cx43-dependent phenotypes during fin regeneration. *Dev Biol* **366**, 195-203

14. Zanata, S. M., Hovatta, I., Rohm, B., and Puschel, A. W. (2002) Antagonistic effects of Rnd1 and RhoD GTPases regulate receptor activity in Semaphorin 3A-induced cytoskeletal collapse. *J Neurosci* **22**, 471-477

15. Aci-Seche, S., Sawma, P., Hubert, P., Sturgis, J. N., Bagnard, D., Jacob, L., Genest, M., and Garnier, N. (2014) Transmembrane recognition of the semaphorin co-receptors neuropilin 1 and plexin A1: coarse-grained simulations. *PLoS One* **9**, e97779

16. Rohm, B., Rahim, B., Kleiber, B., Hovatta, I., and Puschel, A. W. (2000) The semaphorin 3A receptor may directly regulate the activity of small GTPases. *FEBS Lett* **486**, 68-72

17. Negishi, M., Oinuma, I., and Katoh, H. (2005) Plexins: axon guidance and signal transduction. *Cell Mol Life Sci* **62**, 1363-1371

18. Balakrishnan, A., Penachioni, J. Y., Lamba, S., Bleeker, F. E., Zanon, C., Rodolfo, M., Vallacchi, V., Scarpa, A., Felicioni, L., Buck, M., Marchetti, A., Comoglio, P. M., Bardelli, A., and Tamagnone, L. (2009) Molecular profiling of the "plexinome" in melanoma and pancreatic cancer. *Hum Mutat* **30**, 1167-1174

19. Takahashi, T., and Strittmatter, S. M. (2001) Plexina1 autoinhibition by the plexin sema domain. *Neuron* **29**, 429-439

20. Driessens, M. H., Hu, H., Nobes, C. D., Self, A., Jordens, I., Goodman, C. S., and Hall, A. (2001) Plexin-B semaphorin receptors interact directly with active Rac and regulate the actin cytoskeleton by activating Rho. *Curr Biol* **11**, 339-344

21. Wang, Y., He, H., Srivastava, N., Vikarunnessa, S., Chen, Y. B., Jiang, J., Cowan, C. W., and Zhang, X. (2012) Plexins are GTPase-activating proteins for Rap and are activated by induced dimerization. *Sci Signal* **5**, ra6

22. Su, P. C., and Berger, B. W. (2012) Identifying key juxtamembrane interactions in cell membranes using AraC-based transcriptional reporter assay (AraTM). *J Biol Chem* **287**, 31515-31526

23. Xiang, X., Zhang, X., and Huang, Q. L. (2012) Plexin A3 is involved in semaphorin 3F-mediated oligodendrocyte precursor cell migration. *Neurosci Lett* **530**, 127-132

24. Palaisa, K. A., and Granato, M. (2007) Analysis of zebrafish sidetracked mutants reveals a novel role for Plexin A3 in intraspinal motor axon guidance. *Development* **134**, 3251-3257

25. Cirino, P. C., Mayer, K. M., and Umeno, D. (2003) Generating Mutant Libraries Using Error-Prone PCR. in *Directed Evolution Library Creation: Methods and Protocols* (Arnold, F. H., and Georgiou, G. eds.), Humana Press Inc., Totowa, NJ. pp 3-9

26. Carriba, P., Navarro, G., Ciruela, F., Ferre, S., Casado, V., Agnati, L., Cortes, A., Mallol, J., Fuxe, K., Canela, E. I., Lluis, C., and Franco, R. (2008) Detection of heteromerization of more than two proteins by sequential BRET-FRET. *Nat Methods* **5**, 727-733

27. Pfleger, K. D., Seeber, R. M., and Eidne, K. A. (2006) Bioluminescence resonance energy transfer (BRET) for the real-time detection of protein-protein interactions. *Nat Protoc* **1**, 337-345

28. Cheng, H. J., and Flanagan, J. G. (1994) Identification and cloning of ELF-1, a developmentally expressed ligand for the Mek4 and Sek receptor tyrosine kinases. *Cell* **79**, 157-168

29. Birely, J., Schneider, V. A., Santana, E., Dosch, R., Wagner, D. S., Mullins, M. C., and Granato, M. (2005) Genetic screens for genes controlling motor nerve-muscle development and interactions. *Dev Biol* **280**, 162-176

30. Feldner, J., Reimer, M. M., Schweitzer, J., Wendik, B., Meyer, D., Becker, T., and Becker, C. G. (2007) PlexinA3 restricts spinal exit points and branching of trunk motor nerves in embryonic zebrafish. *J Neurosci* **27**, 4978-4983

31. Woolfson, D. N. (2005) The design of coiled-coil structures and assemblies. *Adv Protein Chem* **70**, 79-112

32. Grigoryan, G., and Keating, A. E. (2008) Structural specificity in coiled-coil interactions. *Curr Opin Struct Biol* **18**, 477-483

33. Cohen, C., and Parry, D. A. (1990) Alpha-helical coiled coils and bundles: how to design an alpha-helical protein. *Proteins* **7**, 1-15

34. Takahashi, T., Nakamura, F., Jin, Z., Kalb, R. G., and Strittmatter, S. M. (1998) Semaphorins A and E act as antagonists of neuropilin-1 and agonists of neuropilin-2 receptors. *Nat Neurosci* **1**, 487-493

35. Berger, B. W., Kulp, D. W., Span, L. M., DeGrado, J. L., Billings, P. C., Senes, A., Bennett, J. S., and DeGrado, W. F. (2010) Consensus motif for integrin transmembrane helix association. *Proc Natl Acad Sci U S A* **107**, 703-708

Chapter 3

Interplay of Specific Trans- and Juxtamembrane Interfaces in PlexinA3 Dimerization and Signal Transduction[3a]

[3a]*The work in this chapter has been submitted for publication.*

Abstract

Plexins are transmembrane proteins that serve as guidance receptors during angiogenesis, lymphangiogenesis, neuronal development, and zebrafish fin regeneration with a putative role in cancer metastasis. Receptor dimerization or clustering, induced through extracellular ligand binding but modulated in part by the plexin transmembrane (TM) and juxtamembrane (JM) domains, is thought to drive plexin activity. Previous studies indicate that isolated plexin TM domains interact through a conserved, small-x_3-small packing motif, and the cytosolic JM region interacts through a hydrophobic heptad repeat, but the roles and interplay of these regions in plexin signal transduction remains unclear. In this study, we find disruption of the small-x_3-small motifs in the *Danio rerio* PlexinA3 TM domain enhances dimerization of the TM-JM domain in the AraTM assay by enhancing JM-mediated dimerization, whereas mutations to the cytosolic JM heptad repeat that disrupt dimerization do so even in the presence of TM domain mutations. However, mutations to the small-x_3-small TM interfaces also disrupt PlexinA3 signaling in a zebrafish axonal guidance assay, indicating the importance of this TM interface in signal transduction. Collectively, our results demonstrate that multiple TM and JM interfaces exist in

the PlexinA3 homodimer, and these interfaces independently regulate dimerization important in PlexinA3 signal transduction.

3.1 Introduction

Plexins (plxns) are a group of Type I transmembrane (TM) receptors involved in the guidance of neurons, vascular, and lymphatic vessels during development as well as zebrafish fin regeneration (1-7). Plxns also serve a putative role in cancer metastasis, with altered expression levels or mutations to plxns observed in melanomas and breast, lung, pancreatic, and prostate cancers (8-11). Investigations with plxns' semaphorin (sema) ligands and neuropilin (nrp) co-receptors have also implicated the plxn-nrp-sema pathway as influential to cancer metastasis, with overexpression of SEMA3F inhibiting cancer metastasis in a mouse melanoma model (4,11). As such, understanding the mechanisms necessary for activation of the plxn-nrp-sema signaling pathway may provide insight into design of novel therapeutics as well as their role in a myriad of developmental processes.

Plxns contain an extracellular domain involved in ligand binding, a glycine-rich single-spanning TM domain, and a cytosolic domain (CYTO) involved in signal transduction (1,2,4,12,13). Activity is characterized by CYTO GTPase-activating protein (GAP) activity (3,14-16). An early immunohistological observation that NRP1 and PLXNA1 cluster in regions of high local concentration upon SEMA3A addition in a chick dorsal root ganglion collapse assay led to the premise that receptor dimerization or clustering confers activity (2). Indeed, a RapGAP activity assay on purified CYTO domains of *Mus musculus* PLXNA1, PLXNA2, PLXNA4, and PLXNC1 CYTO suggests plxn CYTO domains dimerized through N-terminal fusions exhibit enhanced activity over the monomeric CYTO domains (16).

Purified murine PLXNA2 extracellular domains and murine PLXNA1, PLXNA3, and human PLXNB1 CYTO domains exhibit only weak homomeric tendencies in solution, however (5,14-17). Removal of the *Mus musculus* PLXNA1 sema-binding domain or extracellular domain confers sema- and nrp-independent collapse activity in a COS-7 growth cone model, indicating PLXNA1 exists in an autoinhibited conformation, and that in the absence of the sema-binding domain, the PLXNA1 TM-CYTO is sufficient for receptor activation (12). Expression of the mouse PLXNA1 CYTO domain alone or with a myristoylation signal fails to induce collapse, though replacement of the human PLXNB1 TM domain with a membrane-anchored CD2 fusion followed by cross-linking enables cellular contraction (12,18,19). As such, membrane-anchored plxn clustering is important for activity, and the TM and juxtamembrane (JM) regions exhibit an inherent tendency to promote plxn homooligomerization (Figure 3.1A).

Previous studies indicate a heptad repeat in the CYTO JM region modulates homomeric interactions in the full-length receptor, with mutations to the JM of *Drosophila* PLXNA and *Danio rerio* PlxnA3 only showing partial activity in axonal guidance assays (14,20). Additionally, the human PLXNA1 TM domain alone exhibits a weak tendency to dimerize in a bacterial adenylate cyclase two-hybrid assay (13,21). Coarse-grained molecular dynamics simulations of the isolated human PLXNA1 TM domain suggest a glycine-rich segment in the TM region largely conserved across Class A plxns may modulate human PLXNA1 homomeric interactions (Figure 3.1B) (13). In particular, this conserved glycine-rich region contains two motifs capable of packing via small-x_3-small interfaces (13). The small-x_3-small motif is a highly conserved sequence-structure motif overrepresented in a wide range of helical TM protein dimers such as glycophorin A and the plxn co-receptor NRP1, in which small residues such as glycine, serine or alanine are placed along one face of the TM helix, creating a specific, ridge-and-groove packing structure that contributes to dimer stability (21-23). A similar series of interfaces is also

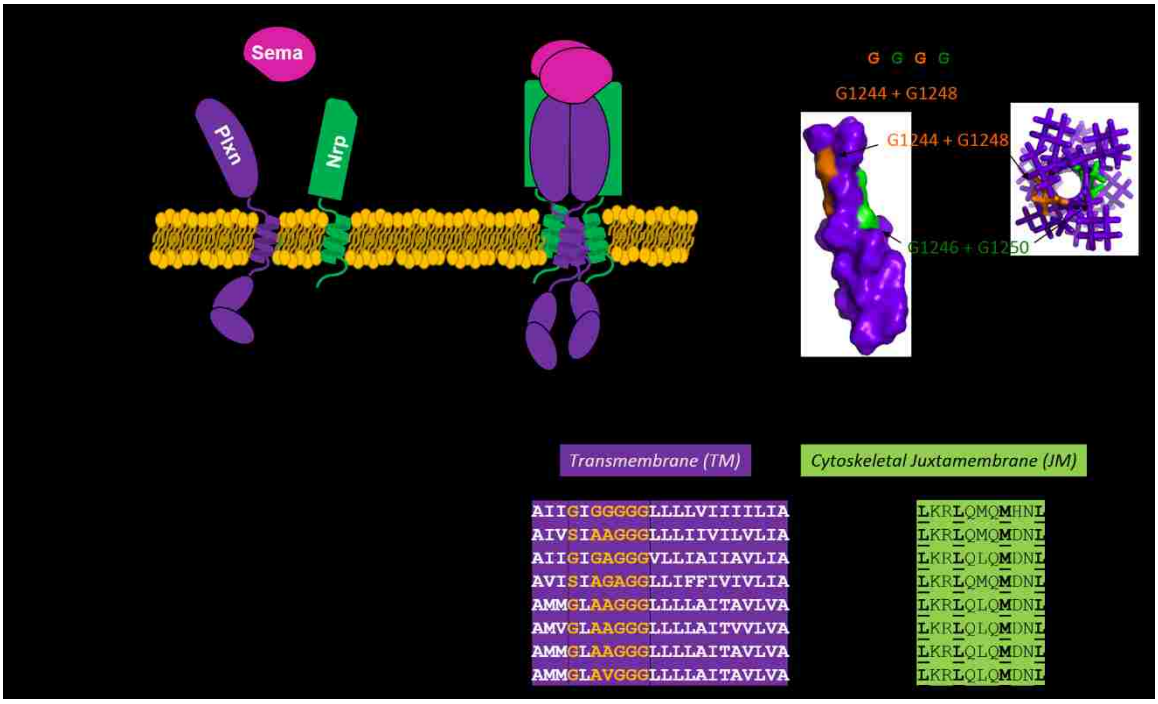

Figure 3.1. Plexin transmembrane and juxtamembrane domains contribute to receptor clustering and activation. (A) Extracellular binding of a semaphorin ligand (Sema) to plexin (Plxn) and neuropilin (Nrp) leads to receptor clustering and activation. (B) A small amino acid-rich region in the transmembrane domain and a cytosolic juxtamembrane heptad repeat are conserved across class A plexins and postulated to modulate homooligomerization. (C) Primary sequence analysis of the glycine-rich *Danio rerio* PlexinA3 transmembrane domain reveals two interfaces capable of participating in small-x_3-small packing motifs. Structural representation of the PlexinA3 transmembrane domain was generated using the asymmetric E_z-*3D* Potential Finder.

present in the *Danio rerio* PlxnA3 TM domain (Figure 3.1C), suggestive of a role in dimerization. However, the relative importance of TM versus JM and interrelationship between TM and JM interactions in PlxnA3 dimerization and signal transduction remain open questions.

In this study, we examine the role of the glycine-rich region of the *Danio rerio* PlxnA3 TM domain on homodimerization and the interplay of TM and JM interactions in PlxnA3 dimerization and signal transduction. Interestingly, we find disruption of the small-x_3-small TM packing motifs through glycine-to-leucine mutations enhances, rather than diminishes,

dimerization of the TM-JM domain. Similarly, extension of the small-x_3-small interfaces through introduction of additional on-interface glycines disrupts, rather than enhances, dimerization. However, mutations to the JM heptad repeat that enhance or diminish dimerization do so even in the presence of TM domain small-x_3-small mutations, suggesting the TM dimer interface is distinct from that of the JM, and the two work in opposition to one another; in other words, the TM small-x_3-small interfaces inhibit JM-mediated TM-JM dimerization. In a zebrafish axonal guidance assay using *sidetracked* (*set*) zebrafish embryos, which exhibit ectopic motor neuron exit points due to a truncation in the *plxnA3* gene (24,25), mutations to the small-x_3-small interfaces result in non-functional (mutation G1246L+G1250L) or only partially functional (mutation G1244L+G1248L) PlxnA3. Collectively, our results demonstrate multiple distinct, functionally important interfaces exist in the PlxnA3 receptor TM and JM that regulate PlxnA3 signaling.

3.2 Materials and Methods

3.2.1 Modelling

A model of the *Danio rerio* PlxnA3 transmembrane domain (amino acids 1241-1262 of NCB Accession # BAF81998.1) (Figure 3.1C) was generated using the asymmetric *E_z-3D* Potential Finder (26).

3.2.2 Plasmids

Cloning for full-length wild-type (WT) *Danio rerio plxnA3* in pcDNA3.1/V5-His-TOPO and the *plxnA3* TM-JM domains (amino acids 1241-1314 of NCB Accession # BAF81998.1) in pAraTM was previously described (20). Mutations were made using the QuikChange II Site-Directed Mutagenesis Kit (Agilent).

3.2.3 AraTM Assay

AraTM measurements and analyses were performed as previously described (20,27). Briefly, electrically-competent SB1676 cells were co-transformed with pAraGFP and the pAraTM construct of interest via electroporation. The transformed cells were grown in selective lysogeny broth (Lennox) medium (LB) overnight, and glycerol stocks were made from the cultures. Cultures for measurements (four per experimental round) were started from these glycerol stocks and allowed to grow 16-24 hours in selective LB, at which time fluorescence (485 nm excitation, 530 nm emission) and absorbance (560 nm) measurements were taken for each culture (and 5-fold serial dilutions of each culture) using a Tecan Infinite F200 multi-well plate reader. Results are reported as the average percent change in slope of fluorescence *vs.* absorbance from WT from three rounds of experiments, with error bars indicating the standard error of the samples plus the standard error of WT samples analyzed in parallel. Expression and orientation in the membrane were confirmed by western blotting and maltose complementation tests, respectively (Figure 3.2).

3.2.4 Zebrafish Care and Embryo Injections

The *set* zebrafish line, provided by Dr. Michael Granato (University of Pennsylvania) was used for this study (24,25). Care for parental zebrafish was previously described (20). Husbandry occurred between adult heterozygous or homozygous *plxna3*/+ zebrafish. This study did not require animal sacrifice. Generation of mutant *plxnA3* RNA, injection into embryos, embryo processing (fixation, staining, imaging, and genotyping), and *set* phenotype classification requirements were as previously described (20). We used previously reported values for occurrence of the *set* phenotype with WT *plxnA3* RNA injections or uninjected *set* zebrafish embryos (20) for our statistical analyses.

250
150
100
75
50
37
25

3.3 Results

3.3.1 Transmembrane Glycines Modulate PlxnA3 Homodimerization

The *Danio rerio* PlxnA3 TM domain contains a glycine-rich region (G_{1244}IGAGGG_{1250}, Figure 3.1C) with two putative interfaces capable of promoting homodimerization via small-x_3-small packing motifs (G1244+G1248 and G1246+G1250). Previous coarse-grained molecular dynamics simulations implied the homologous interfaces in the human PLXNA1 TM domain contribute to dimerization of the isolated TM domain (13). To investigate the role of TM glycines on PlxnA3 TM-JM homodimerization, we employed site-directed mutagenesis in conjunction with the AraTM assay (27). In this assay, the TM domain of interest is expressed as an AraC fusion. Dimerization induced by TM homomeric interactions forms a functional AraC transcription factor, which in turn drives transcription of green fluorescent protein (GFP) regulated by a P_{BAD} promoter. Hence, AraTM cultures expressing TM domains with a stronger propensity to dimerize will exhibit an increased GFP signal over weaker dimer constructs for the same cell density (27).

Our AraTM results illustrate that glycine-to-leucine mutations disrupting the small-x_3-small packing interfaces in the glycine-rich PlxnA3 TM domain actually enhance TM-JM dimerization, either as single point-mutations to a given interface (G1244L, G1246L, G1248L, G1250L; Figure 3.3A), double mutations to eliminate an interface (G1244L+G1248L, G1246L+G1250L; Figure 3.3B) or triple mutations to disrupt both small-x_3-small interfaces (G1244L+G1246L+G1250L and G1246L+G1248L+G1250L; Figure 3.3B). Furthermore, extension of the small-x_3-small motif by placing additional glycines on either interface (L1252G, I1254G) disrupts, rather than enhances, TM-JM dimerization (Figure 3.3A). Collectively, our results indicate small-x_3-small interfaces in the PlxnA3 TM domain negatively regulate TM-JM dimerization (Figure 3.1).

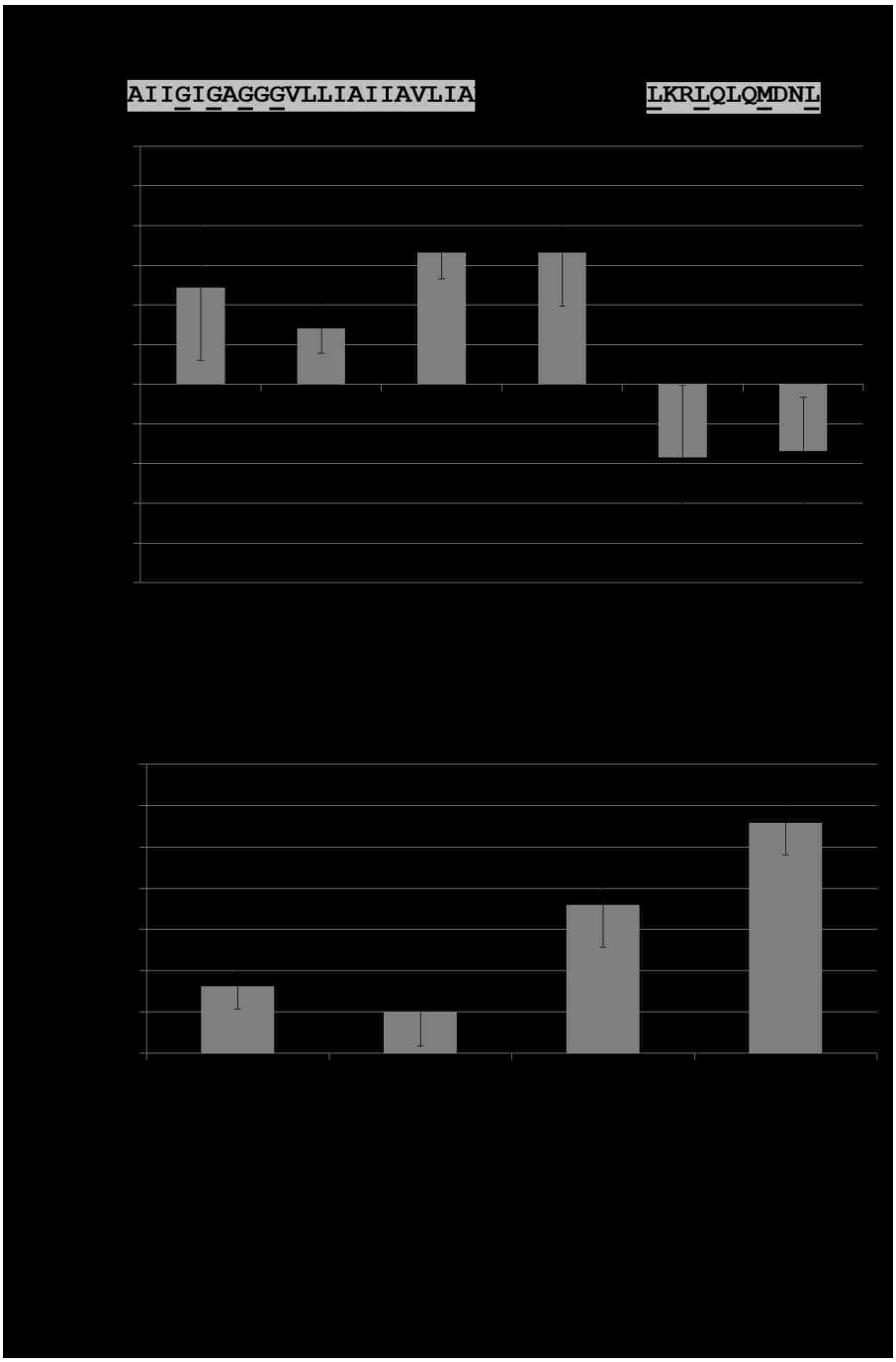

Figure 3.3. (A) Disruption of small-x_3-small interfaces in the PlexinA3 TM domain via point mutations enhance TM-JM dimerization in the AraTM assay. Similarly, extension of the small-x_3-small interfaces via introduction of glycines disrupt TM-JM dimerization. (B) Double and triple mutations disrupting the PlexinA3 TM small-x_3-small interfaces enhance dimerization of the TM-JM in the AraTM assay. Error bars indicate standard error as determined from twelve replicates collected over a minimum of three experiments.

3.3.2 TM and JM Interfaces Independently Regulate PlxnA3 Homodimerization

Previous work has demonstrated a specific heptad repeat in the PlxnA3 JM domain contributes to receptor TM-JM dimerization, with residue M1281 within this heptad repeat acting as a dimerization "switch", in which mutation M1281F disrupts dimerization by destabilizing packing in the hydrophobic core of the JM heptad repeat and mutation M1281L enhances dimerization through enhancing packing in the hydrophobic core of the JM heptad repeat (20). To determine how interactions in the JM interface influence TM-JM dimerization, and what role these interactions play in the observed increase in TM-JM dimerization caused by disruption of the TM small-x_3-small interface, we compared effects of key mutations in the TM region that enhance TM-JM dimerization to mutations in the JM shown previously to enhance or diminish TM-JM dimerization.

As shown in Figure 3.4, mutations to the JM region are dominant versus those in the TM domain; regardless of mutations to the two putative small-x_3-small interfaces of the TM, all of which enhance dimerization, mutations made in conjunction with the disruptive M1281F JM mutation reduce TM-JM dimerization, whereas mutations made in conjunction the enhancing M1281L JM mutation enhance TM-JM dimerization. Furthermore, the enhancements to dimerization through mutation of either of the two small-x_3-small interfaces (Figure 3.3) or M1281L (20) are non-additive; mutation to each domain individually enhances dimerization by less than 25% relative to WT, compared to more than 80% observed with mutation to both TM and JM (Figure 3.4). This suggests the TM small-x_3-small interfaces serve as competitive TM-JM dimers to those formed by the JM heptad repeat interface. Thus, enhancement of the small-x_3-small dimerization interface via introduction of additional on-interface glycines (L1252G, I1254G; Figure 3.3A) strengthens the TM dimer and pulls the TM-JM away from the JM dimer, whereas disruption or removal of the small-x_3-small interfaces through glycine-to-leucine

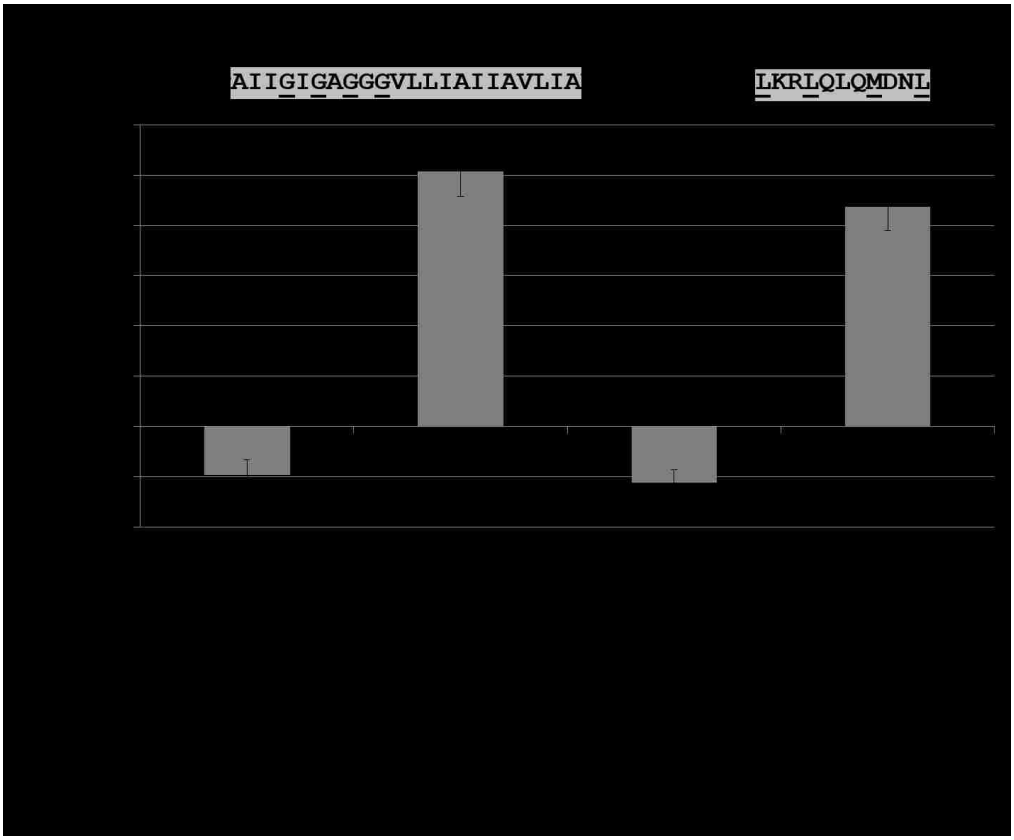

Figure 3.4. Mutations to the PlexinA3 JM domain dominate dimerization tendencies of the TM-JM in the AraTM assay. Error bars indicate standard error as determined from twelve replicates collected over a minimum of three experiments.

mutations (Figure 3.3) removes the TM dimer competition and strengthens the JM dimer. Collectively, our results are consistent with a model in which TM and JM dimerization are competitive, with each providing a distinct interface capable of forming a TM-JM dimer (Figure 3.4).

3.3.3 Glycines in the Transmembrane Domain Modulate PlxnA3 Function in a Zebrafish Axonal Guidance Assay

Zebrafish embryos failing to express membrane-anchored PlxnA3, such as homozygous *set* zebrafish embryos, exhibit anomalous motor neuron patterning, with motor neurons exhibiting atypical branching and ectopic exit points from the spinal cord (Figure 3.5) (24,28). Previous studies demonstrated that *set* embryos injected with WT *plxnA3* RNA show significantly fewer ectopic motor neuron exit points than uninjected *set* embryos (20). We injected *set* embryos while in the single-cell stage with TM-mutant *plxnA3* RNA and examined their motor neurons at 24 hours post fertilization for ectopic exit points, expecting mutations to functionally relevant residues to fail to rescue motor neuron patterning (Table 3.1). Comparisons to WT *plxnA3* RNA-injected and uninjected *set* embryos were made based on previous studies (20).

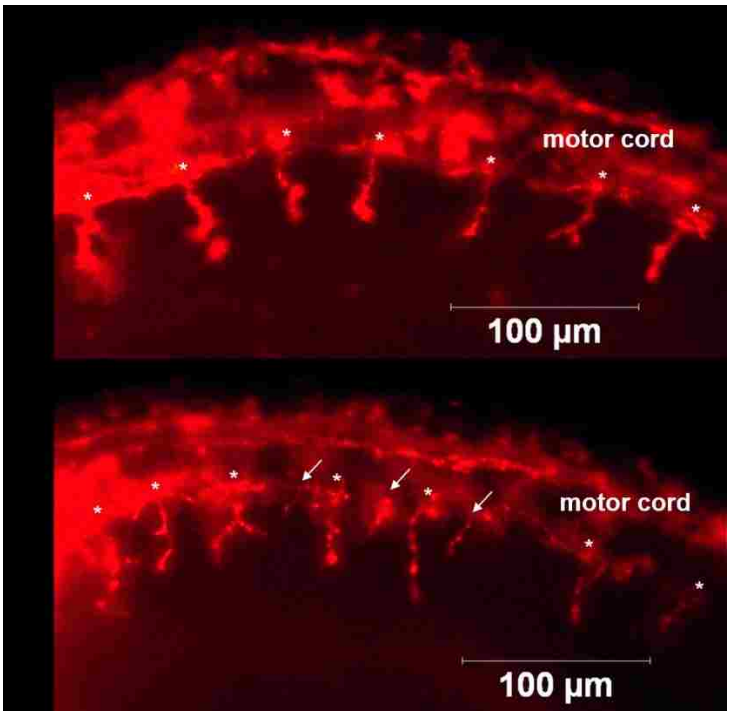

Figure 3.5. Embryos with the *sidetracked* phenotype exhibit ectopic motor neuron exit points (arrows). Endogenous motor neuron exit points are marked with an asterisk. Embryos were 24 hours post fertilization at the time of fixation and are oriented (left-to-right) anterior-to-posterior.

Table 3.1. Percentage of Homozygous *sidetracked* Embryos Exhibiting Phenotype[3b]

Type of RNA Injection	Number of Embryos Evaluated	Percentage of Embryos Exhibiting *sidetracked* Phenotype	P-value Compared to Wild-type *plxnA3* RNA-Injected
G1244L + G1248L	13	62	0.2
G1246L + G1250L	19	74	0.03

[3b]P-values were computed using a Fisher's Exact Test and previously reported values for uninjected and WT embryos (20).

Injection of *set* embryos with G1246L+G1250L *plxnA3* RNA results in significantly more embryos exhibiting the *set* phenotype than WT *plxnA3* RNA-injected embryos (74% of embryos exhibited the *set* phenotype; $p<0.05$ relative to WT as determined by a Fisher's Exact Test, FET). Injection of G1244L+G1248L *plxnA3* RNA partially rescues motor neuron patterning in *set* embryos (62% of embryos exhibited the *set* phenotype, $p>0.05$ compared to WT as determined by FET). Neither mutation resulted in significantly fewer embryos exhibiting the *set* phenotype than the previously reported 80% of uninjected *set* embryos (20). Both of these mutations enhanced dimerization of the TM-JM domains in the AraTM assay (Figure 3.3). Thus, our results are broadly consistent with a model in which destabilizing the TM dimer facilitates formation of a stronger, non-functional JM dimer, where both dimerization motifs contribute to PlxnA3 dependent signaling.

3.4 Discussion

Previous studies suggest plxn function depends on receptor clustering, and that function and clustering are modulated by the TM and JM domains (Figure 3.1) (12,13,16,18-21). In this study, we demonstrate that glycine-to-leucine mutations disrupting putative small-x_3-small

packing interfaces in the TM region of *Danio rerio* PlxnA3 enhance dimerization of TM-JM domains in the AraTM assay (Figure 3.3). Similarly, extension of the small-x_3-small interfaces disrupts dimerization (Figure 3.3). Mutations to the previously established dimer interface in the PlxnA3 JM (20) dominate dimer formation of the TM-JM, with mutations to either TM small-x_3-small interface in conjunction with JM M1281F disrupting dimerization, and mutations to the TM interfaces with JM M1281L enhancing dimerization (Figure 3.4). Functionally, disruption of the PlxnA3 TM interface fails to rescue motor neuron patterning in a zebrafish axonal guidance assay, with G1244L+G1248L exhibiting partial activity and G1246L+G1250L displaying no activity (Figure 3.5 and Table 3.1). Thus, our results point to a model for PlxnA3 dimerization in which the TM and JM both play important, competitive roles in regulating signal transduction (Figure 3.6). A recent coarse-grained molecular dynamics simulation also suggests that the isolated human PLXNA1 TM domain undergoes homooligomerization via two putative small-x_3-small interfaces (13), homologous to the *Danio rerio* PlxnA3 interfaces G1244+G1248 and G1246+G1250 identified in this study, although the role of the JM was not considered in the simulation. Thus, the proposed interaction model for the PlxnA3 TM-JM (Figure 3.6) is consistent with previous work regarding plxn TM domain dimerization, as well as with both functional and biochemical data regarding TM-JM dimerization. Furthermore, these results emphasize the importance of JM interactions in describing models for receptor TM dimerization.

Typically, mutation to small-x_3-small interaction motifs disrupts dimerization, as has been shown with GpA and NRP1 (23,29). This motif promotes TM dimerization by providing a specific interface favorable to steric packing constraints as well as additional side chain associations (22,30-32). Hence, the result that mutations to the PlxnA3 TM small-x_3-small motifs enhance TM-JM dimerization is at first counterintuitive (Figure 3.3). However, the interplay of TM versus JM interfaces as distinct dimers, but both significant in terms of promoting TM-JM

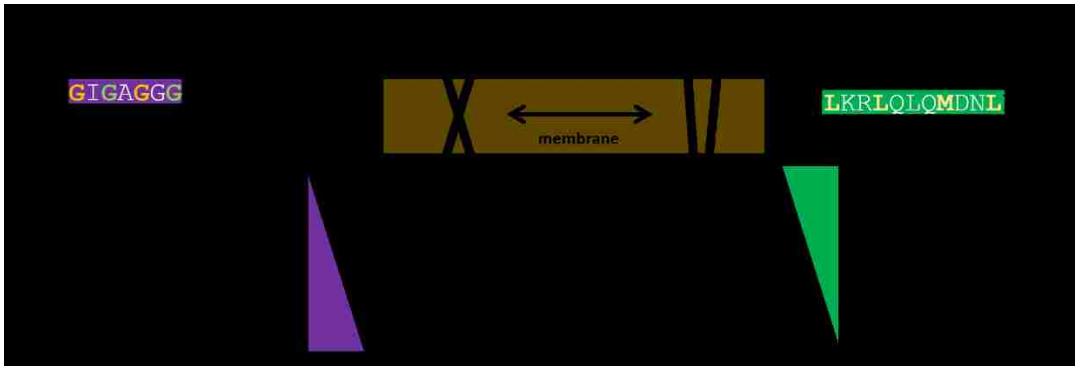

Figure 3.6. Model for competitive TM and JM interactions in regulation of PlexinA3 signal transduction.

dimerization, provides a model (Figure 3.6) in which multiple, competitive dimeric states occur for the TM-JM region, each of which are important in negatively regulating signal transduction. In this sense, the proposed TM-JM model resembles a "push-pull" mechanism used in describing the competition between integrin homo- versus heterodimerization (33). In the case of PlxnA3, the two states (TM dimer and JM dimer) are intrinsic to the receptor and in competition, with mutations that favor either of these interfaces "pulling" the receptor towards that interface and mutations that destabilize either of these interfaces "pushing" the TM-JM towards the other interface. Collectively, our results suggest glycines in the TM domain contribute to dimers driven by small-x_3-small packing motifs that compete with JM-driven dimers, and this competition prevents strong JM dimerization. This mechanism likely contributes to class A plxns flexibility in co-receptor heterodimerization (4,13,21) as well as regulated switchability between active and inactive states.

Our study also indicates that PlxnA3 dimerization does not necessarily correlate with enhanced function (Figure 3.3 and Table 3.1), similar to previous results with mutations in the PlxnA3 JM domain (20). Rather, a specific, dimeric conformation is likely responsible for

regulating activation. Our results for PlxnA3 are similar to previous studies with ErbB2, for which dimerization is required, but not sufficient, for activity; replacement of the ErbB2 TM domain with the GpA TM domain, though dimerized through the GpA small-x_3-small motif, fails to elicit a transformation phenotype (34). It is also analogous to the role of integrin TM domains in integrin activation (33), in which the TM domain has only a modest contribution to receptor dimerization, yet mutations to these TM interfaces have a significant impact on signal transduction (Table 3.1).

In summary, our AraTM results demonstrate that glycines in the *Danio rerio* PlxnA3 TM domain modulate receptor homomeric interactions (Figure 3.3). In particular, small-x_3-small dimerization motifs in the TM domain compete with dimerization driven by the heptad repeat in the JM domain (Figure 3.1). As JM-driven dimerization is dominant in the TM-JM system (Figure 3.4), mutation of the small-x_3-small interfaces results in overall enhancement to TM-JM dimerization. These interfaces both act competitively to regulate signaling, with the TM small-x_3-small interfaces exhibiting no or partial functionality in an embryonic zebrafish axonal guidance assay (Figure 3.5 and Table 3.1). Hence, the interplay of TM versus JM dimerization serves as an important regulatory mechanism in PlxnA3 signal transduction (Figure 3.1). Given other receptors in which JM interactions independently, and often competitively, regulate transmembrane dimerization and signaling (35-38), it will be interesting to see how other receptor systems couple TM and JM interactions to promote both homo- versus heterodimerization as well as signal transduction.

3.5 References

1. Tamagnone, L., Artigiani, S., Chen, H., He, Z., Ming, G. I., Song, H., Chedotal, A., Winberg, M. L., Goodman, C. S., Poo, M., Tessier-Lavigne, M., and Comoglio, P. M. (1999) Plexins are a large family of receptors for transmembrane, secreted, and GPI-anchored semaphorins in vertebrates. *Cell* **99**, 71-80
2. Takahashi, T., Fournier, A., Nakamura, F., Wang, L. H., Murakami, Y., Kalb, R. G., Fujisawa, H., and Strittmatter, S. M. (1999) Plexin-neuropilin-1 complexes form functional semaphorin-3A receptors. *Cell* **99**, 59-69
3. Negishi, M., Oinuma, I., and Katoh, H. (2005) Plexins: axon guidance and signal transduction. *Cell Mol Life Sci* **62**, 1363-1371
4. Kruger, R. P., Aurandt, J., and Guan, K. L. (2005) Semaphorins command cells to move. *Nat Rev Mol Cell Biol* **6**, 789-800
5. Tong, Y., Hota, P. K., Penachioni, J. Y., Hamaneh, M. B., Kim, S., Alviani, R. S., Shen, L., He, H., Tempel, W., Tamagnone, L., Park, H. W., and Buck, M. (2009) Structure and function of the intracellular region of the plexin-b1 transmembrane receptor. *J Biol Chem* **284**, 35962-35972
6. Torres-Vazquez, J., Gitler, A. D., Fraser, S. D., Berk, J. D., Van, N. P., Fishman, M. C., Childs, S., Epstein, J. A., and Weinstein, B. M. (2004) Semaphorin-plexin signaling guides patterning of the developing vasculature. *Dev Cell* **7**, 117-123
7. Ton, Q. V., and Kathryn Iovine, M. (2012) Semaphorin3d mediates Cx43-dependent phenotypes during fin regeneration. *Dev Biol* **366**, 195-203
8. Balakrishnan, A., Penachioni, J. Y., Lamba, S., Bleeker, F. E., Zanon, C., Rodolfo, M., Vallacchi, V., Scarpa, A., Felicioni, L., Buck, M., Marchetti, A., Comoglio, P. M.,

Bardelli, A., and Tamagnone, L. (2009) Molecular profiling of the "plexinome" in melanoma and pancreatic cancer. *Hum Mutat* **30**, 1167-1174

9. Wong, O. G., Nitkunan, T., Oinuma, I., Zhou, C., Blanc, V., Brown, R. S., Bott, S. R., Nariculam, J., Box, G., Munson, P., Constantinou, J., Feneley, M. R., Klocker, H., Eccles, S. A., Negishi, M., Freeman, A., Masters, J. R., and Williamson, M. (2007) Plexin-B1 mutations in prostate cancer. *Proc Natl Acad Sci U S A* **104**, 19040-19045
10. Staton, C. A., Shaw, L. A., Valluru, M., Hoh, L., Koay, I., Cross, S. S., Reed, M. W., and Brown, N. J. (2011) Expression of class 3 semaphorins and their receptors in human breast neoplasia. *Histopathology* **59**, 274-282
11. Bielenberg, D. R., Hida, Y., Shimizu, A., Kaipainen, A., Kreuter, M., Kim, C. C., and Klagsbrun, M. (2004) Semaphorin 3F, a chemorepulsant for endothelial cells, induces a poorly vascularized, encapsulated, nonmetastatic tumor phenotype. *J Clin Invest* **114**, 1260-1271
12. Takahashi, T., and Strittmatter, S. M. (2001) Plexina1 autoinhibition by the plexin sema domain. *Neuron* **29**, 429-439
13. Aci-Seche, S., Sawma, P., Hubert, P., Sturgis, J. N., Bagnard, D., Jacob, L., Genest, M., and Garnier, N. (2014) Transmembrane recognition of the semaphorin co-receptors neuropilin 1 and plexin A1: coarse-grained simulations. *PLoS One* **9**, e97779
14. He, H., Yang, T., Terman, J. R., and Zhang, X. (2009) Crystal structure of the plexin A3 intracellular region reveals an autoinhibited conformation through active site sequestration. *Proc Natl Acad Sci U S A* **106**, 15610-15615
15. Bell, C. H., Aricescu, A. R., Jones, E. Y., and Siebold, C. (2011) A dual binding mode for RhoGTPases in plexin signalling. *PLoS Biol* **9**, e1001134

16. Wang, Y., He, H., Srivastava, N., Vikarunnessa, S., Chen, Y. B., Jiang, J., Cowan, C. W., and Zhang, X. (2012) Plexins are GTPase-activating proteins for Rap and are activated by induced dimerization. *Sci Signal* **5**, ra6

17. Janssen, B. J., Robinson, R. A., Perez-Branguli, F., Bell, C. H., Mitchell, K. J., Siebold, C., and Jones, E. Y. (2010) Structural basis of semaphorin-plexin signalling. *Nature* **467**, 1118-1122

18. Driessens, M. H., Hu, H., Nobes, C. D., Self, A., Jordens, I., Goodman, C. S., and Hall, A. (2001) Plexin-B semaphorin receptors interact directly with active Rac and regulate the actin cytoskeleton by activating Rho. *Curr Biol* **11**, 339-344

19. Zanata, S. M., Hovatta, I., Rohm, B., and Puschel, A. W. (2002) Antagonistic effects of Rnd1 and RhoD GTPases regulate receptor activity in Semaphorin 3A-induced cytoskeletal collapse. *J Neurosci* **22**, 471-477

20. Barton, R., Palacio, D., Iovine, M. K., and Berger, B. W. (2015) A cytosolic juxtamembrane interface modulates plexin a3 oligomerization and signal transduction. *PLoS One* **10**, e0116368

21. Sawma, P., Roth, L., Blanchard, C., Bagnard, D., Cremel, G., Bouveret, E., Duneau, J. P., Sturgis, J. N., and Hubert, P. (2014) Evidence for New Homotypic and Heterotypic Interactions between Transmembrane Helices of Proteins Involved in Receptor Tyrosine Kinase and Neuropilin Signaling. *J Mol Biol* **426**, 4099-4111

22. MacKenzie, K. R., Prestegard, J. H., and Engelman, D. M. (1997) A transmembrane helix dimer: structure and implications. *Science* **276**, 131-133

23. Roth, L., Nasarre, C., Dirrig-Grosch, S., Aunis, D., Cremel, G., Hubert, P., and Bagnard, D. (2008) Transmembrane domain interactions control biological functions of neuropilin-1. *Mol Biol Cell* **19**, 646-654

24. Palaisa, K. A., and Granato, M. (2007) Analysis of zebrafish sidetracked mutants reveals a novel role for Plexin A3 in intraspinal motor axon guidance. *Development* **134**, 3251-3257

25. Birely, J., Schneider, V. A., Santana, E., Dosch, R., Wagner, D. S., Mullins, M. C., and Granato, M. (2005) Genetic screens for genes controlling motor nerve-muscle development and interactions. *Dev Biol* **280**, 162-176

26. Schramm, C. A., Hannigan, B. T., Donald, J. E., Keasar, C., Saven, J. G., Degrado, W. F., and Samish, I. (2012) Knowledge-based potential for positioning membrane-associated structures and assessing residue-specific energetic contributions. *Structure* **20**, 924-935

27. Su, P. C., and Berger, B. W. (2012) Identifying key juxtamembrane interactions in cell membranes using AraC-based transcriptional reporter assay (AraTM). *J Biol Chem* **287**, 31515-31526

28. Feldner, J., Reimer, M. M., Schweitzer, J., Wendik, B., Meyer, D., Becker, T., and Becker, C. G. (2007) PlexinA3 restricts spinal exit points and branching of trunk motor nerves in embryonic zebrafish. *J Neurosci* **27**, 4978-4983

29. Lemmon, M. A., Flanagan, J. M., Treutlein, H. R., Zhang, J., and Engelman, D. M. (1992) Sequence specificity in the dimerization of transmembrane alpha-helices. *Biochemistry* **31**, 12719-12725

30. Russ, W. P., and Engelman, D. M. (2000) The GxxxG motif: a framework for transmembrane helix-helix association. *J Mol Biol* **296**, 911-919

31. Senes, A., Gerstein, M., and Engelman, D. M. (2000) Statistical analysis of amino acid patterns in transmembrane helices: the GxxxG motif occurs frequently and in association with beta-branched residues at neighboring positions. *J Mol Biol* **296**, 921-936

32. Mueller, B. K., Subramaniam, S., and Senes, A. (2014) A frequent, GxxxG-mediated, transmembrane association motif is optimized for the formation of interhelical Calpha-H hydrogen bonds. *Proc Natl Acad Sci U S A* **111**, E888-895

33. Berger, B. W., Kulp, D. W., Span, L. M., DeGrado, J. L., Billings, P. C., Senes, A., Bennett, J. S., and DeGrado, W. F. (2010) Consensus motif for integrin transmembrane helix association. *Proc Natl Acad Sci U S A* **107**, 703-708

34. Burke, C. L., Lemmon, M. A., Coren, B. A., Engelman, D. M., and Stern, D. F. (1997) Dimerization of the p185neu transmembrane domain is necessary but not sufficient for transformation. *Oncogene* **14**, 687-696

35. Deng, W., Cho, S., Su, P. C., Berger, B. W., and Li, R. (2014) Membrane-enabled dimerization of the intrinsically disordered cytoplasmic domain of ADAM10. *Proc Natl Acad Sci U S A* **111**, 15987-15992

36. Oates, J., King, G., and Dixon, A. M. (2009) Strong oligomerization behavior of PDGFbeta receptor transmembrane domain and its regulation by the juxtamembrane regions. *Biochim Biophys Acta* **1798**, 605-615

37. Matsushita, C., Tamagaki, H., Miyazawa, Y., Aimoto, S., Smith, S. O., and Sato, T. (2013) Transmembrane helix orientation influences membrane binding of the intracellular juxtamembrane domain in Neu receptor peptides. *Proc Natl Acad Sci U S A* **110**, 1646-1651

38. Su, P. C., and Berger, B. W. (2013) A novel assay for assessing juxtamembrane and transmembrane domain interactions important for receptor heterodimerization. *J Mol Biol* **425**, 4652-4658

Chapter 4

Cysteines in the Neuropilin-2 MAM Domain Modulate Receptor Homooligomerization and Signal Transduction[4a]

[4a]*The work in this chapter has been accepted for publication as "Cysteines in the neuropilin-2 MAM domain modulate receptor homooligomerization and signal transduction" by Rachael Barton, Alyssa Driscoll, Samuel Flores, Durlav Mudbhari, Theresa Collins, M. Kathryn Iovine, and Bryan W. Berger with* Biopolymers: Peptide Science, *2015.*

Abstract

Neuropilins (NRPs) are transmembrane receptors involved in angiogenesis, lymphangiogenesis, and neuronal development as well as in cancer metastasis. Previous studies suggest that NRPs exist in heteromeric complexes with vascular endothelial growth factors (VEGFs) and VEGF receptors as well as plexins and semaphorins. We determined via site-directed mutagenesis and bioluminescent resonance energy transfer assays that a conserved cysteine (C711) in the Danio rerio NRP2a MAM (meprin, A-5 protein, and protein tyrosine phosphatase μ) domain modulates NRP2a homomeric interactions. Mutation of this residue also disrupts semaphorin 3F binding in NRP2a-transfected COS-7 cells and prevents the NRP2a overexpression effects in a zebrafish vascular model. Collectively, our results indicate the MAM domain plays an important role in defining the NRP2 homodimer structure, which is important for semaphorin-dependent signal transduction via NRP2.

4.1 Introduction

Neuropilins (NRPs) are type I transmembrane (TM) receptors that form heterodimeric complexes with two key classes of signaling TM receptors: plexins and vascular endothelial growth factor receptors (VEGFRs) (1). There are two main NRP receptors (NRP1, NRP2), with multiple extracellular and TM isoforms observed for each *in vivo* (2,3) . NRPs are comprised of two extracellular CUB (complement protein C1r/C1s, Uegf, and Bmp1) domains, two coagulation factor V/VIII (FA V/VIII) domains, one MAM (meprin, A-5 protein, and protein tyrosine phosphatase μ, PTPμ) domain, a single-spanning TM region, and a short cytosolic tail (Figure 4.1A) (1,3-9). The short cytosolic domain (CYTO) for NRPs is in contrast to VEGFRs, which contain a cytosolic tyrosine kinase signaling domain, and plexins, which contain a cytosolic guanine nucleotide exchange factor domain (1). Thus, NRPs are thought primarily to modulate the affinity and specificity of extracellular ligand binding upon co-receptor complex formation (10). In many instances, the co-receptor complex also includes additional cell adhesion molecules (CAMs) such as L1CAM and NrCAM as well as β1 integrins (7,11,12); thus, a functional co-receptor complex may involve three or more receptors at the cell surface. Plexin-NRP co-receptor complexes bind semaphorins (Semas), which are a large class of extracellular, dimeric ligands (20 in total) that act as either attractive or repulsive cues during cell migration in a diverse array of processes including axon guidance, vascular patterning, and bone formation (13-16). Additionally, VEGFR-NRP co-receptor complexes bind vascular endothelial growth factors (VEGFs), which are an equally large family of pro-angiogenic extracellular ligands (17). Thus, NRPs act as key regulators of extracellular signaling through imparting specificity in ligand-co-receptor complex formation.

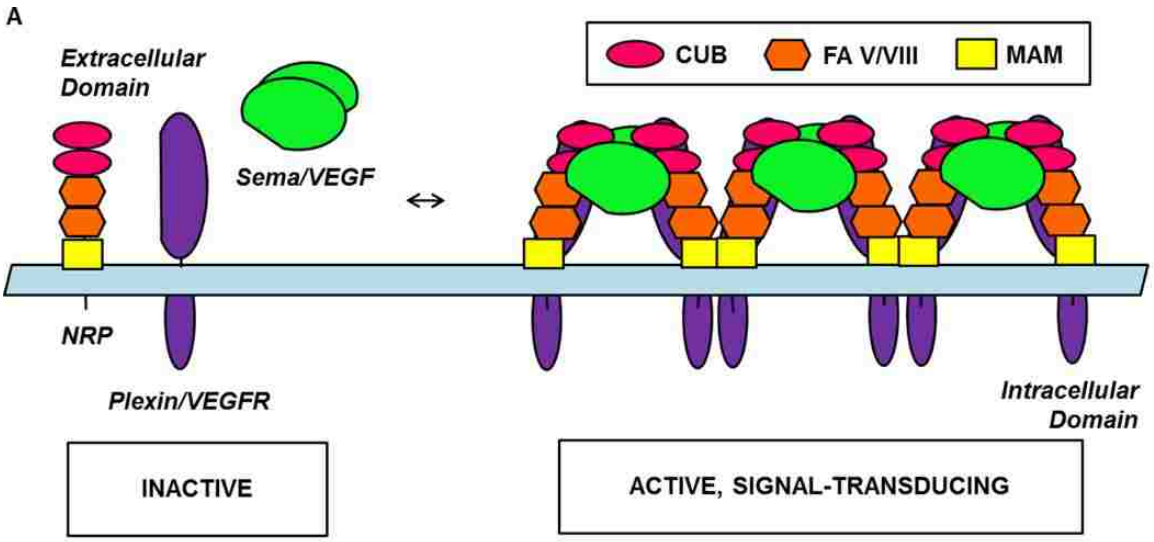

B

LPSHKGLCDFEQGWCGWTLDLDSDFSWVMHSSSKSSALGQSHNLSMGSNSLGNYLYIEASPETQG
QKARLFSPGVDPDTGPLCLMFSYQLEDQGTLRVLLQNKQQEKTLLWSLSGDQQPIWREGRTIIPRSP
DELKVVIEGFFEGTKGHIWIDNIHMSGNTPLEECTQ

Figure 4.1. NRP2a is a transmembrane receptor. (A) NRP2a consists of two CUB domains, two factor V/VIII domains, a MAM domain, a single-spanning transmembrane region, and a short cytosolic tail. NRP homooligomerization may play a role in NRP-plexin-sema and NRP-VEGFR-VEGF signal transduction by promoting aggregation. (B) Primary sequence of the *Danio rerio* NRP2a MAM domain. The MAM domain contains four conserved cysteines that impact homooligomerization in other MAM domain family members.

Given the diversity of biological processes in which Sema and VEGF modulate cell migration, dysregulation of NRP-dependent signaling has been linked to a variety of cancers (6). In particular, Sema3F has been shown to exhibit strong anti-angiogenic activity through binding to NRP2, with forced overexpression of Sema3F in a mouse melanoma model inhibiting tumor angiogenesis (18). NRP2 activation in response to VEGF-C binding is also linked to enhanced autophagy in cancer cells through an mTOR-dependent pathway, allowing them to survive after chemotherapeutic treatment (19). Additional studies have demonstrated the up-regulation of numerous other signaling pathways known to positively influence tumor metastasis in response to NRP2 activation, including chemokine receptor CXCR4 in breast cancers and insulin-like growth

factor-1 receptor in high-grade, PTEN-null prostate cancer (20,21). In general, it has been observed that NRP1 and NRP2 are both overexpressed in multiple cancer types, and in the case of NRP1, positively correlate with tumor progression (4,6,22). Likewise, therapeutics targeted to NRP1 and NRP2 that block signal transduction have shown anti-metastatic potential in multiple cancer types, suggesting NRPs may serve as effective biomarkers that specifically target metastatic tumors (5,23,24). Thus, NRPs act as key regulators of cell migration, and dysregulation of NRP-dependent signaling can lead to enhanced pro-angiogenic tumor growth as well as cancer cell survival post-treatment.

In the case of NRP1-PlexinA1 signaling, it has been observed that the receptors cluster upon Sema3A addition and subsequent signal transduction (25). Forced homodimerization of the PlexinA1, A2, A4, and C1 cytosolic domains also enhances receptor GTPase-activating protein (GAP) activity in an *in vitro* RapGAP assay (26). Collectively, these results suggest plexin homomeric interactions are important for NRP-plexin-sema signal transduction (Figure 4.1A). A low-resolution crystal structure of the CUB and FA V/VIII domains of NRP1 with the four N-terminal PlexinA2 domains bound to Sema3A reveals a 2:2:2 NRP1:PlexinA2:Sema3A stoichiometry, with the CUB domains of NRP1 acting as a linker to stabilize the Sema3A-PlexinA2 complex (27). No major structural rearrangements in NRP1 or PlexinA2 are observed between the Sema3A-liganded and unliganded states, and both the NRP1 and PlexinA2 extracellular fragments in the crystal structure are monomeric in solution (27). Similarly, plexin cytosolic domains appear predominately monomeric in solution with only weak homomeric interactions observed (26,28), implying plexin dimerization and clustering is influenced through the TM domain and proximal regions and/or the NRP co-receptor.

Receptor dimerization or clustering likely influences VEGFR signaling, as well (29,30). Crystal structures of the VEGFR-2 ligand binding domain complexed with VEGF-A or VEGF-E indicate a 2:2 stoichiometry, as do crystal structures of the first NRP1 FA V/VIII domain

complexed with VEGF-A (31,32). In addition to the capabilities of both VEGFR-2 and NRP1 to bind VEGF-A in the absence of the co-receptor, VEGFR-2 and NRP1 interact with each other in the absence of the VEGF-A ligand. While the co-receptor complex may affect ligand binding or receptor internalization upon ligand binding, another model suggests NRPs serve to promote clustering of VEGFRs and subsequent activation (Figure 4.1A) (29,33,34).

The full-length NRP1 receptor appears dimeric when solubilized via western blots and co-immunoprecipitation (co-IP) experiments, as does the full-length NRP2 receptor (8,35-37). Studies on the TM domain of NRP1 indicate that mutations to TM glycines found in a conserved 'G-x_3-G' motif disrupt dimerization of purified NRP1 TM domain peptides, implying a role for the TM domain in NRP1 homodimeric interactions (38). Domain-binding and -deletion studies also suggest homomeric interactions may be facilitated by the NRP juxtamembrane MAM domain (8,35,36). The involvement of the MAM domain in NRP homomeric interactions is further supported by the inability of MAM-deletion constructs to co-IP with the full-length receptor and the ability of an alkaline phosphatase (AP)-tagged NRP2 MAM domain to bind COS cells upon expression of the full-length NRP1 or NRP2 receptors (8,35). Thus, while the NRP transmembrane domain exhibits a G-x_3-G motif, a driving force for NRP2 MAM homomeric interactions and their role in receptor clustering and activation remains unresolved.

MAM domains are also present in meprins and protein tyrosine phosphatase (PTP) subclass IIB proteins. This domain in both meprin α and PTPμ has been shown to influence homomeric interactions (39,40). The MAM domains of neuropilins, PTPμ, and meprin α all contain four conserved cysteines, with the MAM domain of meprin α containing one additional cysteine (39,40). Mutation of this fifth cysteine in a secreted truncated meprin α protein or addition of reducing agent to this same protein results in monomeric meprin α in SDS-PAGE (39). While the PTPμ MAM domain cross-linked in solution runs as a dimer on SDS-PAGE, addition of reducing agent to the cross-linking reaction results in monomeric PTPμ (40).

Collectively, these results suggest cysteine chemistry influences MAM domain interactions in meprin α and PTPμ.

In order to determine if cysteine chemistry in the MAM domain also influences homooligomerization of NRP2, we utilized a series of biochemical and genetic tools to identify the ability of cysteine-mutant constructs to self-interact. Our results indicate cysteines in the *Danio rerio* NRP2a MAM domain, in particular a conserved cysteine (C711), play a significant role in homooligomerization and function. Notably, we predict that a C711-dependent disulfide bond dictates proper formation for the activated, clustered NRP2 (Figure 4.1A). Mutations to select MAM domain cysteines in the full-length receptor in a bioluminescence resonance energy transfer ($BRET^2$) assay enhance dimerization. When expressed in transiently-transfected COS-7 cells, the NRP2a mutation C711S reduces Sema3F binding, signifying a role for this residue in dictating interactions necessary for the activated, clustered state. Furthermore, while injection of wild-type (WT) NRP2a RNA into zebrafish embryos resulted in branched intersegmental vessels (ISVs), injection of C711S mutant RNA resulted in significantly fewer embryos with this NRP2a overexpression phenotype. Collectively, these results indicate cysteine chemistry in the NRP2a MAM domain contributes to the protein's mechanisms for homooligomerization and provides insight into the structural organization of NRP co-receptor complexes important for signal transduction (Figure 4.1A).

4.2 Materials and Methods

4.2.1 Plasmids

Zebrafish are known to express two NRP2 isoforms (a and b) (41). Full-length WT *Danio rerio* NRP2a (NCB Accession # BC162118.1, Thermo Scientific) was generated by PCR for cloning into pcDNA3.1/V5-His-TOPO (Invitrogen) as per manufacturer's instructions with a

C-terminal FLAG-tag, pGFP^2-N3 (BioSignal Packard) as a NheI/HindIII insert, and pRLuc-N1 (BioSignal Packard) at XhoI/HindIII. Mutations were made using the QuikChange II Site-Directed Mutagenesis Kit (Agilent Technologies) as per manufacturer's instructions.

To generate hook-Sema3F, the hook moiety complete with an N-terminal HA-tag and two C-terminal myc-tags was obtained by PCR from the phook-2 plasmid (Invitrogen; residues 2096-3066) provided by Paul Billings (University of Pennsylvania). This construct was subsequently cloned into pcDNA3.1/V5-His-TOPO at HindIII/KpnI with a 5' Kozak sequence and a C-terminal poly-glycine linker. Human Sema3F without a signal sequence (residues 266-2467 of NCB Accession # XM_005265382.2) was then cloned into this plasmid at KpnI/XbaI. The plasmid coding for AP-Sema3F, used as a PCR template to make this construct, was provided by Dr. Roman J. Giger (University of Michigan).

4.2.2. Mammalian Cell Culture

COS-7 cells (ATCC) were maintained as recommended by ATCC, except media was supplemented with 1% (v/v) 100X Antibiotic/Antimycotic solution (100 U/mL penicillin G, 100 µg/mL streptomycin, and 0.25 µg/mL amphotericin B) (Hyclone) and subcultivation ratios ranged from 1:10 to 1:20. Transfections occurred via electroporation with a Bio-Rad Gene Pulser XCell using pre-set COS-7 parameters.

4.2.3 BRET^2 Assay

COS-7 cells were co-transfected via electroporation with a pGFP^2 and a pRLuc construct containing a fusion to full-length NRP2a. Each transfection was split across eight wells in a white, flat-bottomed 96-well plate. Each well represented one replicate, and each transfection represented one round for the specified condition. Cultures were allowed to grow for two days,

and measurements were taken as previously described using a Tecan Infinite F200 multi-well plate reader (42,43). Following measurements, levels of BRET^2 protein expression were confirmed consistent between mutants via western blots (1:1000 dilutions of EGFP mouse monoclonal antibody, Clontech; mouse monoclonal anti-tubulin, Abcam; anti-mouse IgG HRP-linked antibody, Cell Signaling; or 1:2500 dilution of MSX Renilla Luciferase, Millipore) (Figure 4.2).

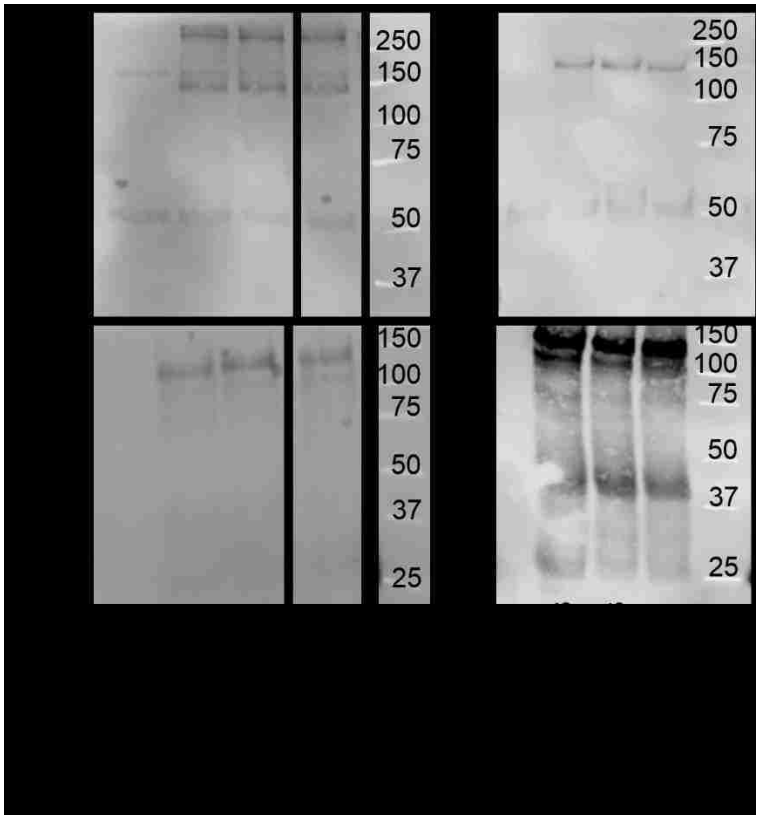

Figure 4.2. NRP2 BRET^2 constructs are expressed in COS-7 cells upon transfection. Ladder markings are in kDa. Anti-RLuc (top), anti-tubulin (top), and anti-GFP (bottom) western blots of cultures co-transfected with NRP2-RLuc and NRP2-GFP fusion constructs. R = NRP2-RLuc fusion (140 kDa), T = tubulin (55 kDa), G = NRP2-GFP fusion (130 kDa).

For analysis, we first considered the total luminescence of individual wells normalized to the average mock total luminescence of the wells for that round. Cultures with total

luminescence values lower than that of the mock-transfected cells were eliminated from subsequent analyses. The ratio of green luminescence to magenta luminescence was computed for each sample, then divided by the average ratio of green luminescence measurements to magenta luminescence measurements for the WT condition for that round of experiments. Results represent the average percent difference from WT and standard error of at least 24 independent replicates, with the standard error of WT samples added to the standard error of the mutants.

4.2.4 NRP2a Overexpression in Zebrafish

Capped NRP2a mRNA was made using the mMESSAGE mMACHINE T7 Transcription Kit (Ambion) as per manufacturer's instructions, with template NRP2a DNA generated from the pcDNA3.1/V5-His-TOPO constructs linearized with XhoI.

Embryos from adult fli1-GFP intercrosses were injected with either NRP2a RNA at 1 µg/µL or miR-2188 morpholino (miR-2188-MO, Gene Tools) at 0.5 mM while in the single-cell stage. At 48 hours post fertilization, chorions were popped and embryos were fixed with 4% paraformaldehyde for 2 hours at room temperature. Embryos were subsequently washed 3x with PBS and imaged at 20X magnification. Embryos were evaluated for ISV branching previously identified as a NRP2a overexpression phenotype (44).

4.2.5 Semaphorin Binding

Cells were transfected via electroporation with WT or mutant NRP2a in pcDNA3.1/V5-His-TOPO. Two days after transfections, all media was removed from the plate and replaced with 50-fold concentrated media from hook-Sema3F transfected cultures, and incubated 1.5-2 hours at 37°C in 5% CO_2. Treated cells were rinsed three times in PBS, then fixed for 30 minutes at room temperature with 4% paraformaldehyde in PBS. Cells were rinsed once in PBS, blocked

for one hour in PBS + 1% (w/v) BSA + 0.5% (v/v) TritonX-100 at room temperature, and incubated in mouse monoclonal anti-myc antibody (Cell Signaling) at 1:2000 in block solution over two nights. Secondary antibody incubation (anti-mouse IgG AlexaFluor 546 or 488) took place over the course of one hour at room temperature. For analysis, twenty fields of confluent cells per condition were then imaged at 20x magnification with consistent exposure and gain per round; subsequently, an observer counted the total number of fluorescent cells per condition.

4.3 Results

4.3.1 Specific Cysteines in the MAM Domain Influence NRP2a Homooligomerization

Previous research suggests the NRP2a MAM domain influences homooligomerization, similar to MAM domains in meprins and protein tyrosine phosphatases (8,35). In particular, four conserved cysteines in the MAM domains of meprin α and PTPμ have been shown to play an important role in stabilizing the homodimer through disulfide bond formation (39,40,45). As these cysteines are also conserved in the NRP2a MAM domain (Figure 4.1B), we hypothesized disulfide bond formation via these four conserved cysteines may also influence NRP2a MAM oligomerization. Comparison of the *Danio rerio* NRP2a MAM domain with the PTPμ MAM domain suggested C636-C643 and C711-C794 are likely to form disulfide bonds (analogous to disulfide bonds C27-C36 and C96-C182 in the PTPμ MAM domain) (46). Therefore, we mutated one or both cysteines in each of the corresponding putative disulfide bonds in the NRP2a receptor and analyzed the effects using the BRET^2 assay (42,43). Mutations were introduced into the full-length NRP2a receptor for both the C-terminal GFP^2-fused and *Renilla luciferase* (RLuc)-fused proteins. The BRET^2 assay relies upon distance between the GFP^2-fused and the RLuc-fused proteins; upon addition of the Deep Blue C substrate, the RLuc tag catalyzes a reaction that causes light to be emitted at 395 nm. This light then excites nearby GFP^2 tags, causing light to be

emitted at 510 nm. Results are characterized by an energy transfer ratio, or the ratio of intensity of light produced by GFP^2 (green fluorescence at 510 nm) to the luminescence signal generated by RLuc (magenta luminescence at 395 nm) (42,43).

As shown in Figure 4.3, the MAM mutants C643S, C711S, and C711S + C794S show significant differences from WT as an enhancement in energy transfer. Thus, the BRET^2 results indicate mutants C643S, C711S, and C711S + C794S enhance oligomerization of full-length NRP2a. Interestingly, the double mutant C636S + C643S did not exhibit significant changes in energy transfer efficiency from the WT receptor, suggesting specific cysteines or combinations of cysteines in the MAM domain influence NRP2a homooligomerization. Collectively, the results imply specific cysteines in the NRP2a MAM domain influence receptor homomeric interactions and subsequent clustering and activation (Figure 4.1).

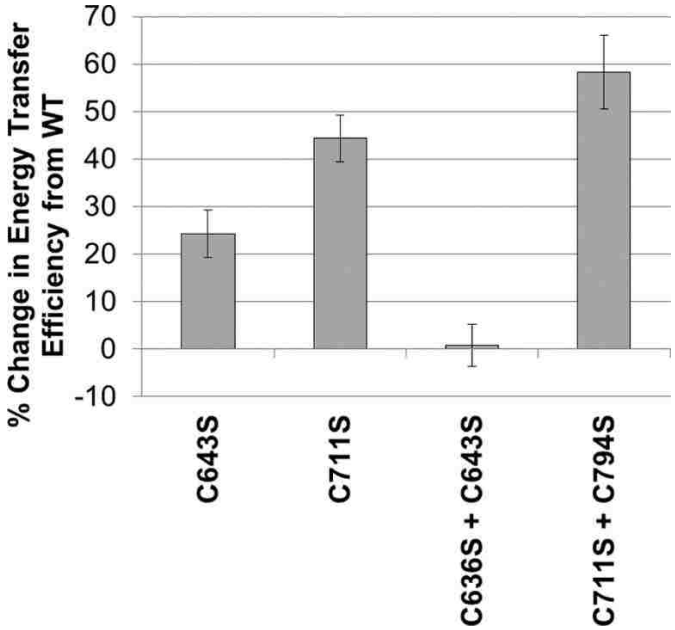

Figure 4.3. Cysteines in the NRP2a MAM domain of influence receptor homooligomerization in a mammalian membrane, as determined by BRET^2. Results were collected from at least three separate transfections of each condition and error bars represent standard error.

4.3.2 Mutations to the NRP2a MAM Domain Influence Overexpression Phenotypes in Zebrafish Vascular Patterning

Previous results demonstrate that knockdown of a microRNA that suppresses NRP2a expression (miR-2188), hence inducing NRP2a overexpression, results in irregular ISV branches in zebrafish embryos. This phenotype is believed to manifest itself through the NRP2a-VEGF pathway (44). One model suggests NRP2a influences VEGF signaling through NRP-VEGF-VEGFR clustering (29). To determine if our cysteine mutations affect signaling in a NRP2a-VEGF pathway, we injected miR-2188-MO or NRP2a mRNA into zebrafish embryos and examined them for the NRP2a overexpression phenotype (Figure 4.4 and Table 4.1).

Of the embryos examined, 16% of those injected with miR-2188-MO and 18% of those injected with WT NRP2a mRNA exhibited branches characteristic of the NRP2a overexpression phenotype. This was significantly more than the 2.5% of uninjected embryos exhibiting ISV branches ($p<0.0005$, as determined via an unpaired two-tailed student t-test assuming equal variance). Embryos injected with cysteine-mutant NRP2a mRNA (C643S, C711S, and C711S + C794S) showed significant increases in NRP2a overexpression compared to the uninjected embryos, as well ($p<0.05$ for C643S and C711S and $p<0.0005$ for C711S + C794S). However, compared to the embryos injected with WT NRP2a mRNA, fewer embryos injected with C711S NRP2a mRNA exhibited the overexpression phenotype ($p<0.05$). This suggests mutation C711S fails to elicit the same functionality as WT NRP2a, possibly due to alterations to receptor oligomeric state and/or tertiary structure as suggested by our $BRET^2$ results (Figure 4.3).

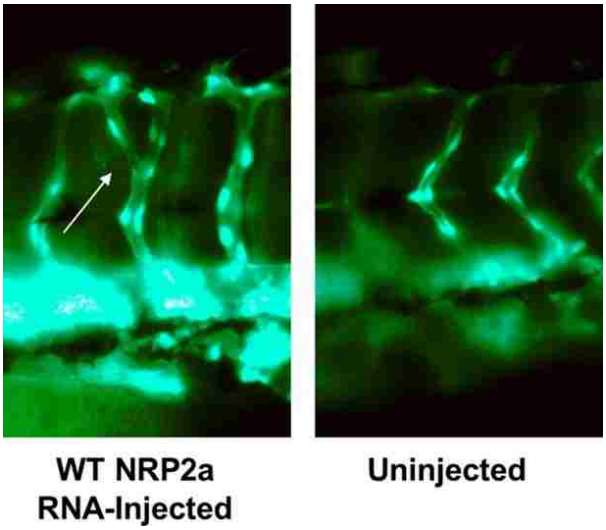

Figure 4.4. WT NRP2a overexpression causes ISV branching in 48 hours post fertilization zebrafish embryos.

Table 4.1. Percentage of fli1-GFP embryos exhibiting ISV branching[4b]

Type of Injection	Number of Embryos Examined	Percentage of Embryos Exhibiting NRP2 Overexpression Phenotype	P-value Compared to Uninjected	P-value Compared to WT NRP2a RNA-Injected
Uninjected	204	2.5	1	6.8×10^{-6}
WT NRP2a RNA	62	18	6.8×10^{-6}	1
C643S NRP2a RNA	54	9.3	0.021	0.19
C711S NRP2a RNA	141	7.8	0.020	0.034
C711S + C794S NRP2a RNA	81	17	4.4×10^{-6}	0.94
miR-2188-MO	43	16	1.1×10^{-6}	0.29

[4b]P-values were determined using an unpaired equal variance two-tailed student t-test.

4.3.3 Mutations to the NRP2a MAM Domain Influence Sema3F Binding

Previous work suggests the NRP1 MAM domain promotes receptor cis- or trans-aggregation, and that these aggregates (of a higher-order than dimer) may be required for activation or interactions with a co-receptor (35). While crystal structures suggest a 2:2:2 NRP1:PlexinA2:Sema3A stoichiometry (27), it is possible that activation of the full-length receptors requires a higher order oligomer than dimer or promotes binding of the semaphorin ligand (Figure 4.1A) (35). Previous results with NRP2 have shown that deletion of the MAM domain reduces receptor affinity for the Sema3F ligand, as determined by reduction in absorbance measurements of COS-7 cells transfected with NRP2 and subsequently treated with an AP- Sema3F (35). To determine a possible functional role of the MAM cysteines in semaphorin binding, we examined Sema3F binding to COS-7 cells transfected with either WT or mutant *Danio rerio* NRP2a. Sema3F acts as a negative regulator of growth cone formation guided by NRP2-Plexin A3, and thus binding of Sema3F is necessary for growth cone collapse (28).

Expression of full-length FLAG-tagged WT NRP2a or mutant C711S + C794S resulted in significant binding of Sema3F compared to mock-transfected cells, as determined by fluorescence microscopy (Figures 4.5A-B). Significantly fewer Sema3F-bound cells were observed in cultures transfected with NRP2a mutant C711S for the same exposure times, indicating a reduction in Sema3F-binding in cells transfected with this mutant. The reduction in Sema3F-binding is likely due to altered oligomeric states or conformational changes in the protein rather than expression levels, as western blots on NRP2a $BRET^2$ constructs exhibit similar expression levels. Our $BRET^2$ (Figure 4.3) results point to C711 as influential to NRP2a homomeric interactions. A model in which the oligomeric state of NRP2a regulates Sema3F-binding, and C711 regulates NRP2a oligomerization, is consistent with these results (Figure 4.1).

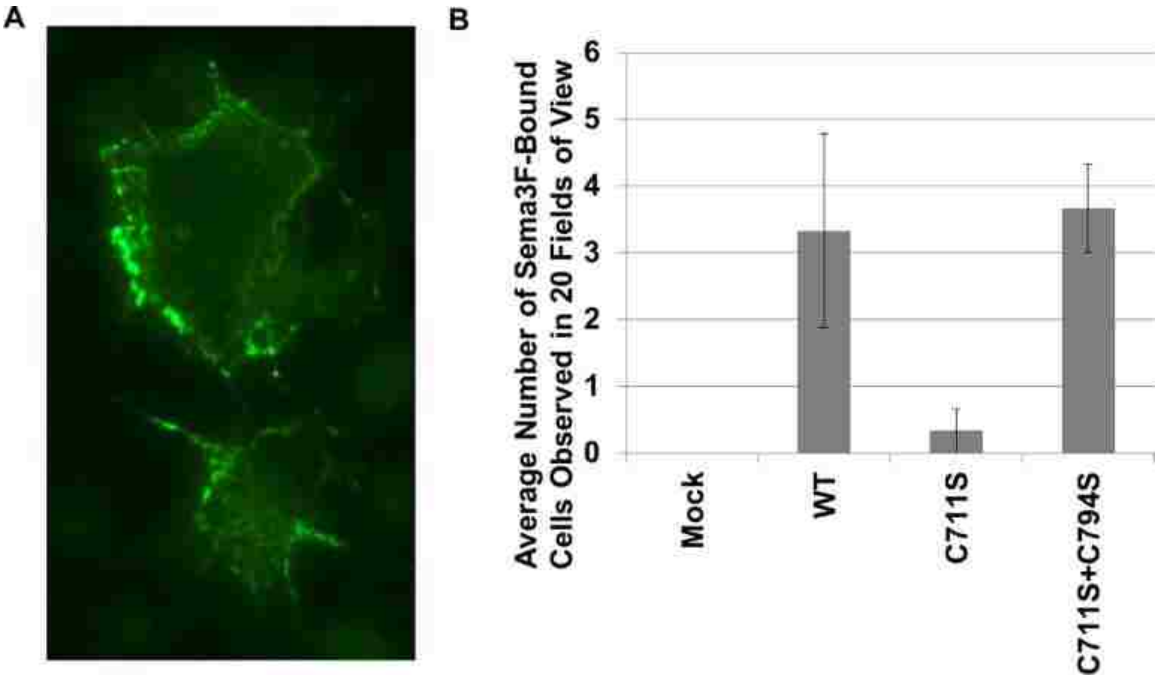

Figure 4.5. Mutant C711S reduces binding of Sema3F to the full-length NRP2a receptor. (A) Representative images of hook-Sema3F-bound cells. (B) Mutant C711S disrupts Sema3F-binding. Cells were transfected with water, WT, or mutant NRP2a constructs and treated with 50x-concentrated hook-Sema3F. Twenty random fields of view for each condition per round (three rounds total) were examined at an exposure time consistent within the round and the total number of Sema3F-bound cells were counted. Error bars indicate standard error.

4.4 Discussion

Previous studies have shown the NRPs exhibit an intrinsic ability to dimerize and aggregate (8,35-37). Here, we identify a conserved cysteine in the MAM domain of NRP2a (C711) that governs homooligomerization when mutated in the context of the full-length receptor in a mammalian cell membrane (Figure 4.3). This mutation also disrupts Sema3F-binding to the full-length receptor (Figure 4.5) and causes less of the NRP2a overexpression phenotype in zebrafish embryo vasculature compared to the WT receptor (Table 4.1). We also identified mutations to conserved cysteines (C711S + C794S) that affect receptor homomeric interactions, as determined by $BRET^2$ (Figure 4.3), but do not disrupt Sema3F-binding (Figure 4.5) or a reduced NRP2a overexpression phenotype in zebrafish vasculature (Table 4.1). Our results

collectively point to a model in which the MAM domain acts as a regulator of the equilibrium between oligomeric states (Figure 4.1) and possibly receptor extracellular domain tertiary structure, thereby controlling semaphorin binding and VEGFR clustering. Furthermore, conserved cysteines govern this equilibrium. Additional structural and functional studies will allow further elucidation of the functional significance of the cysteine mutations.

In particular, one of the principle observations from this work is that the C711S mutation, which is one of four conserved cysteines in the MAM domain, drives dimerization in the context of the full-length receptor (Figure 4.3), suggesting the disulfide bond involving C711 negatively regulates oligomerization. Consistent with previous studies on meprin α and PTPμ MAM domains in which disruption of disulfide bonds resulted in decreased function (39,40,45), the NRP2a C711S mutant exhibits a reduction in Sema3F-binding capabilities as well as in ability to induce a NRP2a overexpression phenotype in zebrafish vasculature (Table 4.1 and Figure 4.5). In PTPμ, mutation of a conserved cysteine disrupted MAM domain interactions between receptors while maintaining the ability to induce cellular aggregation (40). In meprin α, disrupting a conserved MAM domain cysteine resulted in decreased thermal stability of the enzyme, increased proteolytic degradation, and decreased activity towards protein substrates (39). In NRP2a, we find disruption of the C711 disulfide bond triggers oligomerization of the full-length NRP2a receptor (Figure 4.3), which seemingly disrupts Sema3F binding (Figure 4.5) and reduces its ability to induce branching in zebrafish embryo vasculature (Table 4.1). It is likely that the C711S mutation could disrupt the equilibrium between oligomeric states and thereby affect ligand binding (Figure 4.1). Alternatively, the mutation could introduce a conformational change in the monomeric NRP2a structure itself that not only leads to NRP2a oligomerization, but also disrupts ligand binding sites. Our studies do not distinguish between either possibility, but do suggest that residue C711 is important for defining the oligomeric state of NRP2a and the receptor's ability to bind Sema3F and function in a VEGF-dependent system (Figure 4.1).

In summary, we have shown that residues in the NRP2a MAM domain regulate the equilibrium between NRP2a oligomeric conformations which lead to activated, clustered states (Figure 4.1). Cysteines, in particular C711, assist in regulating MAM dimerization, with intact disulfide bonds disrupting clustering of the full-length receptor (Figure 4.3). Regulation of NRP2a MAM domain cysteine chemistry ultimately affects Sema3F-binding, as observed with mutation of residue C711 (Figure 4.5), as well as its ability to act in a VEGF-dependent signaling cascade (Table 4.1). Our results suggest that cysteine interactions in the NRP2a MAM domain regulate oligomeric state and may provide a target site for approaches to modulate NRP homomeric interactions.

4.5 References

1. Zachary, I. C., Frankel, P., Evans, I. M., and Pellet-Many, C. (2009) The role of neuropilins in cell signalling. *Biochem Soc Trans* **37**, 1171-1178
2. Gagnon, M. L., Bielenberg, D. R., Gechtman, Z., Miao, H. Q., Takashima, S., Soker, S., and Klagsbrun, M. (2000) Identification of a natural soluble neuropilin-1 that binds vascular endothelial growth factor: In vivo expression and antitumor activity. *Proc Natl Acad Sci U S A* **97**, 2573-2578
3. Rossignol, M., Gagnon, M. L., and Klagsbrun, M. (2000) Genomic organization of human neuropilin-1 and neuropilin-2 genes: identification and distribution of splice variants and soluble isoforms. *Genomics* **70**, 211-222
4. Bagri, A., Tessier-Lavigne, M., and Watts, R. J. (2009) Neuropilins in tumor biology. *Clin Cancer Res* **15**, 1860-1864
5. Caunt, M., Mak, J., Liang, W. C., Stawicki, S., Pan, Q., Tong, R. K., Kowalski, J., Ho, C., Reslan, H. B., Ross, J., Berry, L., Kasman, I., Zlot, C., Cheng, Z., Le Couter, J.,

Filvaroff, E. H., Plowman, G., Peale, F., French, D., Carano, R., Koch, A. W., Wu, Y., Watts, R. J., Tessier-Lavigne, M., and Bagri, A. (2008) Blocking neuropilin-2 function inhibits tumor cell metastasis. *Cancer Cell* **13**, 331-342

6. Ellis, L. M. (2006) The role of neuropilins in cancer. *Mol Cancer Ther* **5**, 1099-1107
7. Fukasawa, M., Matsushita, A., and Korc, M. (2007) Neuropilin-1 interacts with integrin beta1 and modulates pancreatic cancer cell growth, survival and invasion. *Cancer Biol Ther* **6**, 1173-1180
8. Nakamura, F., Tanaka, M., Takahashi, T., Kalb, R. G., and Strittmatter, S. M. (1998) Neuropilin-1 extracellular domains mediate semaphorin D/III-induced growth cone collapse. *Neuron* **21**, 1093-1100
9. Schwarz, Q., and Ruhrberg, C. (2010) Neuropilin, you gotta let me know: should I stay or should I go? *Cell Adh Migr* **4**, 61-66
10. Kirkbride, K. C., Ray, B. N., and Blobe, G. C. (2005) Cell-surface co-receptors: emerging roles in signaling and human disease. *Trends Biochem Sci* **30**, 611-621
11. Castellani, V., Chedotal, A., Schachner, M., Faivre-Sarrailh, C., and Rougon, G. (2000) Analysis of the L1-deficient mouse phenotype reveals cross-talk between Sema3A and L1 signaling pathways in axonal guidance. *Neuron* **27**, 237-249
12. Falk, J., Bechara, A., Fiore, R., Nawabi, H., Zhou, H., Hoyo-Becerra, C., Bozon, M., Rougon, G., Grumet, M., Puschel, A. W., Sanes, J. R., and Castellani, V. (2005) Dual functional activity of semaphorin 3B is required for positioning the anterior commissure. *Neuron* **48**, 63-75
13. Cheng, H. J., Bagri, A., Yaron, A., Stein, E., Pleasure, S. J., and Tessier-Lavigne, M. (2001) Plexin-A3 mediates semaphorin signaling and regulates the development of hippocampal axonal projections. *Neuron* **32**, 249-263

14. Hayashi, M., Nakashima, T., Taniguchi, M., Kodama, T., Kumanogoh, A., and Takayanagi, H. (2012) Osteoprotection by semaphorin 3A. *Nature* **485**, 69-74

15. Sharma, A., Verhaagen, J., and Harvey, A. R. (2012) Receptor complexes for each of the Class 3 Semaphorins. *Front Cell Neurosci* **6**, 28

16. Torres-Vazquez, J., Gitler, A. D., Fraser, S. D., Berk, J. D., Van, N. P., Fishman, M. C., Childs, S., Epstein, J. A., and Weinstein, B. M. (2004) Semaphorin-plexin signaling guides patterning of the developing vasculature. *Dev Cell* **7**, 117-123

17. Olsson, A. K., Dimberg, A., Kreuger, J., and Claesson-Welsh, L. (2006) VEGF receptor signalling - in control of vascular function. *Nat Rev Mol Cell Biol* **7**, 359-371

18. Bielenberg, D. R., Hida, Y., Shimizu, A., Kaipainen, A., Kreuter, M., Kim, C. C., and Klagsbrun, M. (2004) Semaphorin 3F, a chemorepulsant for endothelial cells, induces a poorly vascularized, encapsulated, nonmetastatic tumor phenotype. *J Clin Invest* **114**, 1260-1271

19. Stanton, M. J., Dutta, S., Zhang, H., Polavaram, N. S., Leontovich, A. A., Honscheid, P., Sinicrope, F. A., Tindall, D. J., Muders, M. H., and Datta, K. (2013) Autophagy control by the VEGF-C/NRP-2 axis in cancer and its implication for treatment resistance. *Cancer Res* **73**, 160-171

20. Goel, H. L., Chang, C., Pursell, B., Leav, I., Lyle, S., Xi, H. S., Hsieh, C. C., Adisetiyo, H., Roy-Burman, P., Coleman, I. M., Nelson, P. S., Vessella, R. L., Davis, R. J., Plymate, S. R., and Mercurio, A. M. (2012) VEGF/neuropilin-2 regulation of Bmi-1 and consequent repression of IGF-IR define a novel mechanism of aggressive prostate cancer. *Cancer Discov* **2**, 906-921

21. Yasuoka, H., Kodama, R., Tsujimoto, M., Yoshidome, K., Akamatsu, H., Nakahara, M., Inagaki, M., Sanke, T., and Nakamura, Y. (2009) Neuropilin-2 expression in breast

cancer: correlation with lymph node metastasis, poor prognosis, and regulation of CXCR4 expression. *BMC Cancer* **9**, 220

22. Harsha, H. C., Kandasamy, K., Ranganathan, P., Rani, S., Ramabadran, S., Gollapudi, S., Balakrishnan, L., Dwivedi, S. B., Telikicherla, D., Selvan, L. D., Goel, R., Mathivanan, S., Marimuthu, A., Kashyap, M., Vizza, R. F., Mayer, R. J., Decaprio, J. A., Srivastava, S., Hanash, S. M., Hruban, R. H., and Pandey, A. (2009) A compendium of potential biomarkers of pancreatic cancer. *PLoS Med* **6**, e1000046

23. Narazaki, M., Segarra, M., and Tosato, G. (2008) Neuropilin-2: a new molecular target for antiangiogenic and antitumor strategies. *J Natl Cancer Inst* **100**, 81-83

24. Pan, Q., Chanthery, Y., Liang, W. C., Stawicki, S., Mak, J., Rathore, N., Tong, R. K., Kowalski, J., Yee, S. F., Pacheco, G., Ross, S., Cheng, Z., Le Couter, J., Plowman, G., Peale, F., Koch, A. W., Wu, Y., Bagri, A., Tessier-Lavigne, M., and Watts, R. J. (2007) Blocking neuropilin-1 function has an additive effect with anti-VEGF to inhibit tumor growth. *Cancer Cell* **11**, 53-67

25. Takahashi, T., Fournier, A., Nakamura, F., Wang, L. H., Murakami, Y., Kalb, R. G., Fujisawa, H., and Strittmatter, S. M. (1999) Plexin-neuropilin-1 complexes form functional semaphorin-3A receptors. *Cell* **99**, 59-69

26. Wang, Y., He, H., Srivastava, N., Vikarunnessa, S., Chen, Y. B., Jiang, J., Cowan, C. W., and Zhang, X. (2012) Plexins are GTPase-activating proteins for Rap and are activated by induced dimerization. *Sci Signal* **5**, ra6

27. Janssen, B. J., Malinauskas, T., Weir, G. A., Cader, M. Z., Siebold, C., and Jones, E. Y. (2012) Neuropilins lock secreted semaphorins onto plexins in a ternary signaling complex. *Nat Struct Mol Biol* **19**, 1293-1299

28. He, H., Yang, T., Terman, J. R., and Zhang, X. (2009) Crystal structure of the plexin A3 intracellular region reveals an autoinhibited conformation through active site sequestration. *Proc Natl Acad Sci U S A* **106**, 15610-15615

29. Whitaker, G. B., Limberg, B. J., and Rosenbaum, J. S. (2001) Vascular endothelial growth factor receptor-2 and neuropilin-1 form a receptor complex that is responsible for the differential signaling potency of VEGF(165) and VEGF(121). *J Biol Chem* **276**, 25520-25531

30. Lemmon, M. A., and Schlessinger, J. (2010) Cell signaling by receptor tyrosine kinases. *Cell* **141**, 1117-1134

31. Brozzo, M. S., Bjelic, S., Kisko, K., Schleier, T., Leppanen, V. M., Alitalo, K., Winkler, F. K., and Ballmer-Hofer, K. (2012) Thermodynamic and structural description of allosterically regulated VEGFR-2 dimerization. *Blood* **119**, 1781-1788

32. Parker, M. W., Xu, P., Li, X., and Vander Kooi, C. W. (2012) Structural basis for selective vascular endothelial growth factor-A (VEGF-A) binding to neuropilin-1. *J Biol Chem* **287**, 11082-11089

33. Shraga-Heled, N., Kessler, O., Prahst, C., Kroll, J., Augustin, H., and Neufeld, G. (2007) Neuropilin-1 and neuropilin-2 enhance VEGF121 stimulated signal transduction by the VEGFR-2 receptor. *FASEB J* **21**, 915-926

34. Karpanen, T., Heckman, C. A., Keskitalo, S., Jeltsch, M., Ollila, H., Neufeld, G., Tamagnone, L., and Alitalo, K. (2006) Functional interaction of VEGF-C and VEGF-D with neuropilin receptors. *FASEB J* **20**, 1462-1472

35. Chen, H., He, Z., Bagri, A., and Tessier-Lavigne, M. (1998) Semaphorin-neuropilin interactions underlying sympathetic axon responses to class III semaphorins. *Neuron* **21**, 1283-1290

36. Giger, R. J., Urquhart, E. R., Gillespie, S. K., Levengood, D. V., Ginty, D. D., and Kolodkin, A. L. (1998) Neuropilin-2 is a receptor for semaphorin IV: insight into the structural basis of receptor function and specificity. *Neuron* **21**, 1079-1092

37. Takahashi, T., Nakamura, F., Jin, Z., Kalb, R. G., and Strittmatter, S. M. (1998) Semaphorins A and E act as antagonists of neuropilin-1 and agonists of neuropilin-2 receptors. *Nat Neurosci* **1**, 487-493

38. Roth, L., Nasarre, C., Dirrig-Grosch, S., Aunis, D., Cremel, G., Hubert, P., and Bagnard, D. (2008) Transmembrane domain interactions control biological functions of neuropilin-1. *Mol Biol Cell* **19**, 646-654

39. Marchand, P., Volkmann, M., and Bond, J. S. (1996) Cysteine mutations in the MAM domain result in monomeric meprin and alter stability and activity of the proteinase. *J Biol Chem* **271**, 24236-24241

40. Cismasiu, V. B., Denes, S. A., Reilander, H., Michel, H., and Szedlacsek, S. E. (2004) The MAM (meprin/A5-protein/PTPmu) domain is a homophilic binding site promoting the lateral dimerization of receptor-like protein-tyrosine phosphatase mu. *J Biol Chem* **279**, 26922-26931

41. Wolman, M. A., Liu, Y., Tawarayama, H., Shoji, W., and Halloran, M. C. (2004) Repulsion and attraction of axons by semaphorin3D are mediated by different neuropilins in vivo. *J Neurosci* **24**, 8428-8435

42. Carriba, P., Navarro, G., Ciruela, F., Ferre, S., Casado, V., Agnati, L., Cortes, A., Mallol, J., Fuxe, K., Canela, E. I., Lluis, C., and Franco, R. (2008) Detection of heteromerization of more than two proteins by sequential BRET-FRET. *Nat Methods* **5**, 727-733

43. Pfleger, K. D., Seeber, R. M., and Eidne, K. A. (2006) Bioluminescence resonance energy transfer (BRET) for the real-time detection of protein-protein interactions. *Nat Protoc* **1**, 337-345

44. Soares, A. R., Reverendo, M., Pereira, P. M., Nivelles, O., Pendeville, H., Bezerra, A. R., Moura, G. R., Struman, I., and Santos, M. A. (2012) Dre-miR-2188 targets Nrp2a and mediates proper intersegmental vessel development in zebrafish embryos. *PLoS One* **7**, e39417

45. Aricescu, A. R., Siebold, C., Choudhuri, K., Chang, V. T., Lu, W., Davis, S. J., van der Merwe, P. A., and Jones, E. Y. (2007) Structure of a tyrosine phosphatase adhesive interaction reveals a spacer-clamp mechanism. *Science* **317**, 1217-1220

46. Aricescu, A. R., Hon, W. C., Siebold, C., Lu, W., van der Merwe, P. A., and Jones, E. Y. (2006) Molecular analysis of receptor protein tyrosine phosphatase mu-mediated cell adhesion. *EMBO J* **25**, 701-712

Chapter 5

Concluding Remarks and Future Work

Receptors involved in axonal guidance have recently been identified as influential during angiogenesis, lymphangiogenesis, skeletal development, and cancer metastasis (1-4). Understanding their activation mechanisms could provide insight into the development of biological systems and may assist in rational design of cancer therapeutics. Here, we have considered two such guidance receptors, plexin A3 (PlxnA3) and neuropilin-2a (Nrp2a), and identified juxtamembrane and transmembrane (TM) interfaces that modulate receptor dimerization as well as function. Specifically, we have demonstrated that a cytosolic juxtamembrane (JM) heptad repeat in *Danio rerio* PlxnA3 modulates homodimerization and signal transduction. In particular, mutations to residue M1281 in the JM can enhance (M1281L) or disrupt (M1281F) dimerization, with the dimer-enhancing mutation exhibiting altered dimeric tendencies even in the presence of a semaphorin (sema) ligand. This mutation also fails to rescue endogenous neuronal patterning in a PlxnA3-knockout zebrafish axonal guidance assay (Chapter 2). We have also demonstrated that the PlxnA3 TM domain modulates dimerization and function by competing with dimerization induced by the JM. In particular, mutation to TM small-x_3-small interfaces enhance dimerization of the PlxnA3 TM + JM domains, while extension of the small-x_3-small interfaces disrupt dimerization. This is due to dominant role of the JM domain on TM + JM dimerization. PlxnA3 with disruptive mutations to these small-x_3-small motifs (enhanced dimerization of the TM + JM) is non-functional or only partially functional in the zebrafish

axonal guidance assay. Hence, enhancing PlxnA3 dimerization does not necessarily enhance function (Chapter 3). With *Danio rerio* Nrp2a, we have demonstrated that cysteines in the juxtamembrane MAM (meprin, A-5 protein, and protein tyrosine phosphatase μ, PTPμ) domain modulate receptor dimerization and ligand-binding. Specifically, mutations to a putative disulfide bond involving residue C711 (mutations C711S and C711S+C794S) enhance dimerization of the full-length receptor. While the double mutation binds Sema3F to a similar extent as the wild-type (WT) protein and exhibits a comparable degree of the Nrp2a overexpression phenotype in a zebrafish vascular patterning model as the WT receptor, the point mutation C711S exhibits reduced ligand binding and a lesser extent of the overexpression phenotype. Collectively, the results suggest Nrp2a residue C711 modulates receptor homooligomerization as well as function (Chapter 4).

Identification of these homomeric interfaces is only the beginning of understanding plxn and nrp signal transduction mechanisms. The work presented in this thesis provides a foundation that may further a number of additional studies, specifically investigating [1] the role of dimerization *vs.* oligomerization *vs.* ligand binding on plxn function, [2] the roles of additional residues in the PlxnA3 TM and JM domains (such as a second small-x_3-small motif in the TM domain and off-interface residues in the TM and JM domains) in modulating homooligomerization and function, [3] structural stability of the PlxnA3 TM domain and cooperative effects of the PlxnA3 extracellular, TM, and JM domains on structure, [4] cooperative effects of the Nrp2a MAM domain with the Nrp2a TM domain or other extracellular domains, [5] behavior of the Nrp2a MAM domain in solution and as a putative therapeutic, and [6] the heteromeric interaction interfaces of nrps and plxns. Application of the knowledge presented in this thesis and subsequent work may augment efforts to rationally design function-altering therapeutics to disrupt tumor growth and cancer metastasis. Additional work with a peptide-based biosurfactant (Appendix A) may also provide a starting point for rational design of

a drug delivery system for hydrophobic active ingredients likely required to modify TM domain dimerization and function.

5.1 The Role of Dimerization, Oligomerization, and Ligand-Binding on Plexin Function

The observation that PLXNA1 and NRP1 cluster upon addition of SEMA3A to chick E7 dorsal root ganglion neurons led to the premise that receptor clustering promotes plxn activity (5). Subsequent studies have since demonstrated that dimerization of the PLXNA1, A2, A4, and C1 cytosolic (CYTO) domains enhances RapGAP activity in solution (6). However, our results with PlxnA3 TM small-x_3-small and JM M1281L mutations demonstrate that enhanced dimerization does not necessarily correlate with enhanced function (Chapters 2 and 3). This may be due to a conformation or oligomeric state of the receptor not conducive to ligand binding [a trait that could be investigated via an alkaline-phosphatase assay previously described (5)], or may be indicative of an alternate activation mechanism that relies upon higher-order oligomeric states for proper function.

Traditionally, membrane protein activation is thought to be triggered by homomeric or heteromeric interactions resulting from [1] translation parallel to the membrane, [2] translation perpendicular to the membrane, [3] rotation about the membrane (resulting in alternate crossing angles between interacting membrane domains), or [4] rotation within the membrane (resulting in alternate residue exposure between interacting membrane domains) (Figure 5.1A) (7,8). A trimeric crystal structure of the PLXNB1 CYTO with an intact JM and the presence of the RhoGTPase Rac1, however, led researchers to postulate membrane-anchored plxns exist in the membrane in a trimeric state, and binding of dimeric sema extracellularly induces network formation by the combination of dimers and trimers (9). This network enhances the plxn local

concentration (Figure 5.1B), and this increase in membrane-anchored concentration causes extension or retraction of the growth cone.

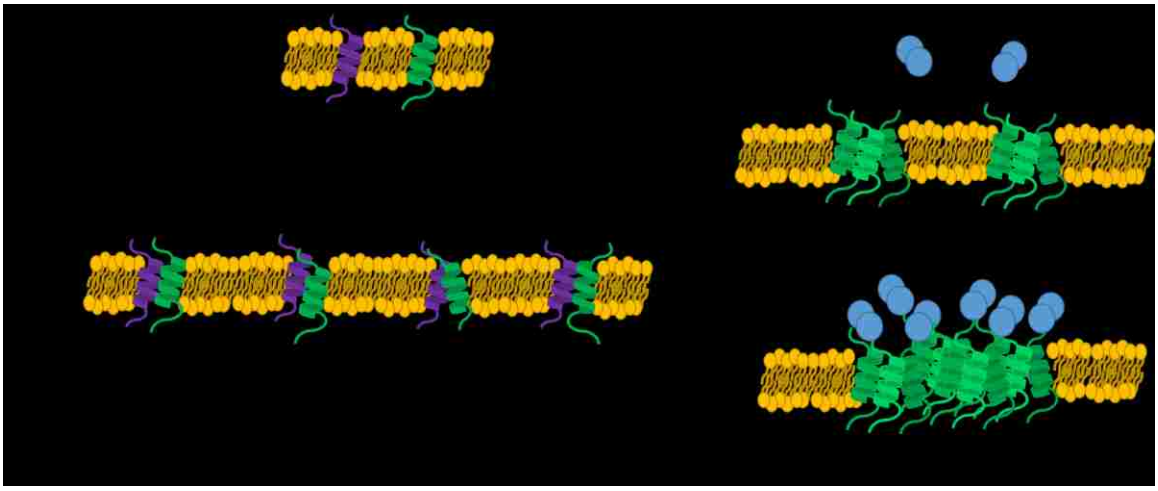

Figure 5.1. Mechanisms of transmembrane protein activation. (A) Traditionally, membrane protein activation is thought to occur through translational or rotational motion. (B) Activation of the plexin transmembrane receptor may rely upon a variation of horizontal translation that results in high local concentration due to clustering caused by a network of dimers and trimers.

Our small-x_3-small and M1281L and mutations, while enhancing PlxnA3 dimerization (Chapters 2 and 3), may fail to induce formation of a larger network. Indeed, previous work with heptad repeats have demonstrated that the location of a hydrophobic residue in a heptad repeat as well as the identity of the hydrophobic residue influences oligomeric state (10,11). For instance, a phenylalanine to methionine mutation in a synthetic phenylalanine zipper causes a shift in oligomeric state from pentamer to tetramer (10-12). Our small-x_3-small and M1281L mutations may enhance PlxnA3 homooligomerization but fail to promote network formation.

Our bioluminescence resonance energy transfer ($BRET^2$) results with the WT receptor also support such a mechanism (Chapter 2). The PlxnA3 receptors alone or co-expressed with a Nrp2a co-receptor and treated with a SEMA3F ligand exhibited similar energy transfer ratios, indicative of similar distances between PlxnA3 receptors even upon PlxnA3-Nrp2a-SEMA3F

complex formation. Our observations could be due to a number of possibilities specific to the experiment; for instance, the concentration of SEMA3F used in the experiments may not have been high enough to enhance PlxnA3 dimerization (13), or that PlxnA3 does not exhibit inherent growth cone collapse activity in the COS-7 cells used in the $BRET^2$ assay indicates co-expression with another protein in COS-7 cells is necessary to effectively assess the structure of the PlxnA3 active state (14). As our results were generated with a truncated receptor, we also cannot refute or support the possibility that the CYTO changes shape upon sema binding, as has been hypothesized (13). However, a mechanism in which the plxn CYTO does not alter shape upon sema binding to the full-length receptor, but rather the receptors form a network, has been theorized in studies with the PLXNB1 CYTO domain (9) and is consistent with our findings.

Further work examining the oligomeric state of the PlxnA3 JM in WT and mutant forms may provide additional structural insight into the plxn activation mechanism. The JM domain in isolation has been expressed and purified in our lab as a thrombin-cleavable maltose-binding protein (MBP) fusion (MBP-JM) (Figure 5.2). Purification of the JM domain from MBP, followed by size exclusion chromatography (SEC), could elucidate the oligomeric tendency of the JM domain and the effect of mutations to residue M1281 on multimer equilibrium. Additionally, understanding the oligomeric equilibrium of the full-length receptor [via immunogold labeling (15), single molecule photobleaching (16), or receptor tracking with quantum dots (17)] and how the function-altering TM and JM mutations alter this equilibrium may elucidate the plxn signaling mechanism and assist in future work entailing rational drug design targeted to manipulate plxn activity.

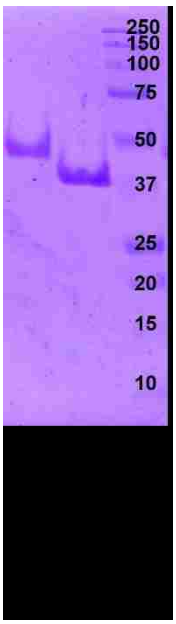

Figure 5.2. The Danio rerio PlxnA3 JM was successfully expressed and purified as a thrombin-cleavable MBP fusion. Ladder markings are in kDa. Expected molecular weights are 48.8 kDa, 42.7 kDa, and 6.1 kDa for the MBP-JM, MBP, and JM, respectively.

5.1.1 Materials and Methods

5.1.1.1 Plasmids

For the MBP-JM fusion construct, a 6-histidine tag, followed by MBP, a poly-glycine linker, and tobacco etch virus cleavage site was cloned into pET42 as an NdeI/BamHI insert. The *Danio rerio* PlxnA3 JM (amino acids 1264-1314 of NCB Accession # BAF81998.1) was subsequently cloned into this plasmid as a BamHI/XhoI insert.

5.1.1.2 Expression and Purification

BL21(DE3) cells (Invitrogen) were transformed via electroporation and stored as glycerol stocks. For expression, cultures were started from glycerol stocks and grown to saturation overnight at 37ºC in LB + 50 µg/mL kanamycin. Cells were then diluted to an optical density (600 nm) (OD_{600}) of 0.4 and allowed to grow an addition 3-6 hours at 20ºC, at which point 1 mM isopropyl β-D-1-thiogalactopyranoside (IPTG) was added to the culture. Cells were collected 16-24 hours post-IPTG induction, re-suspended in lysis buffer (100 mM HEPES, 500 mM sodium

chloride, 10 mM imidazole, and 10% (v/v) glycerol) and lysed via a freeze-thaw process followed by tip sonication. The soluble MBP-JM fusion protein was subsequently purified by nickel chromatography with chelating fast flow resin (GE Healthcare) and imidazole washes ranging from 10 mM to 500 mM in 20 mM HEPES, 500 mM sodium chloride, and 10% (v/v) glycerol. Thrombin cleavage was performed using 1 µL thrombin per 100 µL protein sample incubated at room temperature overnight on a rotisserie.

5.2 The Role of Off-Interface Transmembrane and Juxtamembrane Residues on Plexin A3 Dimerization

Our AraTM results indicate that a glycine-rich region of the PlxnA3 TM domain and a heptad repeat in the JM domain modulate receptor homodimerization (Chapters 2 and 3). Additional residues in these domains may also modulate homodimerization, however. First, the TM domain contains a second small-x_3-small motif in register with the G1246 + G1250 interface; residues involved in this motif (A1258 and A1262) may also contribute to modulation of receptor dimerization (Figure 5.3A). This second small-x_3-small motif is not conserved across species or plxns, but may affect homodimerization of *Danio rerio* PlxnA3. Second, the *Danio rerio* PlxnA3 TM domain contains a fifth, off-interface glycine in the glycine-rich region (G1249) that may modulate receptor dimerization and function (Figure 5.3A). Finally, in the JM domain, side chain interactions between off-interface residues of heptad repeats cause formation of coiled-coils, with salt bridges stabilizing the hydrophobic core of the heptad repeat (10). As such, amino acids adjacent to the JM hydrophobic core may also modulate dimerization. Furthermore, the JM domain of class A plxns contains a conserved off-interface hydrophobic residue (methionine or leucine; L1279 in *Danio rerio* PlxnA3) that may compete with the hydrophobic core of the heptad repeat as a modulation mechanism for dimerization (Figure 5.3A-C).

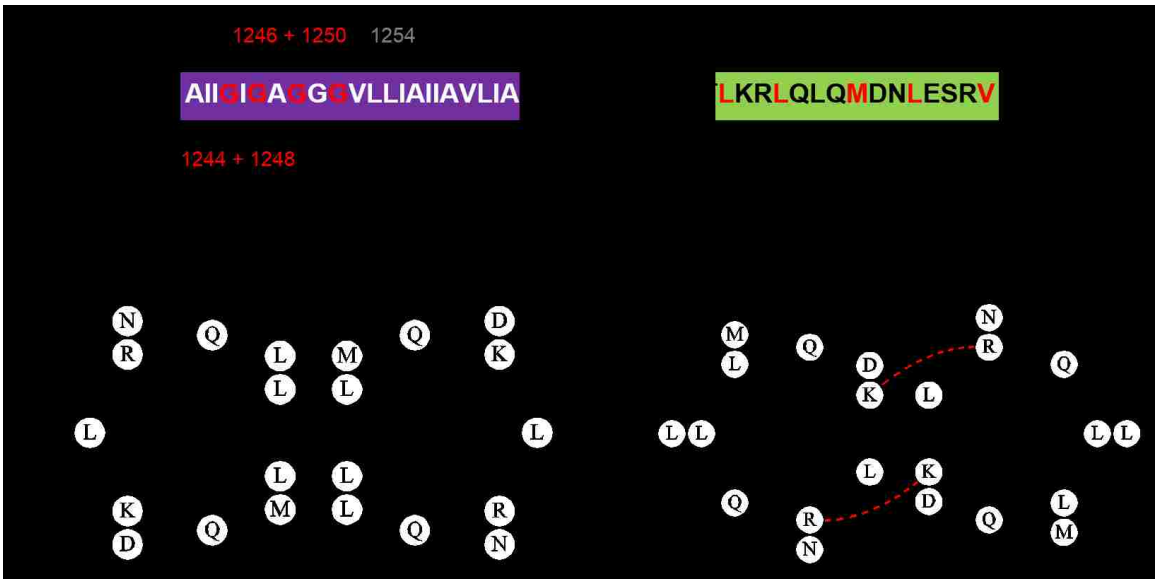

Figure 5.3. Off-interface residues in the TM and JM may modulate receptor dimerization. (A) Sequence of the *Danio rerio* PlxnA3 TM (purple) and JM (green) domains. Two small-x_3-small interfaces in the TM domain and a heptad repeat in the JM domain (red font) modulate TM + JM dimerization (Chapters 2 & 3). Additional off-interface residues, such as G1249 and A1255 in the TM domain, or R1276 and L1279 in the JM domain, may modulate dimerization. Another small-x_3-small interface in-frame with G1246 + G1250 (A1258 + A1262) may also modulate dimerization. (B) Helical wheel diagram of the PlxnA3 JM domain with the heptad repeat at the core of the dimer interface (Chapter 2). (C) Helical wheel diagram of the PlxnA3 JM domain with an alternative leucine (L1279) at the dimer core and predicted disruptive electrostatic interactions (K1275 + R1276) de-stabilizing the interaction. Helical wheel diagrams and salt bridge prediction were generated using DrawCoil 1.0.

Using the AraTM assay performed as described in Chapters 2 and 3 and considering the small-x_3-small motif in the PlxnA3 TM domain in register with the G1246 + G1250 interface (A1258 + A1262), we observe that mutation A1258L also slightly enhances dimerization of the TM + JM domain (Figure 5.4). This is consistent with the model in which dimerization via small-x_3-small motifs in the PlxnA3 TM domain competes with JM-driven dimerization. Mutation to these small-x_3-small packing motifs enhances dimerization by allowing the dominant JM dimer to form (Chapter 3).

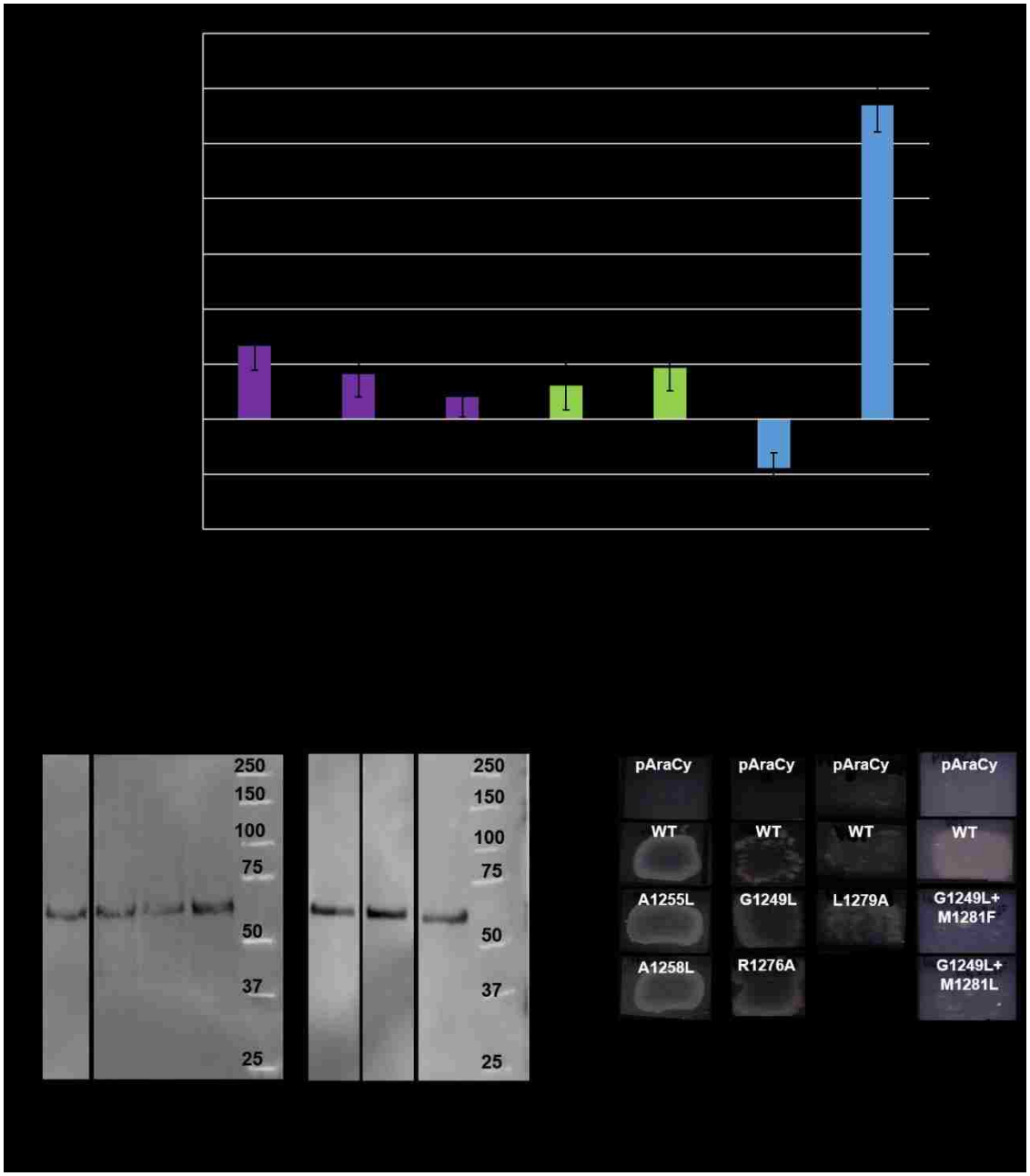

Figure 5.4. Off-interface residues TM and JM residues contribute to dimerization. (A) Off-interface residues in the TM (purple) and JM (green) modulate TM + JM dimerization in the AraTM assay. JM mutations (M1281F and M1281L, Chapter 3) dominate in mutations to both the TM and JM domains (blue). Error bars indicate standard error as determined from a minimum of twelve replicates collected over the course of three experiments. (B) Anti-MBP (1:10,000 dilution, NEB) western blots confirming expression of PlxnA3 TM + JM mutants. Expected molecular weight ~67 kDa. Portions of these western blots appeared in Chapters 2 (right) and 3 (left). (C) Maltose complementation tests on PlxnA3 TM + JM constructs. Each column represents a separate plate. Portions of the plates (the WT or pAraCy controls) may have appeared in Chapters 2 and 3.

Interestingly, off-interface mutation G1249L also enhances dimerization of the *Danio rerio* PlxnA3 TM + JM domains in the AraTM (Figure 5.4). Previous studies with small-x_3-small motifs suggest that large, aliphatic residues (predominately isoleucine and valine, but also leucine) immediately flanking small residues participating in small-x_3-small motifs enhance homomeric interactions (18). This triplet pattern is also overrepresented in a database of transmembrane proteins (19). Hence, mutation G1249L possibly enhances dimerization of the small-x_3-small interfaces. This is in contrast to our previous results in which enhancement to the small-x_3-small interfaces disrupts dimerization of the TM + JM domains (Chapter 3), however, suggesting additional insight is required regarding the mechanism of G1249L enhancement to TM + JM dimerization. In agreement with our previous results (Chapter 3), the impact on dimerization due to mutation G1249L with JM mutations trends the same as JM mutations alone, implying dominant JM-driven dimers in the TM + JM system. Mutation to residue A1255L, also off-interface to all putative small-x_3-small motifs in the PlxnA3 TM domain, also enhances dimerization of the TM + JM domains in the AraTM assay (Figure 5.4). Collectively, these results imply the overall presence of small amino acids in the PlxnA3 TM domain de-stabilize TM + JM dimerization. Possibly, the prevalence of small amino acids allows for close TM-packing of higher-order than dimer, such as the trimer postulated from the crystal structure of the PLXNB1 CYTO (9), which subsequently de-stabilizes JM-driven dimerization (dominant in the AraTM assay, Chapter 3).

Considering off-interface residues of the PlxnA3 JM domain, we observe that mutation L1279A enhances dimerization of the PlxnA3 TM + JM domains in the AraTM assay (Figure 5.4). This is consistent with L1279 being solvent-exposed and in competition with the heptad repeat residues; reduction of the hydrophobic competition through mutation L1279A enhances dimer formation. Mutation R1276A, a mutation to a predicted off-interface residue, also resulted in enhanced oligomerization. Interestingly, this mutation is predicted to remove a putative

repulsive electrostatic interaction between R1276 and K1275 on PLXNA3 JM domains dimerized with L1279 in the hydrophobic core, as determined using DrawCoil 1.0 (Figure 5.3) (11). Hence, residues L1279 and R1276 likely modulate stability of a competitive dimerization motif in the PlxnA3 JM, with appropriate mutation to either enhancing overall dimerization of the TM + JM domains.

Collectively, our results indicate the PlxnA3 TM + JM domains contain a number of additional residues (G1249, A1255, A1258, R1276, and L1279) that disrupt overall TM + JM dimerization. As functional studies suggest strong dimerization inhibits PlxnA3 function (Chapters 2 and 3), these residues likely contribute to modulation of PlxnA3 activity. By inhibiting strong dimerization of the JM domain, these residues allow for PlxnA3 switchability, between active and inactive states as well as amongst co-receptors. Similar specific, but weak interactions govern integrin heterodimerization and function (20). Additional insight regarding the effect of mutations G1249L and A1255L on TM + JM dimerization mechanisms, as well as additional functional tests with mutations A1255L, R1276A, and L1279A (*refer to Section 5.3 for G1249L functional tests*) may further elucidate the mechanisms modulating PlxnA3 activity.

5.3 Structural Stability of the Plexin A3 Transmembrane Domain and Cooperative Effects on Dimerization and Function

Our AraTM results for the PlxnA3 TM and JM domains (Chapters 2 and 3) suggest the intrinsic structures of the two domains compete: the heptad repeat in the JM domain enhances dimerization (Chapter 2), while the surplus of glycines in the TM domain disrupts dimerization (Chapter 3 and Section 5.2). Furthermore, mutations to both the TM and JM domains result in non-additive AraTM signals (Figure 5.5), suggesting domain cooperativity.

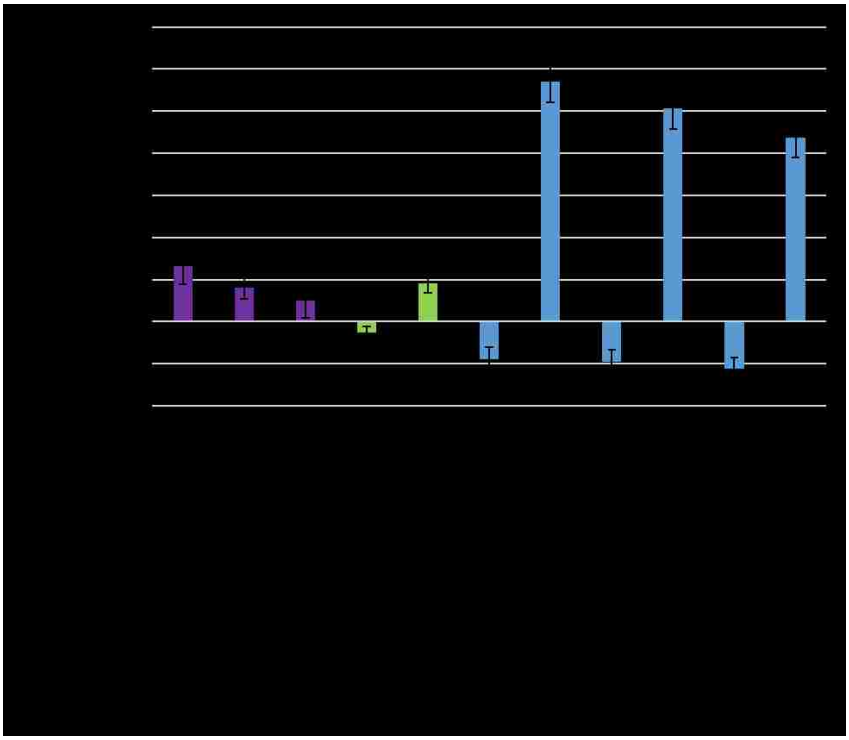

Figure 5.5. Mutations to both TM and JM domains (blue) are non-additive from TM mutations alone (purple) and JM mutations alone (green). Values originally appeared in Chapters 2 and 3 and Section 5.2 and are re-plotted here for clarification.

While quaternary structure is likely to depend on TM and JM domain cooperativity, it is also possible that the domain proximity influences the stability of secondary and tertiary structures. While tertiary and quaternary structure are difficult to de-couple without a means to assess tertiary structure (such as crystal structure determination or small-angle x-ray scattering), secondary structure can be assessed via circular dichroism. Due to the hydrophobicity and low dielectric constant of the membrane environment, secondary structure in TM domains is more stable than in proteins in an aqueous environment (21). Backbone hydrogen bonding, resulting in α-helices and β-sheets, provides energetic recompense for the dehydration of the peptide bond in a hydrophobic environment (22). Hence, single-spanning membrane proteins, such as plxns, are generally considered α-helical. While the glycines in the PlxnA3 TM would be considered 'helix-breakers' in an aqueous environment due to the entropic costs of confining glycine in a

secondary structure (23), the enthalpic benefit from backbone hydrogen bonding induced by secondary structure in a membrane environment allows for their incorporation in membrane α-helices (24). Indeed, glycines are commonly found at the core interfaces of membrane protein dimers due to their small size and enhanced ability to participate in α-carbon hydrogen bonds (18,19,24-27).

Investigation of the secondary structure of the PlxnA3 TM domain indicates a propensity for the domain to form β-sheets in FOS-Choline-15 micelles in the absence of the juxtamembrane domains for concentrations of 0.2-0.6 mg/mL and temperatures of 4ºC -47ºC (Figure 5.6A-B), likely due to aggregation. Addition of 40% tetrafluoroethylene or examination of the peptide in a 1,2-dimyristoyl-*sn*-glycero-3-phosphocholine (DMPC)/1,2-dihexanoyl-*sn*-glycero-3-phosphocholine (DHPC) bilayer induces the anticipated α-helical structure (Figure 5.6C-D). Investigations regarding the structural stability of the PlxnA3 TM peptide in a bicelle, in WT and mutant form, may provide additional insight regarding plxn signaling mechanisms. The presence of the JM heptad repeat [an α-helix, PDB # 3IG3, (13)] may also influence structural stability of the TM domain. The *Danio rerio* PlxnA3 TM + JM domain has been successfully expressed and purified as a thrombin-cleavable ompF-fusion protein (Figure 5.7). Purification of the TM + JM domain from ompF could provide insight into cooperative effects on secondary structure stability. Stoichiometry studies, such as SEC or cross-linking SDS-PAGE, using a purified TM + JM, a purified JM, and the TM peptide available in our lab may also elucidate the putative cooperative role of the TM and JM on modulation of PlxnA3 oligomerization and function.

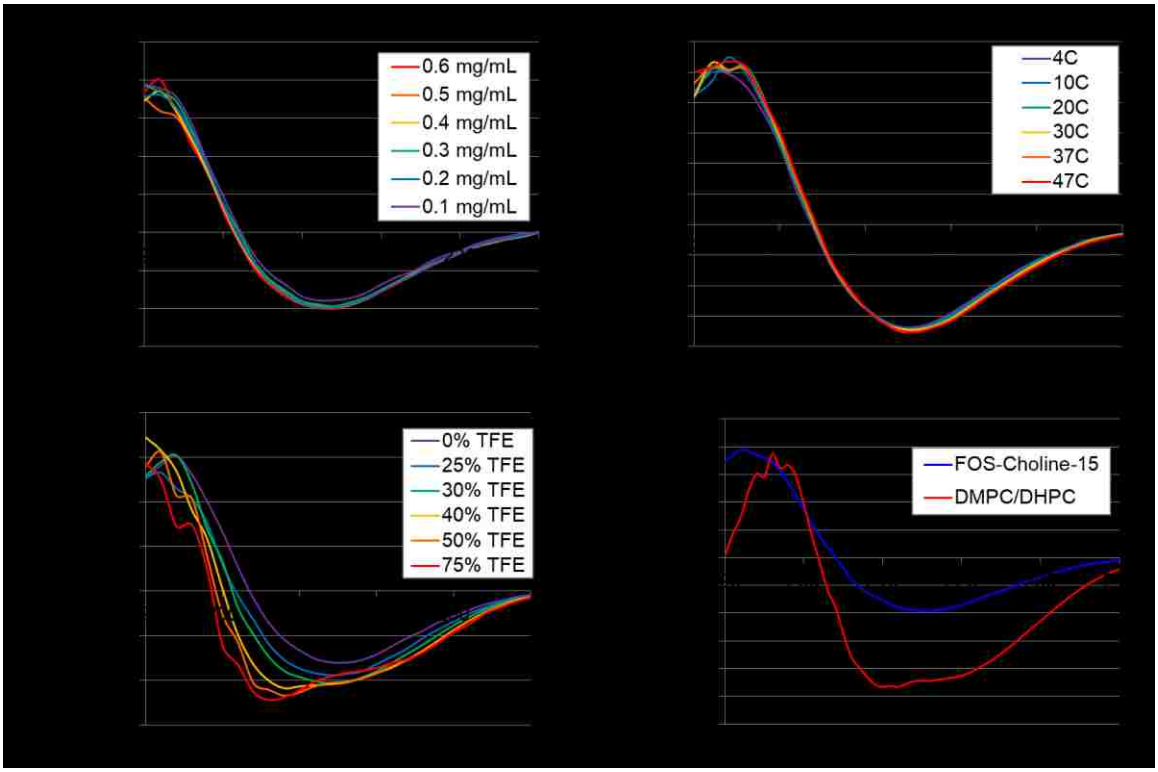

Figure 5.6. CD spectra of the *Danio* rerio PlxnA3 TM domain (A) at various concentrations in FOS-Choline-15, (B) at various temperatures (0.3 mg/mL in FOS-Choline-15), (C) with TFE in (0.3 mg/mL in FOS-Choline-15), and (D) at 0.3 mg/mL in FOS-Choline-15 micelles or DMPC/DHPC bicelles.

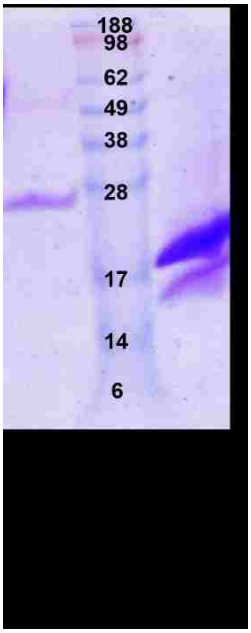

Figure 5.7. The *Danio rerio* PlxnA3 TM + JM was successfully expressed and purified as a thrombin-cleavable ompF fusion. Ladder markings are in kDa. Expected molecular weights are 26.8 kDa, 17.4 kDa, and 9.4 kDa for the ompF-TM + JM, ompF, and TM + JM, respectively.

Additionally, though the JM domain dominates in the TM + JM system (Chapter 3), and mutations to the JM domain in the context of the TM + JM in the AraTM assay agree with BRET^2 results for the TM + JM domains with an intact extracellular domain (Chapter 2), the influence of the TM mutations on a receptor with an intact extracellular domain have not been investigated. That select TM mutations exhibit partial functionality (G1244L+G1248L) whereas others exhibit no functionality (G1246L+G1250L), though both enhance dimerization, implies the possibility of an additional role for these motifs in full-length receptor function. Furthermore, TM mutations exhibit the dominant functional effects, despite JM dominance in TM + JM dimerization (Table 5.1).

Table 5.1. Percentage of Embryos Exhibiting *sidetracked* Phenotype[5a]

Type of Injection	Number of Embryos Examined	Percentage of Embryos Exhibiting the *set* phenotype	P-value Compared to Uninjected	P-value Compared to WT *plxnA3* RNA-injected	Description of Result
Uninjected[5b]	30	80	1	0.003	Non-functional
WT *plxnA3* RNA[5b]	22	36	0.003	1	Functional
M1281F *plxnA3* RNA[5b]	12	33	0.009	1	Functional
M1281L *plxnA3* RNA[5b]	12	50	0.07	0.5	Partially Functional
G1244L + G1248L *plxnA3* RNA[5c]	13	62	0.3	0.2	Partially Functional
G1246L + G1250L *plxnA3* RNA[5c]	19	74	0.7	0.03	Non-functional
G1249L *plxnA3* RNA	14	79	1	0.003	Non-functional

[5a]P-values were determined using Fisher's Exact Test.
[5b]Values were previously reported in Chapter 2.
[5c]Values were previously reported in Chapter 3.

BRET^2 results indeed suggest the PlxnA3 small-x$_3$-small TM interfaces are non-equivalent in the context of the full extracellular, TM, and JM domains (Figure 5.8). In contrast

to AraTM results with just the TM + JM anchored in a bacterial membrane, in which mutations G1244L + G1248L and G1246L + G1250L both enhanced dimerization (Chapter 3), in a mammalian membrane with the intact extracellular domain, mutation G1244L + G1248L does not exhibit significant changes to dimerization relative to the WT receptor, and mutation G1246L + G1250L disrupts dimerization (Figure 5.8). This is in agreement with functional test results with the zebrafish embryo axonal guidance assay, in which injection of G1244L + G1248L *plxnA3* RNA into *sidetracked* (*set*) embryos resulted in partial functionality, with the number of embryos exhibiting the *set* phenotype being not significantly different from the number of embryos injected with WT *plxnA3* RNA. Significantly more *set* embryos injected with G1246L + G1250L *plxnA3* RNA exhibited the *set* phenotype than those injected with WT *plxnA3* RNA (Table 5.1), also in agreement with the BRET^2 results.

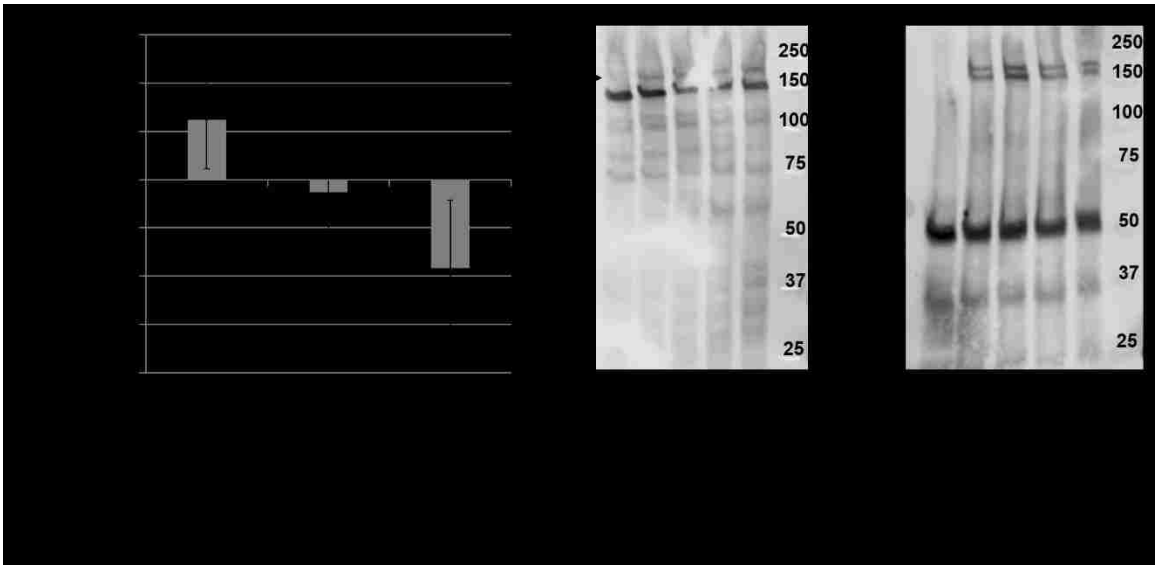

Figure 5.8. Select mutations to the Plexin A3 TM domain influence homooligomerization with a full extracellular domain intact (A) BRET^2 results. Error bars indicate standard error determined from a minimum of forty-six replicates collected over the course of six experiments. Expression of PlxnA3 BRET^2 constructs. (B) Anti-RLuc (1:1,000 dilution, Millipore) western blot of PlxnA3 BRET^2 transfections. Expected molecular weight ~185 kDa (R). (C) Anti-GFP (1:1,000 dilution, Clontech) and anti-tubulin (1:1,000 dilution, Abcam) western blot of PlxnA3 BRET^2 transfections. Expected molecular weights ~176 kDa (PlxnA3-GFP^2, G) and ~50 kDa (tubulin, T).

The disruption to PlxnA3 dimerization by G1246L + G1250L in the BRET^2 assay is also in agreement with studies on the small-x_3-small TM motifs in glycophorin A (GpA) and NRP1, in which mutation to the small-x_3-small packing motif disrupted receptor dimerization (28,29). Hence, with the extracellular domain intact, the TM interface G1246 + G1250 serves to drive receptor dimerization, even with the dominant JM-driven dimer observed in the AraTM assay (Chapter 3). It is therefore possible that the extracellular domain also plays a cooperative role in modulating receptor dimerization.

To further understand the role of mutations to the TM domain on dimerization with an intact extracellular domain, we examined the *Danio rerio* PlxnA3 mutant G1249L in the BRET^2 assay. Similar to AraTM results with the TM + JM domain (Section 5.2), mutation G1249L enhances dimerization of the TM + JM domains with an intact extracellular domain (Figure 5.8). These results are consistent with previous studies of small-x_3-small motifs in which a valine, isoleucine, or leucine immediately adjacent to residues participating in small-x_3-small motifs (*e.g.*, mutation G1249L is adjacent to interfaces G1244 + G1248 and G1246 + G1250) enhances dimerization (18). Hence, in a receptor with the full extracellular domain, mutant G1249L may enhance the small-x_3-small packing motif for either the G1244 + G1248 or G1246 + G1250 interface through enhancement of the ridge in the ridge-and-groove structure characteristic of this motif. Furthermore, in the zebrafish axonal guidance assay, *plxnA3* RNA injections with the G1249L mutation also fail to rescue WT motor neuron patterning, exhibiting no functionality in the assay (similar to mutation G1246L+G1250L) (Table 5.1). This result validates a role for the PlxnA3 TM in modulation of receptor dimerization and subsequent function.

Collectively, these results corroborate earlier findings (Chapters 2 and 3) that enhanced PlxnA3 dimerization does not enhance function of the receptor (mutation G1249L; Figure 5.8 and Table 5.1). Additionally, our BRET^2 results indicate disruption to the small-x_3-small interface G1246 + G1250 disrupts dimerization of the PlxnA3 TM + JM upon inclusion of the full

extracellular domain, in contrast to our AraTM results (Chapter 3). This result implies cooperativity of the extracellular domain with the TM + JM domains in modulation of receptor dimerization. As deletion of the PLXNA1 sema-binding domain renders the PLXNA1 receptor constitutively active (14), the sema-binding domain may also serve to modulate receptor dimerization in the absence of ligand. Additional $BRET^2$ studies with a full CYTO domain, in addition to investigations with TM structural stability, may further elucidate the mechanism of plxn activation.

5.3.1 Materials and Methods

5.3.1.1 Plasmids and Peptides

For the ompF-TM + JM fusion, the *Danio rerio* PlxnA3 TM + JM (amino acids 1241-1314 of NCB Accession # BAF81998.1) was cloned into pOmpF (30) as a SacI/XhoI insert. The TM peptide (amino acids 1238-1263 of NCB Accession # BAF81998.1, with two flanking lysines on each end) was synthesized at the University of Pennsylvania. $BRET^2$ constructs were cloned as previously described (Chapter 2) (31).

5.3.1.2 Expression and Purification of ompF-TM + JM

BL21(DE3) cells (Invitrogen) were transformed with the pOmpF plasmid containing the TM + JM insert via electroporation and stored as glycerol stocks. For expression, cultures were started from glycerol stocks and grown to saturation overnight at 37ºC in LB + 50 µg/mL kanamycin. Cells were then diluted 1:1000 into ZYP + 50 µg/mL kanamycin and allowed to grow overnight at 37ºC. Cells were collected 16-24 hours post-dilution, washed once in cold 1x PBS, then re-suspended in cold PBS and lysed via a freeze-thaw process followed by tip

sonication. Following sonication, the insoluble fraction was collected by centrifugation at 18000g for 10 minutes.

The ompF-TM + JM fusion protein was subsequently solubilized in 2% sarkosyl in 20 mM Tris (pH 8) by shaking incubation at 37ºC for 15 minutes, bath sonication for 15 minutes, and an additional shaking incubation at 37ºC for 15 minutes. Centrifugation was used to separate the soluble and insoluble fractions. The soluble fraction was subsequently passed over a nickel chromatography column with chelating fast flow resin (GE Healthcare), washing the material with 10 column volumes of 10 mM imidazole in 2% sarkosyl in 20 mM Tris (pH 8), then one column volume each of 50, 100, 300, and 500 mM imidazole in 1% FOS-Choline-15 in 20 mM Tris (pH 8). Thrombin cleavage was performed using 1 µL thrombin per 100 µL protein sample incubated at room temperature overnight on a rotisserie.

5.3.1.3 BRET^2 Assay

Transfections, growth conditions, and measurement conditions for truncated PlxnA3 homooligomerization in the BRET^2 assay were previously described (Chapter 2) (31). Results are reported as the average percent change in the ratio of green to magenta luminescence measurements from WT samples analyzed in parallel. Only samples with total luminescence values greater than that of the average mock total luminescence for that round were included in analyses. Results were collected from six separate transfections for each condition and a minimum of seven wells per transfection. Error bars indicate standard error, calculated as described for the AraTM assay.

5.4 Cooperative Effects of the Neuropilin-2a MAM Domain with Other Intramolecular Domains

Our BRET^2 results with the full-length *Danio rerio* Nrp2a receptor indicate select cysteine mutations in the MAM domain enhance receptor dimerization (Chapter 4). Previous studies with the NRP1 TM domain also indicate the importance of a double small-x_3-small motif in NRP1 TM-driven dimerization (29). The Nrp2a TM sequence is similar to that of Nrp1; however, an alanine insertion alters the small-x_3-small motif and introduces an alternative small-x_3-small packing mode (Figure 5.9). To quickly screen the influence of additional cysteines in the MAM domain on receptor dimerization, as well as select TM domain residues, we analyzed WT and mutant forms of the *Danio rerio* Nrp2a MAM-TM-CYTO domains in the AraTM assay as described in Chapters 2 and 3.

Figure 5.9. *Danio rerio* Nrp1 and Nrp2a transmembrane sequences. Nrp1 exhibits two small-x_3-small motifs (red). An alanine insertion in the Nrp2a transmembrane sequence yields an additional small-x_3-small motif (blue).

Our results indicate that mutation of any glycine capable of participating in small-x_3-small interactions in the Nrp2a TM domain disrupts MAM-TM-CYTO dimerization (Figure 5.10), implying the TM domain may be capable of interacting through multiple small-x_3-small motifs. This flexibility may contribute to switchability between co-receptors.

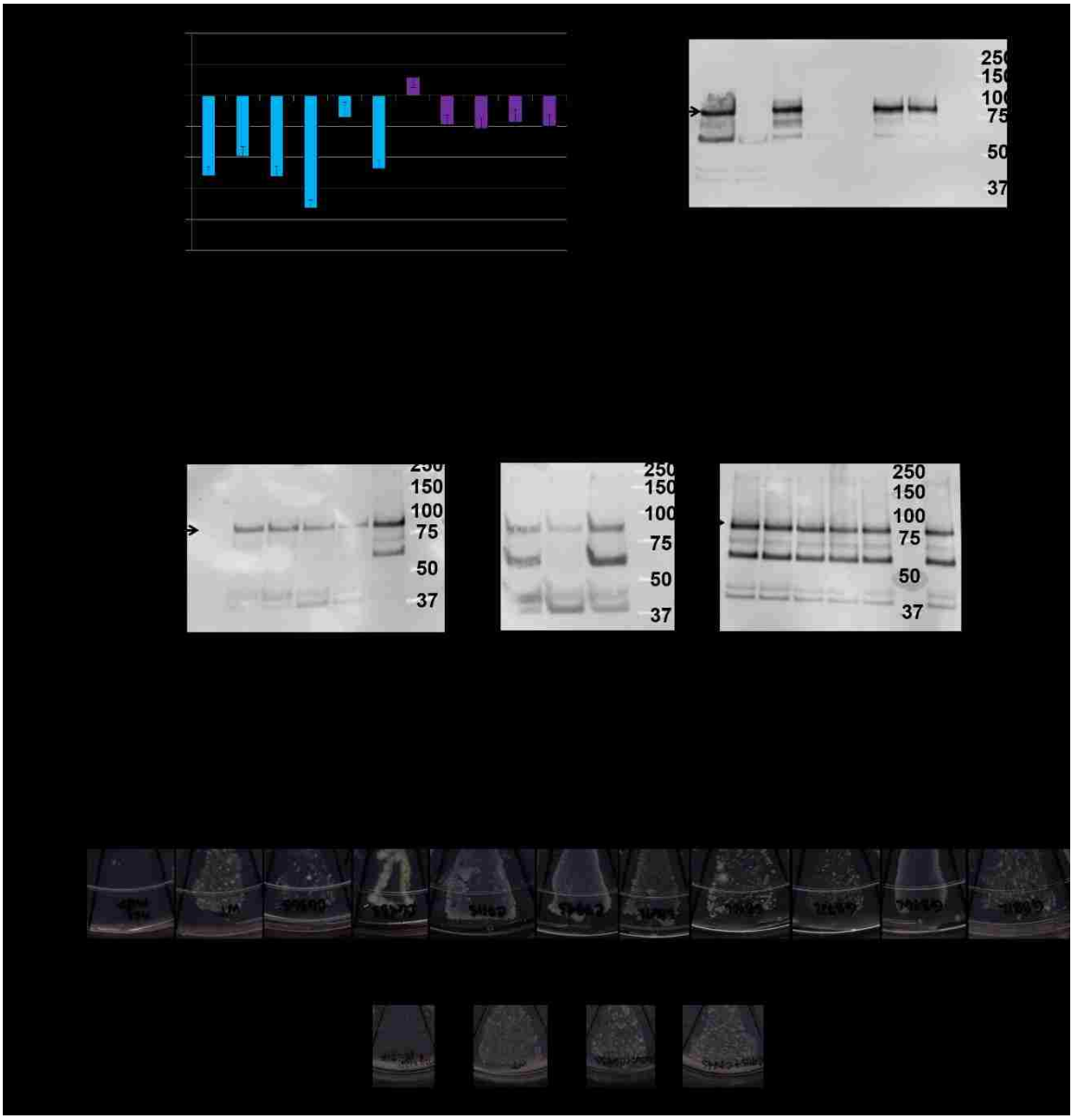

Figure 5.10. Mutations to the Nrp2a MAM and TM domains alter MAM-TM-CYTO homodimerization in the AraTM assay. (A) Specific residues in the Nrp2a MAM (blue) and TM (purple) domains modulate homodimerization of the MAM-TM-CYTO domains, as determined using the AraTM assay. Results were collected over the course of at least three experiments and error bars indicate standard error. (B) An anti-MBP western blot on samples from a spheroplast protection assay reveals WT Nrp2a MAM-TM-CYTO is correctly oriented in the cell membrane. WC = whole cell lysate, P = periplasm, SP = spheroplast, S = supernatant, PK = Proteinase K, NP40 = Nonidet P-40. Ladder markings are in kDa, Nrp2a MAM-TM-CYTO is ~ 92 kDa. (C) Anti-MBP western blot of AraTM constructs, as expressed by SB1676 cells in AraTM measurements. (D) Mutant constructs orient themselves correctly in the cell membrane, as determined by a maltose complementation test (growth on a plate with maltose as the sole sugar source signifies correct orientation).

Considering MAM domain cysteine mutations in the context of the MAM-TM-CYTO domain in a bacterial membrane, modest disruption (>20% of WT signal) to dimerization occurred for mutations C636S, C643S, and C711S, with greater disruptive effects (>30% of WT signal) observed for C794S (Figure 5.10). The double mutant C711S + C794S also disrupted Nrp2a MAM-TM-CYTO dimerization, whereas the double mutant C636S + C643S had negligible effect on dimerization. These results are broadly consistent with the observation that the disulfide bonds involving C711S and C794S regulates MAM oligomeric state (Chapter 4). While the magnitude of change from WT is similar to that exhibited by the mutations in the full-length receptor in the $BRET^2$ assay (Chapter 4), the directionality is inversed (cysteine mutations to full-length Nrp2a enhance dimerization of the full-length receptor, Chapter 4, but disrupt dimerization of the MAM-TM-CYTO, Figure 5.10) (Figure 5.11). Hence, while our results indicate an importance for cysteines in the regulation of MAM oligomerization, the mechanism by which MAM disulfide bonds directly affect receptor clustering is unclear, though all results indicate an importance for residue C711. Our AraTM results suggest that intact disulfide bonds promote dimerization of the MAM-TM-CYTO domain, whereas our $BRET^2$ results suggest a disulfide bond involving C711 disrupts dimerization of the intact MAM domain and the full-length receptor. It is also important to note that the inversion between AraTM and $BRET^2$ results with Nrp2a are thus far specific to the MAM domain; mutation to the Nrp2a TM small-x_3-small motif disrupted dimerization in both assays (Figure 5.11). The differences could be explained by differences in the assays and/or by domain cooperativity.

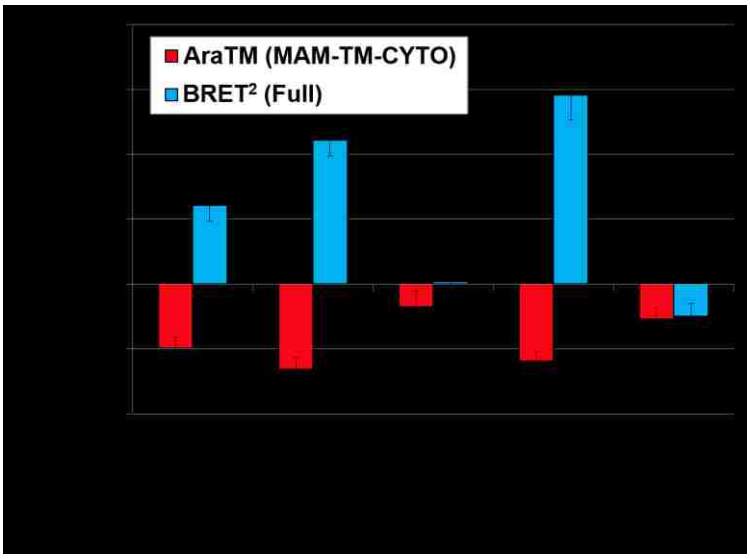

Figure 5.11. A comparison of Nrp2a MAM-TM-CYTO constructs in AraTM and full-length constructs in BRET^2 suggest mutations to the TM domain (G872L) disrupt homodimerization in both assays, suggesting the switch from dimer-disrupting (AraTM) to dimer-enhancing (BRET2) was specific to MAM domain mutations. Error bars indicate standard error. Mutations are those presented in Chapter 4 and Figure 5.10, re-plotted for comparative purposes.

The principles governing reporter mechanisms for the AraTM and BRET^2 assays are fundamentally different. The AraTM assay depends upon dimerization forming a functional promoter, whereas the BRET^2 assay relies upon distance between interacting receptors. Hence, the impact of receptor clustering *vs.* dimerization may impact the two assays differently. When assessed via NativePAGE, less of the GFP^2-fused C711S BRET^2 construct runs at the apparent molecular weight of a dimer (compared to the WT protein) (Figure 5.12). Given similar expression levels (Chapter 4), this suggests C711S tends to form higher-order structures. This possibility does not broadly explain the BRET^2 and AraTM discrepancies (Figure 5.11), however, as point mutant C643S and double mutants C636S + C643S and C711S + C794S all display similar oligomerization patterns to WT (Figure 5.12). As another possible difference between the BRET^2 and AraTM assays, while maltose complementation tests and the spheroplast assay confirmed orientation of the AraTM constructs in bacterial cells (Figure 5.10), surface expression

of the BRET^2 constructs was not confirmed. If the cysteine mutations disrupted receptor folding, they may have altered receptor trafficking. A high intracellular concentration of mutant Nrp2a constructs in the BRET^2 assay may have resulted in an artificially high signal.

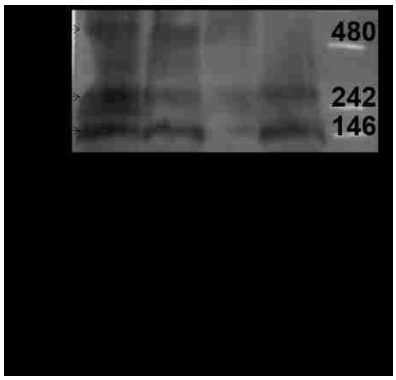

Figure 5.12. A NativePAGE western blot of Nrp2a-GFP^2 constructs suggest the full-length receptor homo-oligomerizes, and MAM mutant C711S promotes homomeric aggregation. Ladder markings in kDa, expected molecular weight of monomeric WT NRP2-GFP^2 is 130 kDa. Apparent molecular weights are marked as M (monomer), D (dimer), and T_4 (tetramer).

Alternatively, domain cooperativity may explain the apparent discrepancy in AraTM and BRET^2 results (Figure 5.13). The small-x_3-small TM dimerization motif, for instance, may compete with the MAM-driven dimer, with the net effect resulting in a decrease in MAM-TM-CYTO dimerization with the MAM dimer-stabilizing mutations C711S and C711S + C794S. Such a mechanism was observed with PlxnA3 TM and JM domains (Chapter 3). Additional studies suggest the NRP1 MAM-TM-CYTO domain cannot co-immunoprecipitate (co-IP) membrane-anchored, glycophosphatidylinositol-linked NRP1 CUB-FA V/VIII-MAM domains, further indicating the possibility that MAM domain interactions can be disrupted by the presence of other NRP domains or that TM domain interactions are strong enough to prevent MAM interactions (32). Comparing previous NRP1 domain-deletion experiments, where deletion of the MAM domain alone allowed for co-IP of NRP1 (32), but deletion of an additional N-terminal 57 nucleotides eliminated this ability (33), results would suggest the region between the MAM

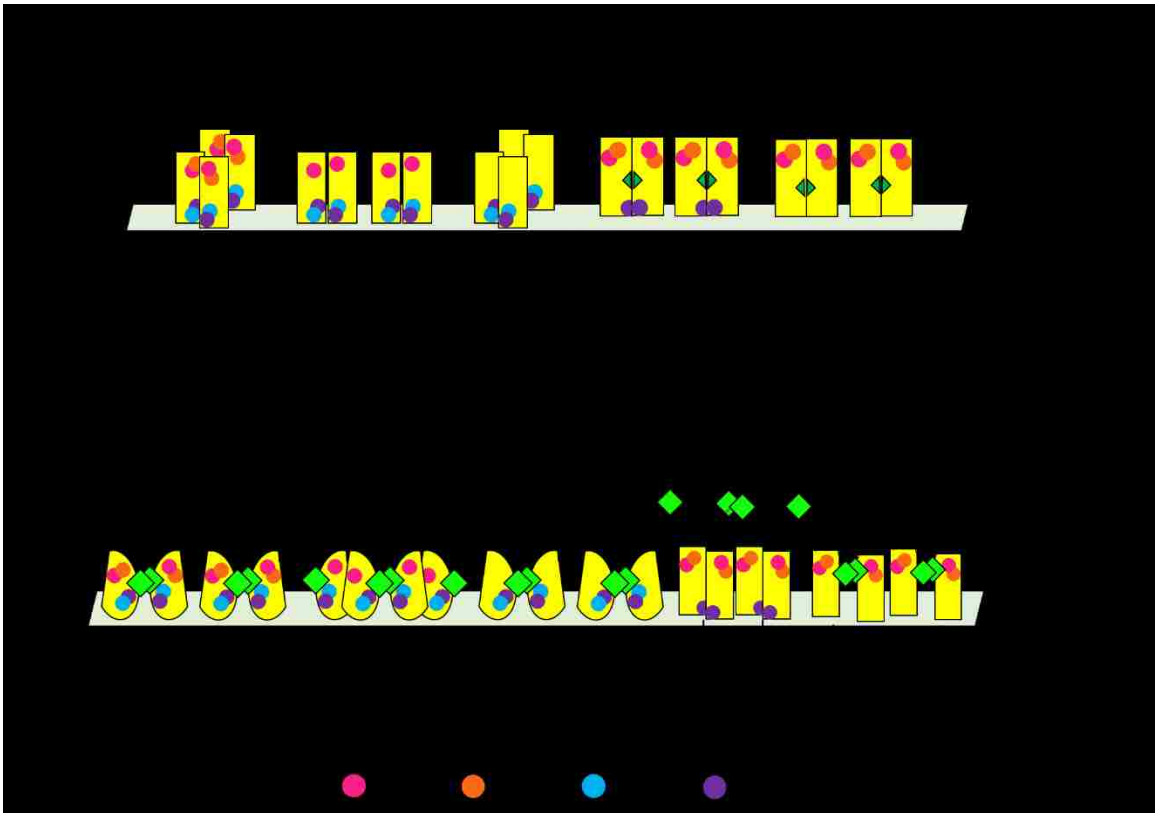

Figure 5.13. Cooperative effects between the MAM domain and other domains may define oligomeric state and conformation of the full-length receptor. (A) In the context of MAM-TM-CYTO (*AraTM assay*), mutations to select cysteines disrupt dimerization. MAM-driven dimerization (via disulfide bonds, *circle pairs*, or another driving force, *green triangle*) may compete with TM-driven dimerization (*arrows*). An intact C711 and C794, no lone cysteines, and shielding of other driving forces (e.g., *burial of the green triangle by intact C711 and C794 disulfide bonds*) allow for native TM interactions. (B) In the full-length receptor (*BRET*^{2} *assay*), select cysteine mutations enhance dimerization. Residues C711 and C794 may cooperate with another extracellular domain, defining the overall shape (e.g., *semi-ovals* vs. *squares*). A requirement to satisfy disulfide bonds (*C643S and C711S*) or better shape complementarity (*C711S + C794S*) may bring receptor cytosolic domains closer together. The requirement to satisfy disulfide bonds, combined with an overall change in receptor shape, may also disrupt ligand binding (*C711S, Chapter 4*).

domain and second FA V/VIII domain may play a cooperative role with the MAM domain to regulate receptor dimerization. Interestingly, previous research indicates that this linker region contains an O-linked glycosylation site necessary for chemotactic migration of mature dendritic cells, suggesting glycosylation likely also plays a role in NRP function, though whether it also influences homooligomerization and other functions remains to be determined (34-36). The

hypothesis that other domains likely cooperatively influence Nrp2a MAM domain interactions and alter full-length receptor clustering is also consistent with previous studies on PTPμ, in which the MAM domain and a C-terminal Ig domain form a structural unit, and cooperativity of this unit with fibronectin type III repeats is necessary for homomeric interactions and functionality (37). Furthermore, a disulfide bond between PTPμ MAM residues C96 and C182 (homologous to residues C711 and C794 in the *Danio rerio* NRP2a MAM domain) stabilizes interdomain interactions and an L-shaped structure in the PTPμ extracellular domain (38). Thus, a disulfide bond involving C711 may form additional interactions with residues in adjacent domains to regulate the dimeric versus oligomeric state. Our studies thus far do not distinguish between the mechanisms, but do suggest that residue C711 is important for defining the oligomeric state of Nrp2a, which is critical for nrp-pxln-sema signaling (Chapters 2-4).

A number of additional studies could be used to confirm the discrepancy between the AraTM and $BRET^2$ results and elucidate the possibility of cooperativity between the MAM domain and other domains. Mutations to both the MAM domain and the small-x_3-small motifs in the TM domain could elucidate which motif dominates MAM-TM-CYTO dimerization (as was done to the PlxnA3 TM and JM domains to determine that the JM-driven dimer dominates in the TM + JM system, Chapter 3). Confirmation of surface expression in the $BRET^2$ assay via biotinylation studies or surface antibody labeling may also provide insight into the cause of the discrepancy. Expression and purification of the Nrp2a extracellular domain in both WT and mutant form, followed by small angle x-ray scattering, may provide structural information regarding the role of MAM domain cysteines on overall shape of the extracellular domain. Such a construct was successfully cloned into a pET28a vector in our lab; however, as bacterial expression systems have not yet been proven to generate a properly-folded receptor, re-cloning into a plasmid suitable for mammalian or insect cell expression may be required for accurate structural studies. Finally, Nrp2a WT, C711S, and C711S + C794S MAM-TM-CYTO constructs

(rather than the full extracellular domain) could be analyzed in the BRET^2 assay and compared to results from the AraTM assay. In the event that the MAM-TM-CYTO BRET^2 constructs exhibit surface expression and cysteine mutations as dimer-disrupting, consistent with the AraTM assay, cloning the constructs depicted in Figure 5.14, followed by analysis in the BRET^2 assay, could identify the minimum extracellular domain length necessary for the switch from dimer-disruptive to dimer-promoting behavior.

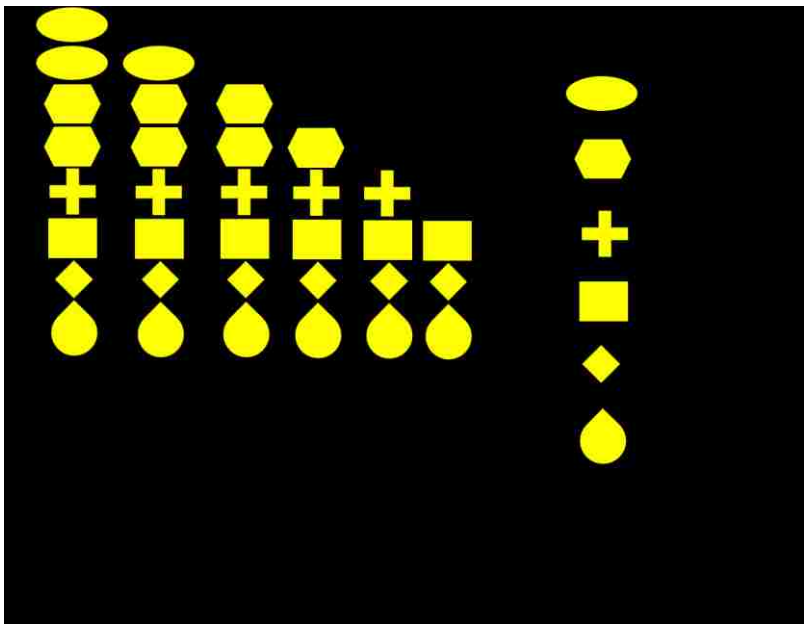

Figure 5.14. Constructs to investigate via BRET^2 to elucidate putative cooperative partners of the MAM domain. Extracellular domain constructs could also be evaluated by small angle x-ray scattering if oligomerization studies imply domain cooperativity.

By elucidating a mechanism for Nrp2a oligomerization, we can better define functionally relevant intra- and intermolecular interfaces. Understanding domains and interfaces crucial to Nrp2a homooligomerization could inform rational drug design that promotes or disrupts clustering of nrp-plxn-sema complexes and subsequent signal activation. Discrepancies between our AraTM and BRET^2 results (Figure 5.11), as well as previous results with other proteins

containing MAM domains (38), suggest the possibility that domain cooperativity also plays a role in regulating oligomeric state and provides additional interfaces suitable for drug targeting.

5.4.1 Materials and Methods

5.4.1.1 Plasmids

For the AraTM assay, nucleotide sequences of the MAM-TM-CYTO domains (residues 629-921 of NCB Accession # AAI62118.1) of the WT construct and mutants were generated via PCR from the pcDNA3.1/V5-His-TOPO constructs described in Chapter 4 and subsequently cloned into the pAraTM plasmid (39) as an EcoRI/XhoI insert. For expression of the Nrp2a extracellular domain in a bacterial system, the extracellular domain without a signal peptide (residues 25-796 of NCB Accession # AAI62118.1) was cloned into pET28a as an NheI/XhoI insert. Likely due to a Taq error, the cloned construct contains a mutation (P62L) in the first CUB domain.

For investigation of Nrp2a domain cooperativity in the BRET^2 assay, 'A' and 'B' constructs (refer to Figure 5.14) for WT, C711S, and C711S + C794S Nrp2a have been successfully cloned into both a pGFP^2 plasmid and a pRLuc plasmid for BRET^2 studies. The WT Nrp2a 'C' and 'D' constructs in a pGFP^2 plasmid and the WT Nrp2a 'D' construct in a pRLuc plasmid have also been cloned. These constructs were generated by ligation-independent cloning using the full-length ('A') constructs described in Chapter 4. Constructs contained a predicted signal-peptide sequence for the full-length receptor (residues 1-27 of NCB Accession # AAI62118.1), followed by amino acids encoding for residues 219-927 ('B' constructs), 267-927 ('C' constructs), 428-927 ('D' constructs), 593-927 ('E' constructs), or 629-927 ('F' constructs) of NCB Accession # AAI62118.1.

Domain-deletion constructs for the extracellular domain were also cloned into pET28a as EcoRI/XhoI inserts for domain cooperativity investigations on a bacterially-expressed soluble protein in the event that such an expression system is deemed useful. These constructs lack the signal peptide, start with the amino acid delineated for the BRET^2 constructs, and conclude with residue 796 of NCB Accession # AAI62118.1.

5.4.1.2 AraTM Assay

Electrically-competent SB1676 (The E. Coli Genetic Stock Center, Yale University) were co-transformed with the pAraGFP plasmid and the Nrp2a MAM-TM-CYTO domain subcloned into plasmid pAraTM. Confirmation of proper membrane integration for each construct as well as quantification of homodimerization was performed as previously described (31), but for maltose complementation, growth on maltose-supplemented plates occurred over the course of one week. Results are reported in terms of the average percent change from WT in slope of GFP fluorescence *vs.* absorbance determined from a minimum of 12 independent replicates. Error bars indicate the standard error of these samples with the standard error from WT added to these values.

5.4.1.3. NativePAGE Western Blots

For full-length Nrp2a homooligomerization, cells were transfected as for BRET^2 (Chapter 4), but with the GFP^2-fusion construct only and the entirety of each transfection seeded into one well of a gelatin-coated 6-well dish. Each well was subsequently trypsinized and re-suspended in 66 μL PBS. One-fourth of this aliquot was used per condition per well on a 3-12% NativePAGE gel, with sample preparation performed as per manufacturer's instructions with 1% n-dodecyl-β-D-maltoside and 2.5% glycerol, with and without 2.5% β-mercaptoethanol (BME) (reducing and non-reducing, respectively). Electrophoresis, transfer to a PVDF membrane, and

subsequent processing of the membrane occurred as per manufacturer's instructions. Blots were blocked for one to two hours at room temperature in 5% milk in TBS + 1% Tween-20 (TBST). Antibodies were diluted 1:1000 (EGFP mouse monoclonal antibody, Clontech; mouse monoclonal anti-tubulin, Abcam; anti-mouse IgG HRP-linked antibody, Cell Signaling) in this block solution. Incubation in primary antibody occurred overnight at 4°C, and incubation in secondary antibody occurred for one hour at room temperature. Development occurred with the ECL Plus Western Blotting Detection System (GE Healthcare), and imaging with a Molecular Dynamics Storm 840. Confirmation that roughly equivalent cell mass was present in each sample was determined via an anti-tubulin SDS-PAGE western blot (Figure 5.12).

5.5 Behavior of the Neuropilin-2a MAM Domain in Solution

Our studies with cysteine mutations in the MAM domain involved this domain anchored to the cell membrane (Chapter 4 and Section 5.4). Behavior of this domain in isolation may provide additional insight into the MAM cysteine regulatory mechanism on Nrp2a dimerization. Additionally, as the NRP2 MAM domain in isolation binds to NRP1 and NRP2 receptors (40), the purified MAM domain, or a rationally-designed homolog, may also be useful as a peptide to alter nrp function. To study the MAM domain in the absence of membrane anchorage, we have expressed this domain using a bacterial expression system both in isolation and as an MBP-fusion and analyzed select constructs via NativePAGE, SDS-PAGE (as cross-linked entities), and SEC to examine oligomeric tendencies as well as via CD and in tryptophan fluorescence studies to gain insight into secondary and quaternary/tertiary structure.

As protein migration via NativePAGE relies not only upon molecular weight, but also the protein's charge distribution and shape, the actual oligomeric state cannot be directly determined from NativePAGE (41). However, shifts in native oligomeric state can be assessed using this

technique. As such, we used this technique to examine MBP-fused MAM domains with cysteine mutations or in the presence of reducing agent (Figure 5.15). The WT Nrp2a MBP-MAM domain preferentially forms a complex with the apparent molecular weight as a dimer as observed by NativePAGE (Figure 5.15), with a higher-order oligomer and aggregates also observed. The apparent dimer persisted in the presence of 2.5% BME (Figure 5.15B), suggesting the protein is actually monomeric or that the complex formed is independent of intermolecular disulfide bonds.

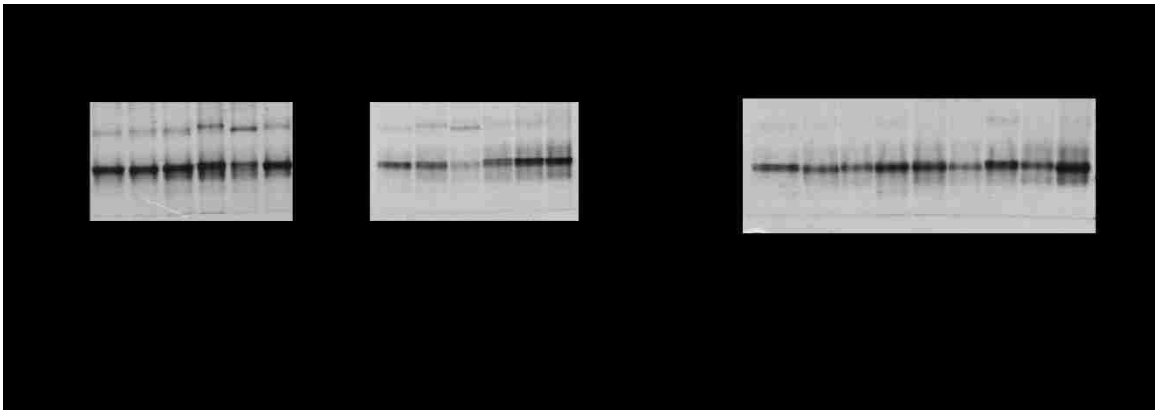

Figure 5.15. NativePAGE on MBP-MAM. (A) NativePAGE gels on purified MAM-MBP mutants illustrates mutations of cysteines C711 and C794 in the MAM domain influence the equilibrium of oligomeric states. (B) In the presence of the reducing agent β-mercaptoethanol, a band at the apparent dimer molecular weight persists. Ladder markings in kDa, expected molecular weight of monomeric WT MAM-MBP is 62.5 kDa. D marks apparent molecular weight of a dimer, H marks higher-order oligomer.

To elucidate what role the conserved cysteines may play in the oligomeric potential of the Nrp2a MAM domain, we generated a series of purified MBP-MAM domain mutants and compared their ability to oligomerize via NativePAGE (Figure 5.15). For mutants C636S and C643S, the overall distribution of oligomeric states is similar to that of WT MBP-MAM, with the

major band corresponding to an apparent molecular weight of a dimer with some higher-order oligomer present. For C711S and C794S, however, this distribution is shifted as compared to that of WT, with both mutants exhibiting an increase in the ratio of amount of higher-order oligomer to amount of apparent dimer observed. Additionally, for C711S, the band corresponding to the higher-order oligomer is shifted slightly to a larger molecular weight relative to the other higher-order oligomer bands observed for both WT and mutants. These results suggest C711 and C794 play a role in regulating the equilibrium between homomeric interactions of the Nrp2a MAM domain. These residues likely define the interfacial conformation leading to Nrp2a clustering and subsequent activation.

To examine whether mutations to cysteines in the MAM domain could have additive effects influencing MAM oligomeric state, we made a series of double-mutants including C636S + C643S, C636S + C711S, C643S + C711S, and C711S + C794S. All double mutations exhibited similar distributions of apparent dimer and higher-order oligomer as WT MBP-MAM (Figure 5.15). This suggests the disruptions caused by single point mutations to cysteines in the MAM domain are not additive in the MBP-fused peptide in a native environment, and further implies residues other than the conserved cysteines play a role in regulating Nrp2a MAM domain oligomeric states. We speculate these other residues can correct for disruptions caused by missing cysteines; however, having C711 alone or C794 alone provides a driving force to shift the equilibrium of Nrp2a MAM oligomeric states to a higher-order. Collectively, our NativePAGE results indicate that, for the MBP-MAM fusion, residues C711 and C794 contribute to modulation of oligomeric states.

To examine behavior of the Nrp2a MAM domain in isolation, we employed cross-linking, followed by SDS-PAGE for accurate molecular weight analysis of the resulting compounds. The purified WT Nrp2a MAM domain preferentially forms a monomer as observed

by SDS-PAGE (Figure 5.16), with dimer also observed independent of the presence or absence of cross-linker (BS3). Without a DTT reducing agent, monomer is observed at roughly four-fold the intensity of dimer, as indicated by ImageJ analyses. The dimer persists in the presence of DTT, but the intensity of the dimer band is slightly reduced (<10%), suggesting cysteines may be involved in formation of the observed MAM dimer via SDS-PAGE. To better understand the role of disulfide bonds formed by specific cysteines in Nrp2a MAM domain oligomerization, we examined the oligomeric state of the purified MAM domain with single and double cysteine mutations via SDS-PAGE. Comparison of the *Danio rerio* Nrp2a MAM domain with the PTPμ MAM domain suggested C636-C643 and C711-C794 are likely to form disulfide bonds (analogous to disulfide bonds C27-C36 and C96-C182 in the PTPμ MAM domain) (Chapter 4) (38). Therefore, we mutated one or both cysteines in each of the corresponding putative disulfide bonds in the Nrp2a MAM domain to determine whether the predicted cysteines play a specific role in MAM monomer-dimer equilibrium. Cross-linking and SDS-PAGE results for mutants C643S and C636S + C643S are both similar to WT MAM, where addition of reducing agent increases the ratio of monomer to dimer. The dimer band for C711S and C711S + C794S, however, remains slightly more pronounced in the presence of DTT than the dimer band of WT (<10%). Collectively, these results suggests C711 plays a role in regulating the equilibrium between monomeric and dimeric states of the isolated Nrp2a MAM domain, with mutation C711S promoting dimer formation (consistent with our $BRET^2$ results, Chapter 4). This is consistent with the idea that a disulfide bond involving C711 in the WT Nrp2a MAM domain acts to negatively regulate the transition from MAM monomer to dimer. Hence, mutation of this residue (C711S) promotes dimer formation (Figure 5.16 and $BRET^2$ results, Chapter 4).

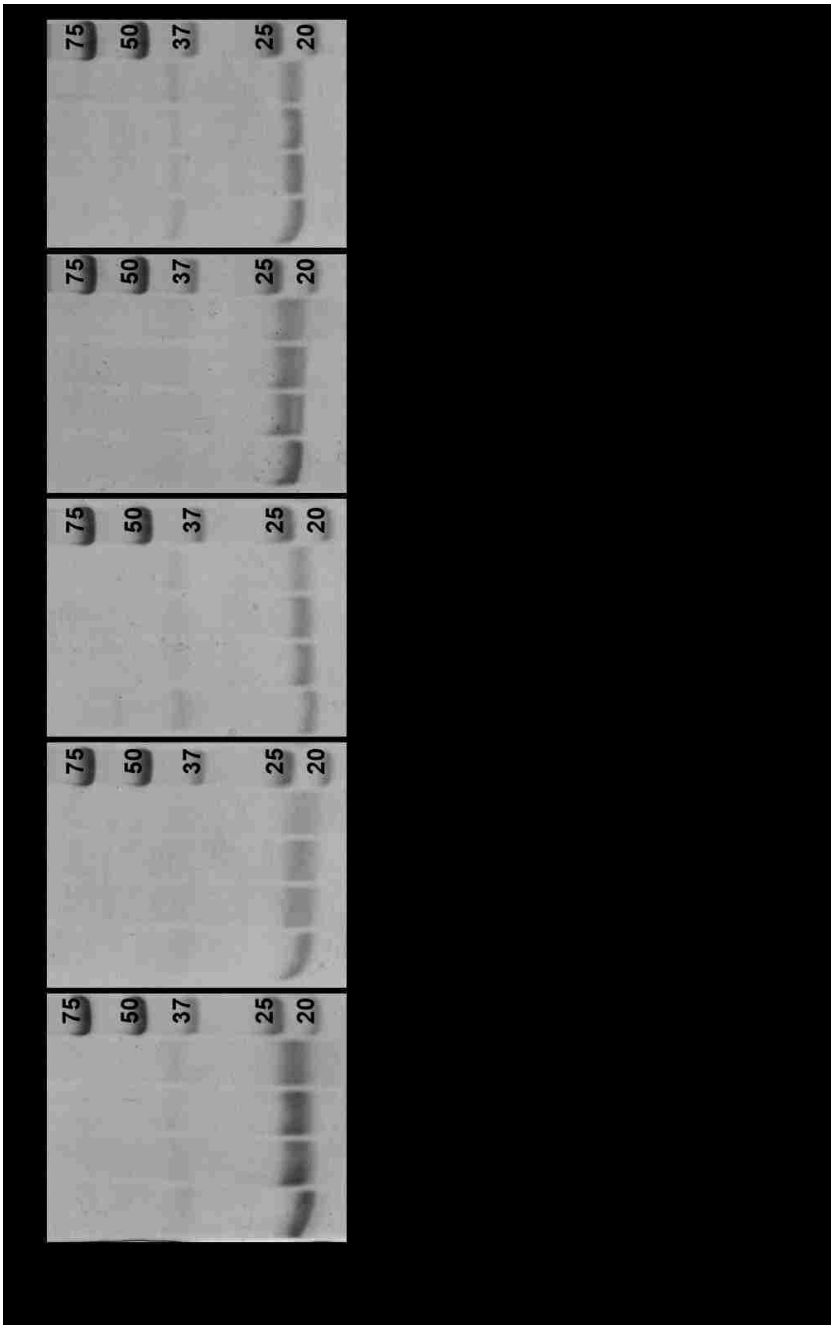
75
50
37
25
20
75
50
37
25
20
75
50
37
25
20
75
50
37
25
20
75
50
37
25
20

As a final method of analysis of the oligomeric state of the Nrp2a MAM peptide, we examined the WT and mutant peptides via SEC. WT and mutant constructs exhibit peaks consistent with the molecular weights of monomer as well as an oligomer with a molecular weight consistent with that of 16 MAM domains (Figure 5.17). While this isolated MAM domain oligomer likely does not reflect the oligomeric state of the full-length receptor, the MAM mutant C711S exhibited an increase in the ratio of the absorbance values of oligomer to monomer (Figure 5.17). This is consistent with a model in which mutation C711S enhances receptor clustering, as was observed with the full-length receptor via NativePAGE (Section 5.4, Figure 5.12). Mutation C711S + C794S in the isolated MAM domain did not show significant changes in the ratio of oligomer to monomer absorbance from WT, consistent with our NativePAGE (Figure 5.15) results.

Collectively, our results further indicate cysteine chemistry in the MAM domain regulates Nrp2a MAM homomeric interactions, and mutation C711S enhances homooligomerization, be it by enhancing dimerization of the full-length receptor ($BRET^2$ results, Chapter 4), enhancing aggregation of the full-length receptor (Section 5.4, Figure 5.12), promoting formation of a higher-order structure when fused to MBP and analyzed via NativePAGE (Figure 5.15), maintaining a higher ratio of dimer to monomer when purified and analyzed via cross-linking and SDS-PAGE (Figure 5.16), and promoting oligomerization when purified and analyzed via SEC (Figure 5.17).

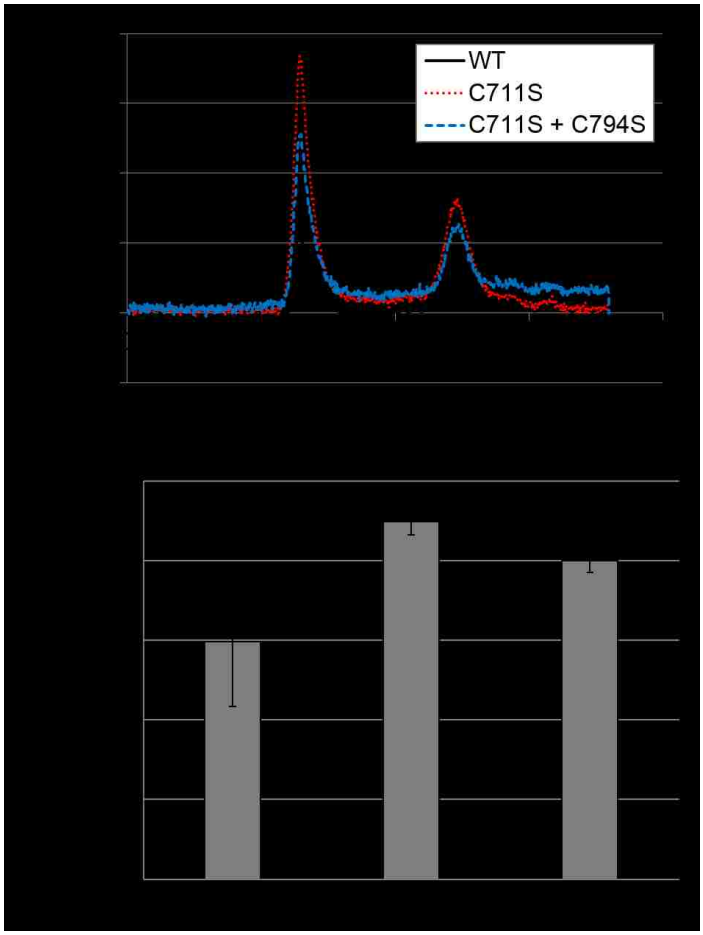

Figure 5.17. The Nrp2a MAM domain exists as monomer and oligomer in PBS, as determined by size-exclusion chromatography. (A) Chromatograms for Nrp2a MAM domain constructs. (B) Ratios of absorbance intensity of oligomer to monomer for Nrp2a MAM domain constructs. Comparisons to WT suggest mutation C711S promotes oligomer formation.

The importance of C711 in regulating Nrp2a MAM tertiary and/or quaternary structure was further confirmed by tryptophan fluorescence studies on the isolated peptide (Figure 5.18), which contains six tryptophan residues. To note, the CD spectra of WT Nrp2a MAM and each individual MAM domain mutant are indistinguishable from one another, and each exhibits a characteristic spectra with minimum at 215 nm, indicative of a β-sheet (Figure 5.19) (42). Crystal structures of the MAM domains of PTPμ and promeprin β have indicated MAM domains in other

receptors are also largely β-sheet, consistent with the CD measurements (37,38,43). Thus, mutations to conserved cysteines in the MAM domain do not significantly alter the secondary structure of the Nrp2a MAM domain. Compared to the barycentric mean fluorescence of free tryptophan (368.5 ± 0.8 nm), the barycentric mean fluorescence of the MAM domain is blue-shifted (354.0 ± 0.6 nm), as would be expected for a folded protein with buried tryptophan residues (Figure 5.18). Mutants C711S and C711S + C794S exhibit red-shifted barycentric mean fluorescence values compared to the WT protein (356.9 ± 0.7 nm and 357.1 ± 0.7 nm, respectively), suggesting the tertiary and/or quaternary structures formed by these mutants do not quench tryptophan residues as extensively as the WT protein. Mutants C643S and C636S + C643S exhibited similar barycentric mean fluorescence values as the WT protein (355.1 ± 0.7 nm and 354.8 ± 0.6 nm, respectively), implying similar solvent exposure as the WT protein.

The addition of reducing agent altered tryptophan quenching for the WT and C711S MAM domains, suggesting slight changes in tryptophan burial in the absence of disulfide bonds (Figure 5.18). For the WT MAM domain, addition of TCEP results in a significant increase in integrated fluorescence intensity (38.0 ± 0.2%), consistent with a model in which intra- or intermolecular disulfide bonds stabilize a tertiary structure in which tryptophan residues are buried within the folded protein. Interestingly, for mutant C711S, addition of TCEP decreases integrated fluorescence intensity (29.4 ± 0.2%). This suggests an alternate tertiary or quaternary structure is formed by mutation C711S in which a disulfide bond prevents tryptophan quenching, unlike WT MAM. Mutants C643S, C636S + C643S, and C711S + C794S exhibit less significant changes in integrated fluorescence intensity than WT or C711S (<5%), suggesting the burial of hydrophobic tryptophan in these mutations is not affected by specific disulfide bonds formed.

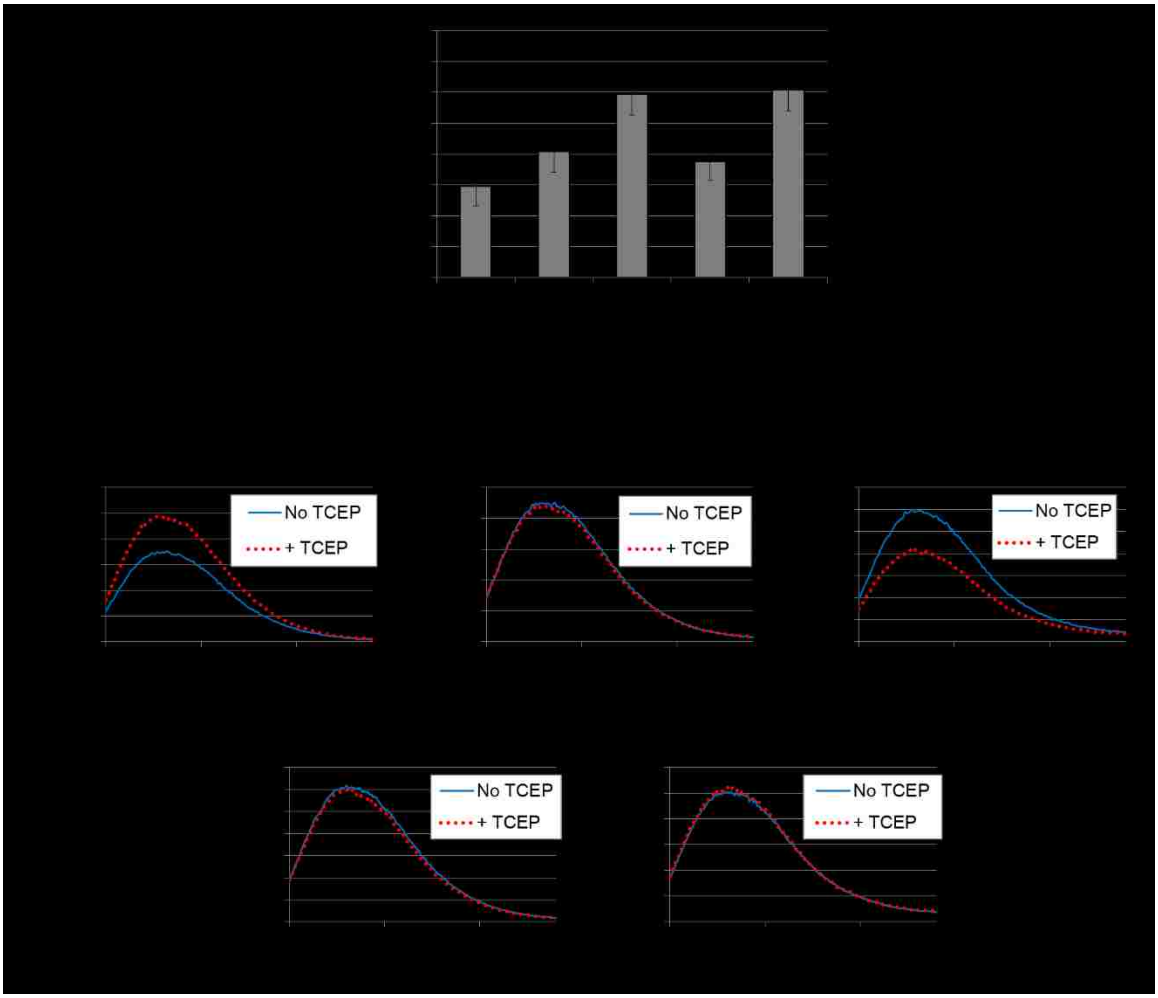

Figure 5.18. Tryptophan fluorescence studies on the Nrp2a MAM domain suggest mutant C711S exposes alternate interfaces compared to WT. (A) Shifts in barycentric mean fluorescence values from free tryptophan suggest the isolated Nrp2a MAM domain tertiary and/or quaternary structures allow for tryptophan burial. Mutants C711S and C711S + C794S exhibit different folding from WT. Error bars indicate standard deviation from three spectral acquisitions. (B) Trends in fluorescence intensity suggest disulfide bonds play a role in tryptophan burial in the WT and C711S Nrp2a MAM domains, with disulfide bonds allowing WT to bury more tryptophan and causing C711S to expose more tryptophan.

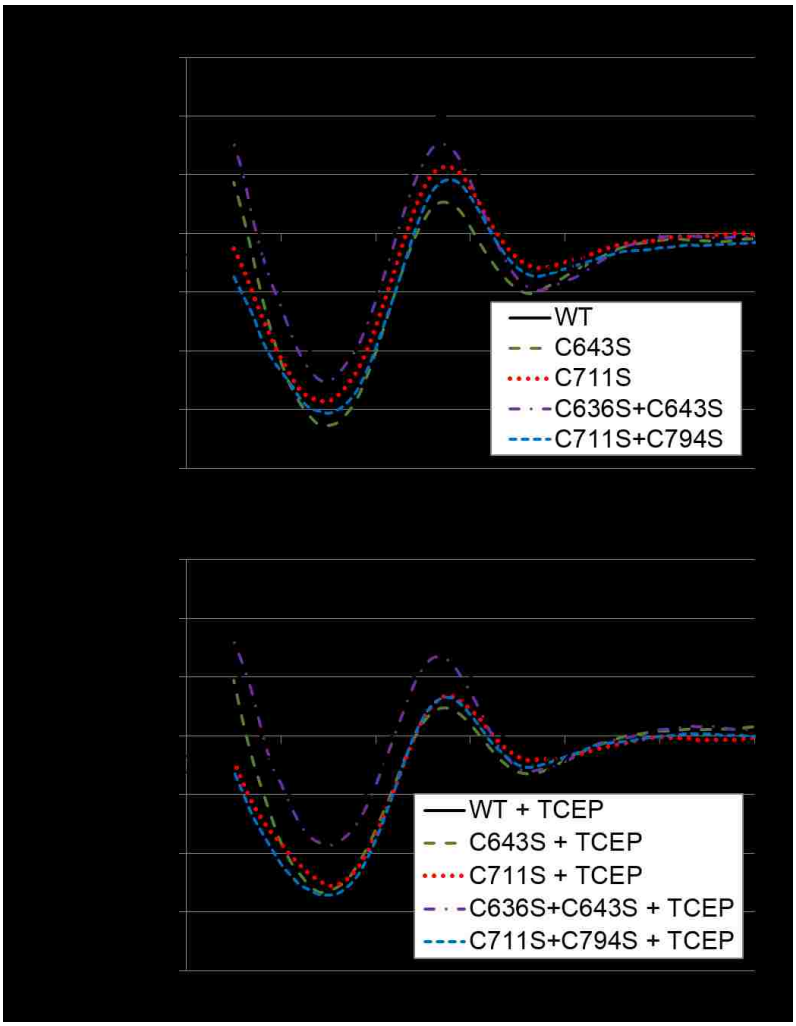

Figure 5.19. Circular dichroism spectra of Nrp2a MAM domains in PBS. WT and mutant constructs exhibit β-sheet characteristics, in the absence (A) or presence (B) of TCEP.

Collectively, our BRET[2] (Chapter 4), AraTM (Section 5.4, Figure 5.10) gel electrophoresis (Figures 5.15 and 5.16 and Section 5.4, Figure 5.12), SEC (Figure 5.17), and tryptophan fluorescence (Figure 5.18) results suggest that Nrp2a MAM domain oligomerization relies upon cysteines that likely form disulfide bonds, and that all cysteines within the Nrp2a MAM domain are not equivalent. The mutations affect quaternary structure equilibrium (gel electrophoresis and SEC, Figures 5.15, 5.16, and 5.17) but do not affect secondary structure (CD,

Figure 5.19). Under native conditions, C711 likely plays a dominant role in defining the equilibrium between Nrp2a oligomeric states and/or tertiary structure versus the other cysteines present in the Nrp2a MAM domain.

While our results suggest cysteines play a key role in regulating the equilibrium between MAM oligomeric states (Figures 5.15, 5.16, and 5.17, Chapter 4, and Section 5.4), they do not play the only role in MAM dimerization, as is apparent by the perseverance of dimer in the isolated MAM domain in the presence of reducing agent (Figure 5.16). As SDS also did not eliminate dimer, we can presume that hydrophobic interactions also contribute to dimer formation. These results are in contrast to investigations of the PTPμ MAM domain, which runs as a monomer in the presence of SDS and reducing agent (44).

To further understand our findings, and to identify other residues that putatively modulate homooligomerization, we developed a model for the *Danio rerio* Nrp2a MAM domain based on the crystal structure of the PTPμ MAM domain (PDB # 2C9A) (37) using MODELLER (45) and PyMOL (46) (Figure 5.20A). The model suggests the four conserved cysteines (C636, C643, C711, C794) present in Nrp2a MAM are all arranged on the same face of the MAM domain (Figure 5.20A). Our tryptophan fluorescence studies (Figure 5.18), gel electrophoresis (Figures 5.15 and 5.16), SEC (Figure 5.17), AraTM (Section 5.4, Figure 5.10), and $BRET^2$ results (Chapter 4) suggest C711 is particularly influential to this interface. Interestingly, unlike the PTPμ MAM domain crystal structure, in which each of the four conserved cysteines are within sufficient proximity to form intramolecular disulfide bonds (44), our model suggests that the Nrp2a MAM cysteines C711 and C794 are sufficiently separate (9.3 Å, as determined using PyMOL) that they cannot form an intramolecular disulfide bond (Figure 5.20B). This hypothesis is supported by our experimental results illustrating mutation to C711 or C794 disrupts MAM domain oligomerization (Figures 5.15 and Section 5.4, Figure 5.10). Furthermore, as mutations

C711S and C794S in the pure MBP-MAM domain do not exhibit an enhanced propensity to form the higher-order oligomer over WT in the presence of 2.5% BME (Figure 5.15), the possibility exists that C711 and C794 form an intermolecular disulfide bond. Further studies, such as the two-step alkylation procedure used previously to determine that PTPμ MAM domains form intramolecular disulfide bonds (44), are required to investigate this possibility. Indeed, the macrophage migratory inhibitory factor protein undergoes local conformational changes in order to form a disulfide bond over longer-than-optimal distances (47), and as such, our model does not eliminate the possibility that residues C711 and C794 form an intramolecular disulfide bond. Such a feature may play a role in domain cooperativity, with additional extracellular domains forcing intramolecular disulfide bonds in the full-length receptor, and their absence in the MAM-TM-CYTO constructs removing a driving force to form intramolecular disulfide bonds in the AraTM assay (Section 5.4).

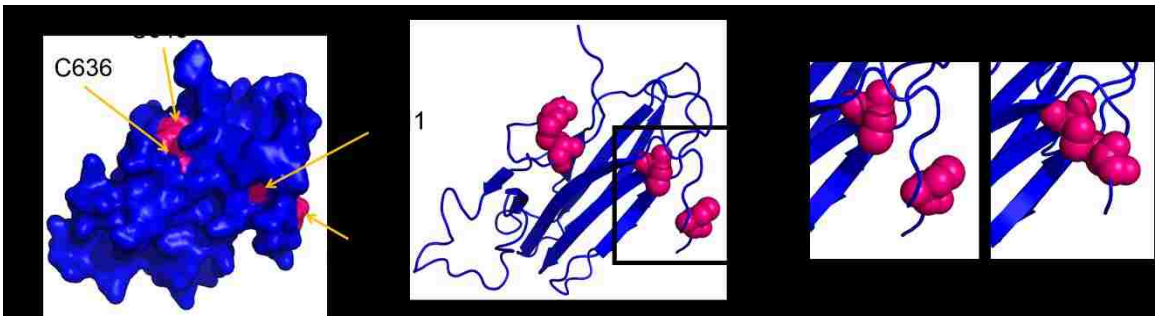

Figure 5.20. Homomeric Nrp2a interactions likely occur via a cysteine-rich interface in the MAM domain. (A) A model of the Nrp2a MAM domain, based on a crystal structure of the PTPμ MAM domain, supports the theory of a cysteine-rich interface that stabilizes dimerization, as the four cysteines lie on the same interface. (B) Our model suggests not all cysteine pairs of the NRP2 MAM domain (left) are close enough to form intramolecular disulfide bonds, in contrast to the MAM domain of PTPμ (right).

Using RosettaDock (48) and the hypothesis that residues C711 and C794 both lie on the MAM homodimer interface, we developed a model to find low-energy configurations for the Nrp2a MAM dimer that contain C711 and C794 in the dimer interface. We examined the ten lowest dimeric energy configurations generated and selected the model with the highest percentage buried accessible surface area (ASA) across the dimer interface (Figure 5.21A). We then used this model to predict residues other than C711 and C794 that may influence Nrp2a MAM dimerization. In particular, we identified M713, which flanks the key residue C711 that regulates MAM dimerization, and N782 as key residues buried in the predicted MAM dimer interface. M674, R697, and R750 are predicted off-interface residues and, as such, expected to have null effects on dimerization. To test our predictions, we generated mutants (M713W, R750E, N782Q, M674W, and R697E) and characterized their effects on MAM-TM-CYTO oligomerization in AraTM. As shown in Figure 5.21B, both mutations to predicted interfacial residues in our dimer model (M713W and N782Q) caused significant disruption of MAM-TM-CYTO dimerization, whereas a predicted null-mutation (M674W) had no significant effect on MAM-TM-CYTO dimerization. Thus, these results provide evidence to support the model for the Nrp2a homodimer (Figure 5.21A). The predicted null-mutations R697E and R750E also disrupted dimerization. This could possibly be due to disruption of long-range interactions that promote dimerization, or could be an indication of other interfaces involved in MAM dimerization.

To examine our model of the Nrp2a MAM domain further, we additionally investigated the M713W, N782Q, and M674W mutations as MBP-MAM constructs on a NativePAGE gel (Figure 5.21E). Predicted off-interface residue M674W exhibited similar oligomerization patterns as WT, in agreement with the AraTM results (Figure 5.21). Predicted interfacial mutation M713W also appeared similar to WT, rather than mutations C711S or C794S; possibly

R697
N782
C711
C794
250
150
100
75
50
37

this mutation is permissive to the WT oligomeric pattern with the MAM domain alone, compared to with the TM-CYTO domain attached in the AraTM assay (Figure 5.21). Predicted interfacial mutation N782Q disrupted formation of the construct at the apparent dimeric molecular weight. This change from WT oligomeric patterning is consistent with the AraTM results (Figure 5.21) and suggests that this residue also lies at the MAM domain homomeric interface and may be one of the unknown residues assisting in dimer formation.

These results provide further evidence of the importance of electrostatic and hydrophobic interactions in Nrp2a MAM dimerization (identified in our cross-linking SDS-PAGE results, Figure 5.16), as the predicted interfacial mutations that resulted in decreased dimer formation in the context of the MAM-TM-CYTO domain were non-cysteines (residues N782 and M713) (Figure 5.21). The results also provide further support of a possible homomeric interface containing C711 and C794, in agreement with our C711 and C794 NativePAGE (Figure 5.15) and AraTM (Section 5.4, Figure 5.10) results. This interface regulates the intermediate dimeric conformation of the Nrp2a MAM domain, which can ultimately control full-length receptor clustering (Chapter 4). The residues predicted by our model, as well as the MAM domain cysteines, in particular C711, may be adjustable residues for fine-tuning the MAM peptide for its use as a putative therapeutic.

In summary, analysis of a bacterially-expressed MAM peptide has further confirmed the importance of MAM domain cysteines, in particular residue C711, in modulation of homodimerization. We have furthermore used this information to develop a model of the Nrp2a MAM domain, and used this model to predict additional residues influential to MAM dimerization. The MAM peptide expressed by insect or mammalian cells, in conjunction with domain cooperativity experiments (Section 5.4), may further define the role of the MAM domain in modulation of nrp signaling. Additional functional studies with the peptide, and rationally-

designed mutations of the peptide predicted from our model, will elucidate the feasibility of use of the peptide to regulate nrp-dependent signaling.

5.5.1 Materials and Methods

5.5.1.1 Plasmids

For MBP-fusion constructs, a 6-His tag, followed by MBP, a poly-glycine linker, and tobacco etch virus cleavage site was cloned into pET42 as an NdeI/BamHI insert. The pET28 multiple-cloning site between BamHI and XhoI was subsequently cloned into this plasmid at BamHI/XhoI. The Nrp2a MAM domain (residues 629-796 of NCB Accession # AAI62118.1) and mutants were then cloned into this plasmid as EcoRI/XhoI inserts. To generate isolated MAM domain constructs, the Nrp2a MAM domain (residues 629-796 of NCB Accession # AI62118.1) in WT or mutant form was cloned into pET28(a) at EcoRI/XhoI.

5.5.1.2 Expression and Purification of Nrp2a MAM and MBP-MAM Constructs

Plasmids containing the Nrp2a MAM or MBP-MAM genes were transformed into BL21(DE3) cells (Invitrogen) and stored as glycerol stocks. Expression and purification of MBP-MAM was conducted using the same protocol as that for the PlxnA3 MBP-JM (Section 5.1.2.2).

For MAM expression without the MBP fusion, cultures were started from glycerol stocks and grown to saturation overnight at 37°C in LB + 50 μg/mL kanamycin. Cells were then diluted to an OD_{600} of 0.8 and allowed to grow an additional 1 hour at 18°C, at which point 1 mM IPTG was added to the culture. Cells were collected 16-24 hours post-IPTG induction, re-suspended in PBS (pH 7.4) and lysed using freeze-thaw and tip-sonication. The MAM protein was subsequently extracted from the insoluble portion of the sonication using 3M urea. The urea

extraction was dialyzed against 100-fold excess DNAse/RNAse buffer (10 mM Tris at pH 7.5, 2.5 mM magnesium chloride, and 0.5 mM calcium chloride) overnight at 4°C and treated with 5 µM DNAse I + 5 µM RNAse A for two hours at room temperature. The protein was subsequently purified by nickel affinity chromatography with chelating sepharose fast flow resin (GE Healthcare) and imidazole washes ranging from 10 mM to 500 mM in 20 mM HEPES, 500 mM sodium chloride, and 10% (v/v) glycerol. Purity of at least 90% was confirmed by SDS-PAGE using 12% polyacrylamide gels cast as previously described without addition of SDS to the polyacrylamide gel formulation (49); *i.e.*, protein gels used to study Nrp2a MAM oligomerization were comprised of a resolving portion [375 mM Tris at pH 8.8, 12% (w/v) acrylamide:bis-acrylamide (29:1), 1 mg/mL ammonium persulfate, and 0.04% (v/v) Temed] and a stacking portion [125 mM Tris at pH 6.8, 5% (w/v) acrylamide:bis-acrylamide (29:1), 1 mg/mL ammonium persulfate, and 0.1% (v/v) Temed]. Gels were run in MES-SDS-PAGE running buffer (50 mM MES, 50 mM Tris, 1 mM EDTA, 0.1% SDS) at 100-250V, and staining occurred in Coomassie solution. Purified protein samples were subsequently dialyzed against 0.2x PBS (pH 7.4), lyophilized, and re-hydrated to a 20-50X concentration with water. Samples were then dialyzed against 1000-fold excess 2 mM phosphate buffer (pH 7.4; CD and tryptophan fluorescence) or 1X PBS (pH 7.4; SEC) overnight at 4ºC. Saturated protein concentrations were determined via absorbance measurements at 280 nm and normalized to 0.5 g/L. For SEC and cross-linking SDS-PAGE, samples were subsequently reduced using 5% (v/v) BME and dialyzed against 1000-fold excess PBS (pH 7.4) for 16 hours at 4ºC. Saturated protein concentrations were again determined and normalized to 0.3 g/L prior to loading for SEC.

5.5.1.3 NativePAGE Gels

Following purification, MBP-MAM samples were subsequently dialyzed against 2 mM Tris at pH 8 to remove imidazole. Samples were then lyophilized and re-hydrated to a 50X

concentration with water. Saturated protein concentrations were determined via absorbance measurements at 280 nm, and protein concentrations were normalized to 1 g/L with 100 mM Tris at pH 8 + 5% (v/v) BME. Samples were then dialyzed against 1000-fold excess 20 mM Tris at pH 8 three times at 4°C (8 hours per round of dialysis) to remove BME. MBP-MAM homooligomerization was subsequently analyzed via Coomassie-stained 3-12% NativePAGE gels (Life Technologies) according to manufacturer's instructions. Roughly 18 μg of protein and 3% (v/v) glycerol were loaded in the sample buffer per condition.

5.5.1.4 Cross-linking

Cross-linking experiments were performed as previously described (44), using protein at 0.2 g/L, 20-fold molar excess BS3 (Thermo Scientific), and 25 mM DTT in reducing conditions. Prior to cross-linking, samples were dialyzed against 0.2X PBS (pH 7.4), lyophilized, and re-hydrated to a 20-50X concentration with water. Samples were then dialyzed against 1x PBS (pH 7.4) and saturated protein concentrations were determined via absorbance measurements at 280 nm. Sample concentrations were normalized to 0.3 g/L with 1x PBS at pH 7.4 + 5% (v/v) BME. Samples were dialyzed against 1000-fold excess PBS at pH 7.4 for 16 hours at 4°C. SDS-PAGE was performed using 12% SDS-PAGE gels made as described in Section 5.5.2.2 and run in MES-SDS-PAGE running buffer (Section 5.2.2.2), and fixed, stained, and de-stained following the procedures for the manufacturer's instructions for NativePAGE gels (Invitrogen), but with staining occurring for 16 hours and de-staining for 4 hours. Roughly 4 μg of protein and 2% (v/v) glycerol were loaded per condition. Intensity of bands were determined by the gel analysis function of ImageJ (50).

5.5.1.5 Size Exclusion Chromatography

Samples (15µL per injection) were passed over a TSKgel G3000SW column (Tosoh Bioscience) equipped with the appropriate guard column using an Agilent 1100 series high performance liquid chromatography system. The mobile phase consisted of PBS run at 0.1 mL/min. Detection of MAM species occurred at 280 nm. Fibrinogen (Sigma), bovine serum albumin (New England Biolabs), and RNAse A (Sigma) were used to generate a molecular weight calibration curve. Serial dilutions of RNAse A were used to confirm absorbance linearity up to at least 8 absorbance units.

5.5.1.6 Tryptophan Fluorescence Measurements

Measurements occurred as previously described (30), but in 2 mM phosphate buffer (pH 7.4). Reduction of disulfide bonds occurred with 1 mM tris(2-carboxyethyl)phosphine (TCEP) over the course of ten minutes. Free tryptophan measurements occurred using 0.5 g/L tryptophan.

5.5.1.7 Circular Dichroism

Measurements occurred as previously described (30), but at 20ºC in 2 mM phosphate buffer (pH 7.4) and scanned from 180 nm to 300 nm. This buffer was also used for background subtraction. Reduction of disulfide bonds occurred with 1 mM TCEP.

5.5.1.8 Homology Modeling and Docking

Homology modeling of the monomeric *Danio rerio* Nrp2a MAM domain was performed using MODELLER (45) with the crystal structure of the PTPμ MAM domain (PDB 2C9A) as the template structure (37). The dimer model was generated using RosettaDock (48). Solvent-accessible surface area (ASA) was determined using VADAR 1.8, employing the Shrake definitions for Van der Waals radii and polar/nonpolar/charged accessible surface area (51). Percentage of the ASA buried was defined by

$$\%\ buried\ ASA = \frac{ASA_A + ASA_B - ASA_{A+B}}{ASA_A + ASA_B} \times 100$$

where the subscripts A and B represent monomeric MAM domains utilized in building the model, and the subscript A+B represents the dimeric output of RosettaDock.

5.6 Heteromeric Interaction Interfaces of Neuropilins and Plexins

Our studies thus far have investigated homomeric interactions of nrps and plxns. With PlxnA3, we have identified residues in both the TM (Chapter 3) and JM (Chapter 2 and Section 5.3) influential to homodimerization. With Nrp2a, we have identified residues in the MAM domain (Chapter 4) influential to homodimerization. However, as function relies upon both receptors, identification of a heteromeric interface could provide additional insight into the plxn-nrp-sema mechanism of activation.

In addition to identifying nrp-plxn interaction interfaces, insight into the heteromeric interaction interfaces amongst nrps and plxns would also be beneficial for rational drug design. For instance, SEMA3C binding in sympathetic and sensory axons relies upon the presence of both NRP1 and NRP2 (40,52). Studies suggest nrps may interact heteromerically via their MAM domains (40) as well as their TM domains (53). A recent study also suggested PLXNA1 and

PLXNB1 may associate via their TM domains (53), though confirmation of this in full-length receptors or a functional relevance has yet to be determined.

The DN-AraTM assay is well-suited for studying heterodimer interfaces of TM and juxtamembrane domains in the context of a bacterial membrane (54). In this assay, a TM and juxtamembrane domain of interest are expressed as fusions to an AraC protein (similar to the AraTM assay, but with an HA-tag from an ampicillin-resistant plasmid, pAraTMwt, rather than a myc-tag from a kanamycin-resistant plasmid) ('TM_1-AraC'). This plasmid is co-transformed with [1] a spectinomycin-resistant plasmid encoding GFP regulated by a P_{BAD} promoter and [2] a plasmid encoding WT or mutant form of the TM and juxtamembrane domains of an interacting protein, fused to an AraC protein with a mutation that disrupts its functionality as a transcription factor ('TM_2-AraC*') (backbone plasmid pAraTMdn). As such, interactions between the TM_1-AraC and TM_2-AraC* constructs compete with homodimerization of TM_1-AraC, the functional transcription factor. This competition results in a decrease in GFP expression. As such, mutations in the TM domain to TM_2-AraC* that disrupt heterodimer formation exhibit a stronger GFP signal than an interacting WT TM domain; similarly, mutations enhancing heterodimerization will express less GFP than the WT TM in the TM_2-AraC* construct (54).

To investigate the heteromeric interfaces between *Danio rerio* PlxnA3 and Nrp2a, the PlxnA3 TM + JM and Nrp2a MAM-TM-CYTO have been successfully cloned into both the pAraTMwt and pAraTMdn plasmids, though PlxnA3-Nrp2a heterodimer measurements are still needed. Additionally, the TM-CYTO and MAM-TM-CYTO domains of five human membrane-anchored NRP2 isoforms (NRP2a(0), NRP2a(17), NRP2a(22), NRP2b(0), and NRP2b(5); Figure 5.22) and the MAM-TM-CYTO domains of the membrane-anchored NRP1 isoform have also been cloned into the pAraTMwt plasmid ('-AraC' constructs) for investigation of nrp heteromeric interfaces. The MAM-TM-CYTO domains of NRP2a(22), NRP2b(0), and NRP1 have also been cloned into the pAraTMdn plasmid ('-AraC*' constructs).

Figure 5.22. Primary sequence comparison of human neuropilins. (A) Alignment of human membrane-anchored neuropilin MAM-TM-CYTO sequences. TM-CYTO domains are indicated by red font, whereas MAM-TM-CYTO domains are both black and red font. Bolded residues are those predicted to be in the membrane environment. (B) The primary sequence of all NRP TM domains exhibit at least one small-x_3-small motif. Different colors indicate different small-x_3-small motifs.

Considering first homodimerization (where higher slopes of GFP fluorescence *vs.* absorbance equate with increased dimerization), our studies thus far indicate the NRP2b constructs (TM-CYTO or MAM-TM-CYTO) homodimerize to a stronger extent than the equivalent NRP2a constructs (Figure 5.23A). Additionally, for the NRP2a TM-CYTO constructs, the shorter the isoform, the stronger it dimerizes, though better western blotting is needed to confirm equivalent expression levels before we can make this conclusion. If expression levels are equivalent, it is possible that the presence of additional residues creates a steric disruption to TM dimerization. Our results may suggest that the NRP2 TM-CYTO domains dimerize more strongly than the MAM-TM-CYTO domains; however, this may be an artifact of unequal expression levels (Figure 5.23B).

To better understand NRP2a, NRP2b, and NRP1 homodimer and heterodimer interfaces, we considered the primary sequences of the TM domains. All exhibit at least two small-x_3-small TM motifs (Figure 5.22). We made a series of mutations to the NRP2a(22), NRP2b(0), and NRP1 MAM-TM-CYTO-AraC* (heterodimer competition) constructs to disrupt (glycine, alanine, or serine to leucine mutations) or enhance (alanine to glycine mutations) the small-x_3-small motifs. The NRP1 and NRP2a(22) WT- and mutant-AraC* constructs were co-expressed with WT NRP1, NRP2a(22), or NRP2b(0) MAM-TM-CYTO-AraC constructs to assess heterodimerization.

As indicated in Figure 5.24, both WT NRP1 and WT NRP2a(22) MAM-TM-CYTO domains heterodimerize with NRP1, NRP2a(22), and NRP2b(0) MAM-TM-CYTO domains, as indicated by the decrease in GFP signal compared to the homodimer constructs upon heterodimer co-expression. Considering first the NRP1 homodimer interface (Figure 5.25), we observe that NRP1 G868L MAM-TM-CYTO-AraC* does not heterodimerize with WT NRP1 MAM-TM-CYTO-AraC as well as the WT NRP1 MAM-TM-CYTO-AraC* heterodimer competition (indicated by the higher GFP expression upon NRP1 MAM-TM-CYTO-AraC co-expression with

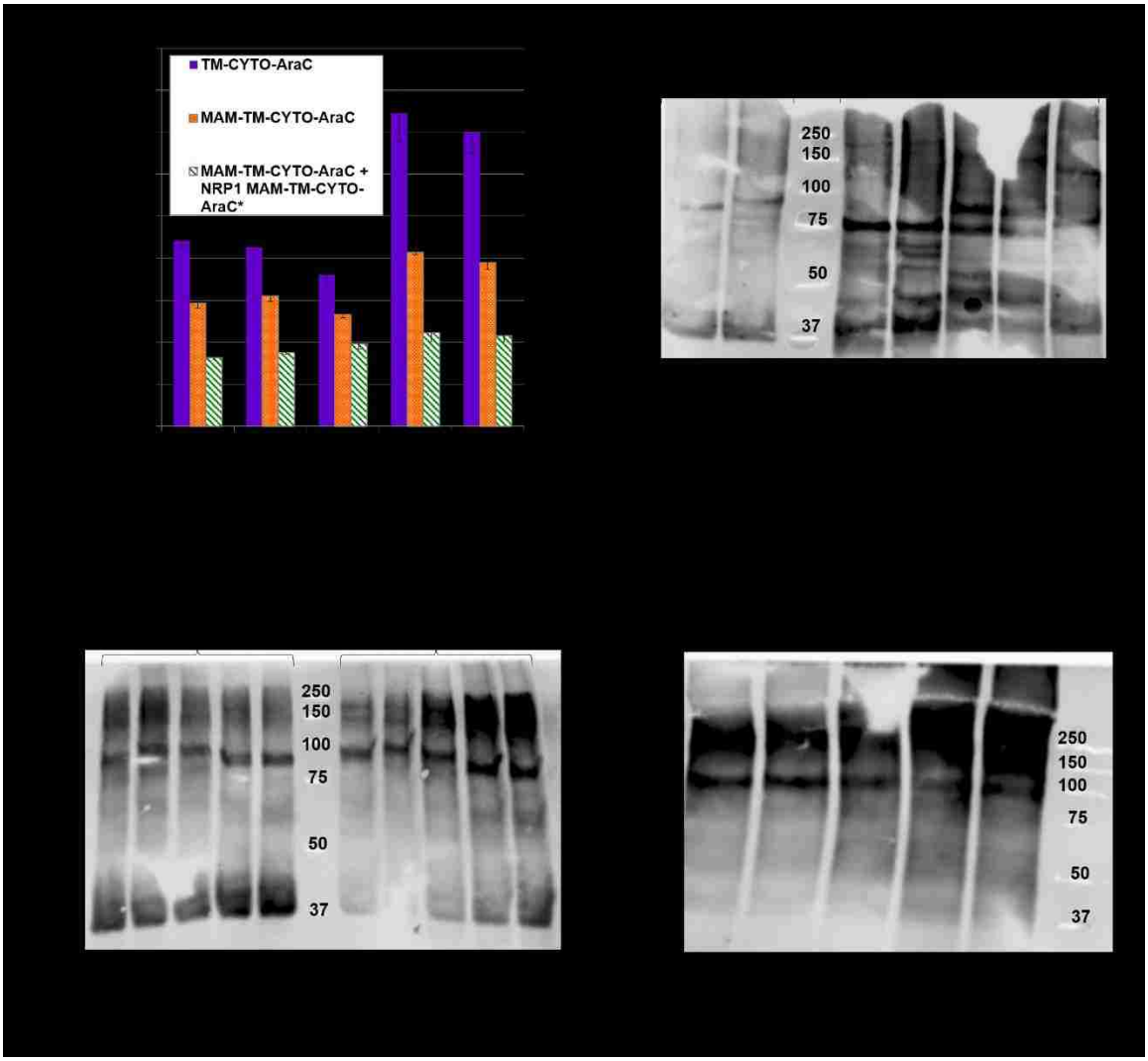

Figure 5.23. DNAraTM measurements of human NRP2 homodimerization and NRP1-NRP2 heterodimerization. (A) DNAraTM measurements for NRP2 TM-CYTO-AraC homodimerization, NRP2 MAM-TM-CYTO-AraC homodimerization, and NRP2 MAM-TM-CYTO-AraC heterodimerization with NRP1 MAM-TM-CYTO-AraC*. Results represent average values of a minimum of 15 samples collected over the course of three experiments. Error bars indicate standard error. (B) An anti-HA (1:1,000, Cell Signaling) western blot indicates NRP2 TM-CYTO-AraC constructs may express better than NRP2 MAM-TM-CYTO-AraC constructs. (C) NRP2 MAM-TM-CYTO-AraC constructs express in equivalent levels independent of NRP1 MAM-TM-CYTO-AraC* co-expression, as indicated by an anti-HA (1:1,000, Cell Signaling) western blot. (D) NRP1 MAM-TM-CYTO-AraC* is expressed in all heterodimer conditions tested in the DNAraTM assay, as indicated by an anti-myc (1:1,000, Cell Signaling) western blot. Expected molecular weights are roughly 75 kDa for TM-CYTO-AraC constructs and 90 kDa for MAM-TM-CYTO-AraC and MAM-TM-CYTO-AraC* constructs.

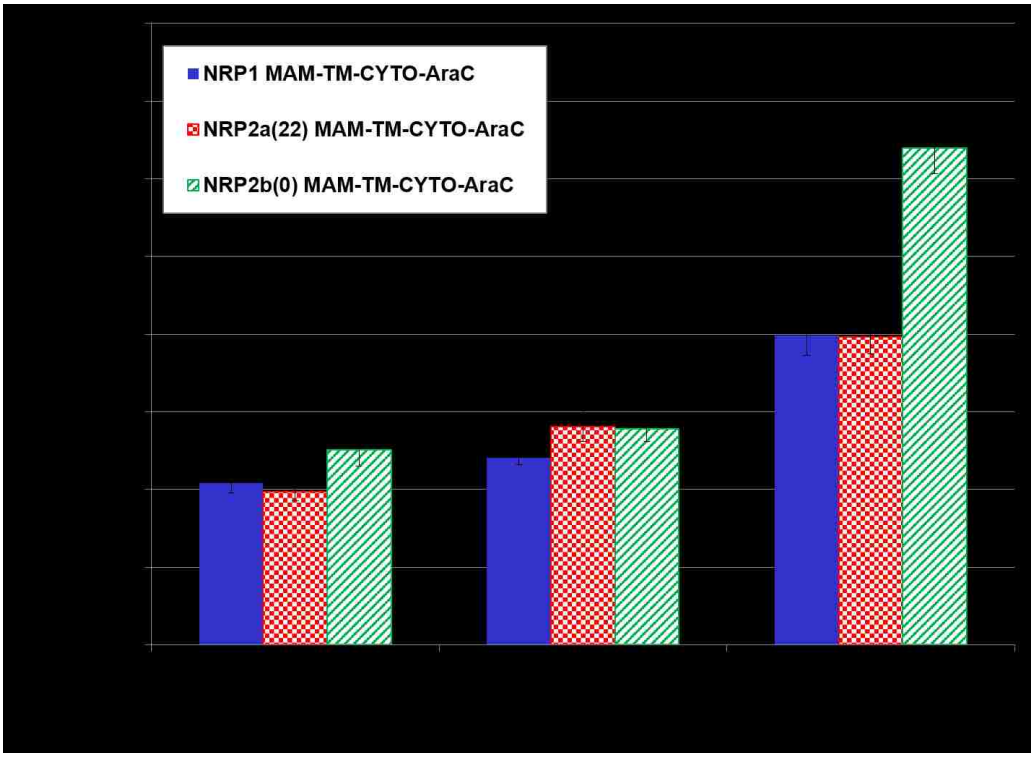

Figure 5.24. NRP1 and NRP2a(22) MAM-TM-CYTO-AraC* constructs heterodimerize with NRP1, NRP2a(22), and NRP2b(0) MAM-TM-CYTO-AraC constructs in the DNAraTM assay, as indicated by decreased level of GFP expression for a given culture density upon co-expression of MAM-TM-CYTO-AraC* with the MAM-TM-CYTO constructs. Values represent average slopes of fluorescence *vs.* absorbance collected from a minimum of 22 replicates collected over the course of six experiments. Error bars indicate standard error.

the G868L NRP1 MAM-TM-CYTO-AraC* heterodimer construct, compared to NRP1- MAM-TM-CYTO AraC co-expression with the WT NRP1 MAM-TM-CYTO-AraC* heterodimer construct). Hence, residue G868 likely contributes to the NRP1 dimer interface. This is in loose agreement with a previous study in which triple mutation to all three residues participating in the NRP1 small-x_3-small motif (G868, G872, and G876) disrupted dimerization. Constructs G872L NRP1 MAM-TM-CYTO-AraC* and G876L NRP1 MAM-TM-CYTO-AraC* heterodimerize with the WT NRP1 MAM-TM-CYTO-AraC to the same extent as WT NRP1 MAM-TM-CYTO-AraC*, suggesting these residues may be less influential in defining the NRP1 homodimer interface. However, our current results do not measure the extent of homodimerization of the

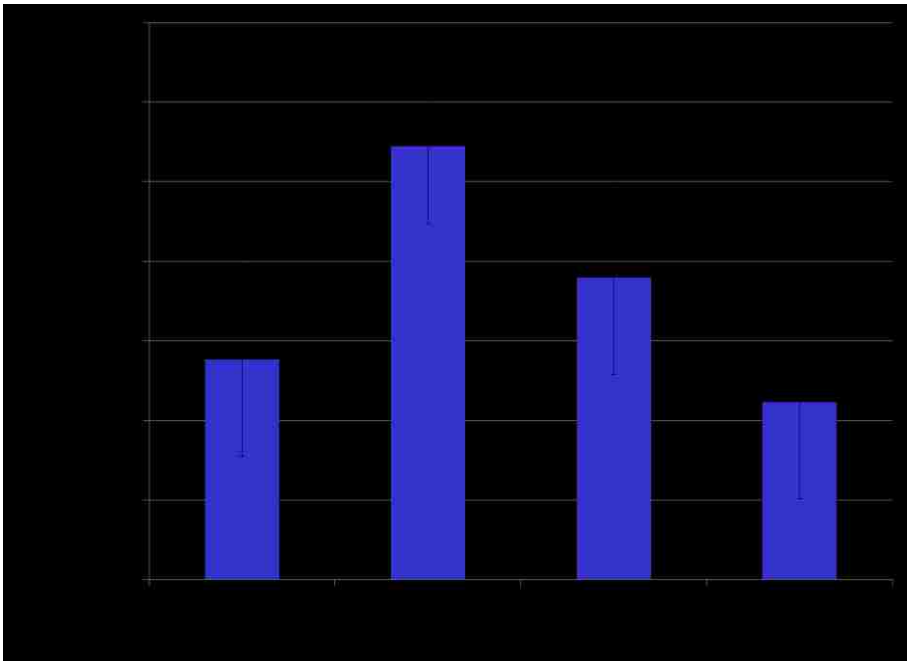

Figure 5.25. NRP1 MAM-TM-CYTO-AraC heterodimerization with NRP1 MAM-TM-CYTO-AraC* competition. Results represent the average value from a minimum of 22 samples collected over the course of six experiments. Error bars indicate standard error.

mutant constructs and hence cannot rule out the possibility that mutations G872L and G876L homodimerize less strongly than the WT receptor.

Mutation G868L to NRP1 MAM-TM-CYTO-AraC* also disrupts heterodimerization with NRP2a(22) MAM-TM-CYTO-AraC (Figure 5.26), as does NRP1 mutation G872L. These results suggest NRP1 residues G868 and G872 are important for NRP1-NRP2a(22) dimerization. In contrast, mutations G868L, G872L, and G876L to NRP1 MAM-TM-CYTO-AraC* enhance heterodimerization with NRP2b(0) MAM-TM-CYTO-AraC (Figure 5.27). Possibly, homodimerization of the WT NRP1 MAM-TM-CYTO-AraC* via a small-x_3-small motif disrupts its capacity to heterodimerize with NRP2b(0). By disrupting the small-x_3-small motif with mutations G868L, G872L, and G876L, we make the NRP1 MAM-TM-CYTO-AraC* construct more accessible to interactions with the NRP2b(0) MAM-TM-CYTO-AraC construct. Additional

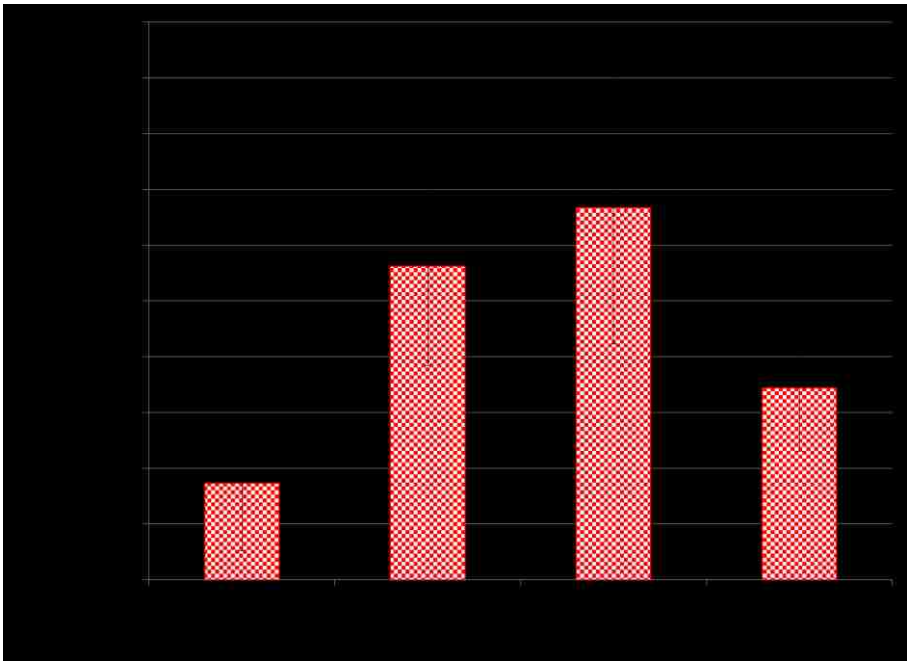

Figure 5.26. NRP2a(22) MAM-TM-CYTO-AraC heterodimerization with NRP1 MAM-TM-CYTO-AraC* competition. Results represent the average value from a minimum of 22 samples collected over the course of six experiments. Error bars indicate standard error.

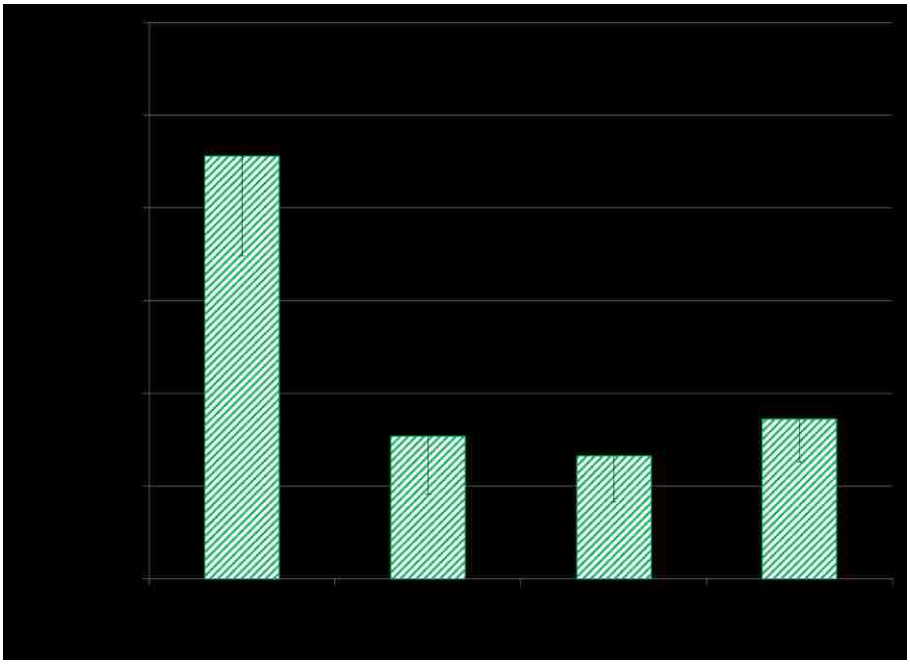

Figure 5.27. NRP2b(0) MAM-TM-CYTO-AraC heterodimerization with NRP1 MAM-TM-CYTO-AraC* competition. Results represent the average value from a minimum of 22 samples collected over the course of six experiments. Error bars indicate standard error.

simulation work may elucidate how our mutagenesis results correlate with receptor heterodimerization.

Considering NRP2a(22) MAM-TM-CYTO-AraC heterodimerization with NRP2a(22) MAM-TM-CYTO-AraC* constructs (Figure 5.28), we observe that mutation G876L disrupts heterodimerization relative to the WT NRP2a(22) MAM-TM-CYTO-AraC* construct, whereas mutations G880L and A884L (both on the same putative small-x_3-small interaction interface as G876) enhances heterodimerization. Our results suggest that the G876-G880-A884 interface influences dimerization; the mechanism, however, is unclear. The mutation enhancing this small-x_3-small motif (A884G) does not alter heterodimerization relative to the WT NRP2a(22) MAM-TM-CYTO-AraC* construct, nor do disruptive mutations to the second putative small-x_3-small interface (A881L and G885L). Previous research indicates that introduction of large aliphatic

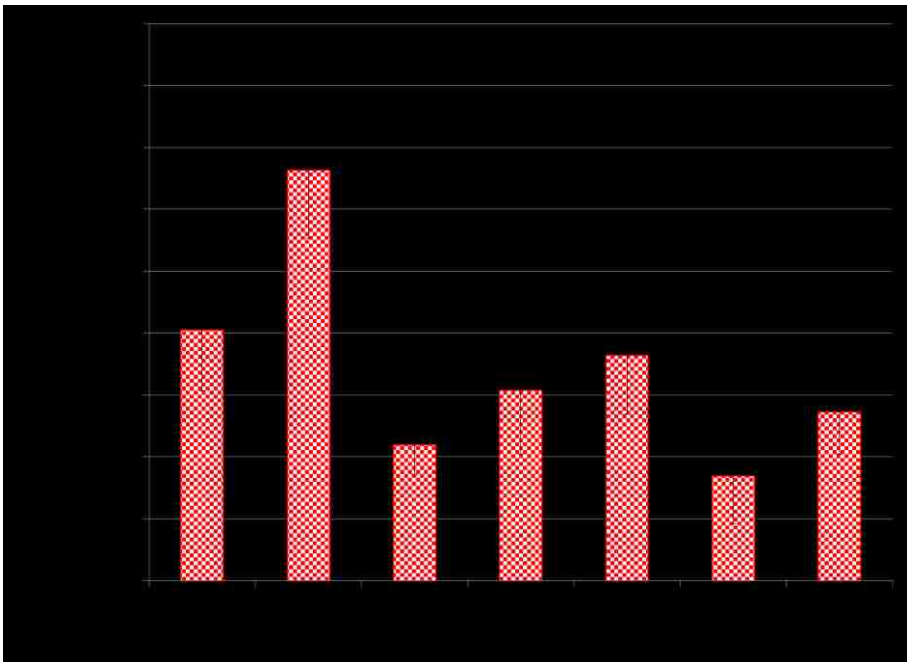

Figure 5.28. NRP2a(22) MAM-TM-CYTO-AraC heterodimerization with NRP2a(22) MAM-TM-CYTO-AraC* competition. Results represent the average value from a minimum of 22 samples collected over the course of six experiments. Error bars indicate standard error.

residues at locations immediately preceding or anteceding residues forming the interface of the small-x_3-small motifs can enhance dimerization (18). Preference for the location of the large residue depends on the size of other off-interface residues. It is possible that mutations G880L and A884L enhance dimerization by promoting small-x_3-small dimerization via residues A881 + G885, such that the dimerization motif is [Large][Small]xx[Large][Small], as has been observed as an over-represented motif in backbones with predominately alanine at the second 'x' position (18). Alternatively, some other packing motif may drive dimerization. Integrin heterodimerization, for instance, relies upon an intact V-x_3-I-x_3-G interface (20). Simulation studies may provide further insight into the NRP2a(22) TM dimerization mechanism.

If we consider mutations to NRP2a(22) affecting NRP2a(22) MAM-TM-CYTO-AraC* heterodimerization with NRP1 MAM-TM-CYTO-AraC (Figure 5.29), we observe that mutations G876L and G880L (on the same small-x_3-small interface) as well as mutation G885L (on a different small-x_3-small interface) disrupt heterodimerization relative to the WT NRP2a(22) MAM-TM-CYTO-AraC* construct. Neither mutation A881L (on the same small-x_3-small interface as G885) nor mutations A884L and A884G (on the same small-x_3-small interface as G876 and G880) affect heterodimerization. As such, maintaining intact glycines appears to be of greater importance than total maintenance of the small-x_3-small dimerization motif. Again, simulation studies would clarify the meaning of this result and possibly elucidate a packing motif different than the small-x_3-small dimer interface.

In the NRP2a(22)-NRP2b(0) heterodimer interface (Figure 5.30), we find two NRP2a(22) mutations disruptive to NRP2a(22) MAM-TM-CYTO-AraC* and NRP2b(0) MAM-TM-CYTO-AraC heterodimerization: G876L and A884G. Both residues lie on the same helical face; however, if we expected this interface to participate in a standard small-x_3-small packing motif, mutation A884G should have enhanced dimerization. Hence, the dimerization mechanism is still

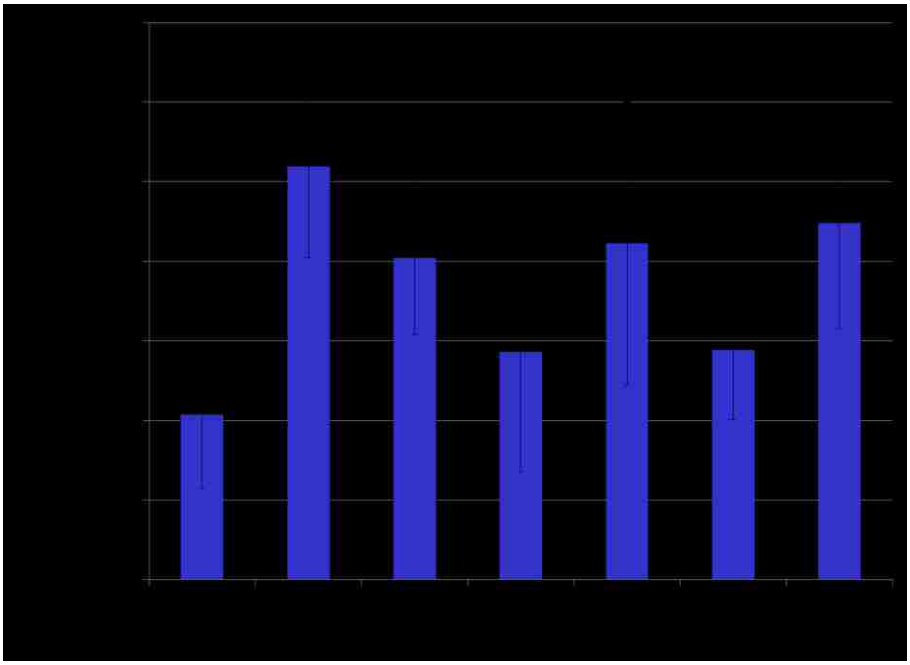

Figure 5.29. NRP1 MAM-TM-CYTO-AraC heterodimerization with NRP2a(22) MAM-TM-CYTO-AraC* competition. Results represent the average value from a minimum of 22 samples collected over the course of six experiments. Error bars indicate standard error.

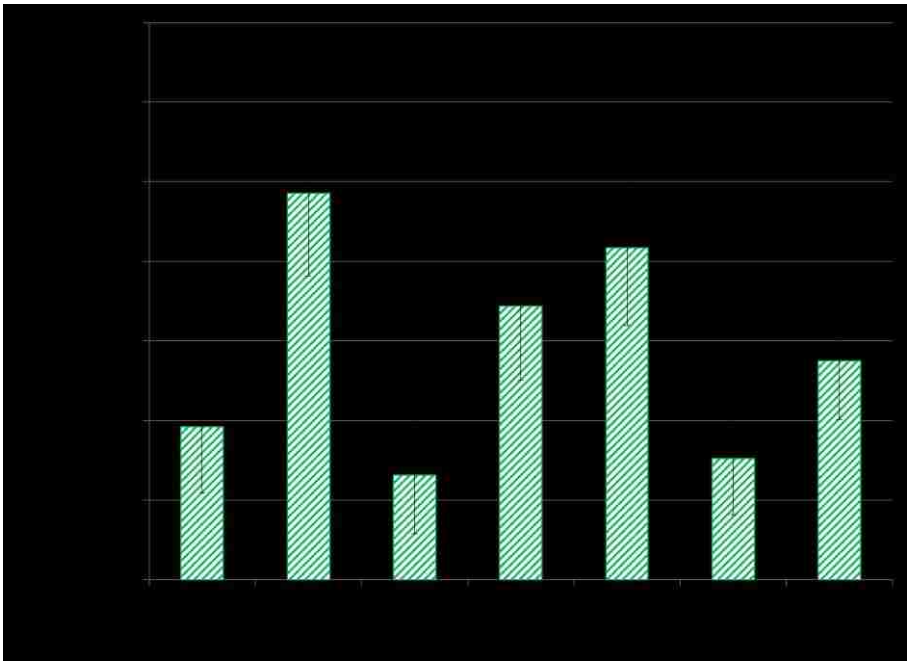

Figure 5.30. NRP2b(0) MAM-TM-CYTO-AraC heterodimerization with NRP2a(22) MAM-TM-CYTO-AraC* competition. Results represent the average value from a minimum of 22 samples collected over the course of six experiments. Error bars indicate standard error.

elusive. It is possible that an alternating small-large dimer interface, as has been observed with integrins (20), may govern NRP2a(22)-NRP2b(0) heterodimerization.

Collectively, our results indicate a role for the small residues in the NRP1 and NRP2a(22) TM domains in modulation of receptor dimerization, though further work is needed to elucidate a mechanism. Simulation studies will provide additional insight, as will DN-AraTM results on investigations of mutagenesis to NRP2b(0) MAM-TM-CYTO-AraC* heterodimerization with NRP1, NRP2a(22), and NRP2b(0) MAM-TM-CYTO-AraC constructs. Mutations to the NRP2b(0) putative small-x_3-small interfaces were recently cloned in our lab for such studies. This work could provide a foundation for understanding NRP heteromeric interfaces, providing structural insight into their activation mechanisms as co-receptor complexes.

5.6.1 Materials and Methods

5.6.1.1 Plasmids

The pAraTM multiple cloning site (SacI through KpnI) was cloned into both pAraTMdn and pAraTMwt for ease of use. In pAraTMwt, a linker (sequence RQLPTAAPEPAK, and a methionine to valine mutation immediately following) was also cloned between the multiple cloning site and the AraC protein. Subsequently, nrp TM-CYTO or MAM-TM-CYTO domains as designated by Table 5.2 were cloned between EcoRI and XhoI.

Table 5.2. Neuropilin Cloning Domains in the DNAraTM Assay.

Gene	Source NCBI Accession Number	TM-CYTO Residues	MAM-TM-CYTO Residues
NRP1	NP_003864.4	800-923	643-923
NRP2a(0)	AAC51788.1	791-909	640-909
NRP2a(17)	AAI43609.1	791-926	640-926
NRP2a(22)	NP_957718.1	791-931	640-931
NRP2b(0)	AAG41403.1	791-901	640-901
NRP2b(5)	AAG41404.1	791-906	640-906

5.6.1.2 DN-AraTM Measurements

DN-AraTM measurements and western blotting to confirm expression (Figure 5.31) were performed as previously described (54), except 24 hours lapsed between IPTG-induction and sample measurement, rather than 6 hours.

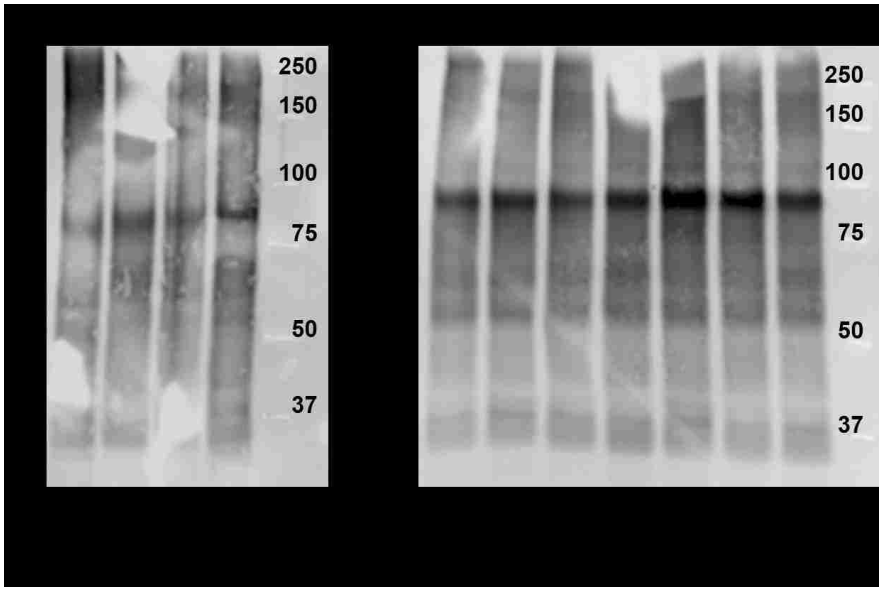

Figure 5.31. Anti-myc (1:1,000, Cell Signaling) western blot confirming expression of (A) NRP1 and (B) NRP2a(22) MAM-TM-CYTO-AraC* DNAraTM constructs. Expected molecular weights of WT constructs are 91 kDa and 92.5 kDa for NRP1 and NRP2a(22), respectively. Ladder markings are in kDa.

5.7 Final Remarks

Understanding plexin and neuropilin signal transduction mechanisms is of interest from a developmental biology perspective as well as in the study of cancer metastasis. Transmembrane dimerization, via the membrane or juxtamembrane domains, is one modulation mechanism for receptor activity. We demonstrate that, in the plexin-neuropilin system:

[1] A cytosolic juxtamembrane heptad repeat modulates PlxnA3 homodimerization, with a conserved methionine preventing strong receptor dimerization. The core of the heptad repeat forms a switchable interface that modulates homooligomerization and activity.

[2] A series of small residues in the PlxnA3 transmembrane domain offer dimerization motifs that compete with dimerization induced by the juxtamembrane heptad repeat. These residues prevent strong receptor dimerization, allowing for switchability between binding partners and active/inactive states. Mutation of these residues disrupts PlxnA3 function; as such, enhanced dimerization does not correlate with heightened function.

[3] Cysteines in the Nrp2a MAM domain modulate homomeric interactions, with mutations disrupting ligand binding and signal transduction.

Our results provide insight into the mechanisms regulating plexin-neuropilin signaling and demonstrate that enhancing receptor dimerization is not sufficient for increasing receptor activity. Our work defining the receptor homomeric interfaces will hopefully augment future efforts to modulate activity, allowing for rational design of targeted therapeutics.

5.8 References

1. Autiero, M., De Smet, F., Claes, F., and Carmeliet, P. (2005) Role of neural guidance signals in blood vessel navigation. *Cardiovasc Res* **65**, 629-638
2. Ton, Q. V., and Kathryn Iovine, M. (2012) Semaphorin3d mediates Cx43-dependent phenotypes during fin regeneration. *Dev Biol* **366**, 195-203
3. Kruger, R. P., Aurandt, J., and Guan, K. L. (2005) Semaphorins command cells to move. *Nat Rev Mol Cell Biol* **6**, 789-800

4. Sakurai, A., Doci, C. L., and Gutkind, J. S. (2012) Semaphorin signaling in angiogenesis, lymphangiogenesis and cancer. *Cell Res* **22**, 23-32

5. Takahashi, T., Fournier, A., Nakamura, F., Wang, L. H., Murakami, Y., Kalb, R. G., Fujisawa, H., and Strittmatter, S. M. (1999) Plexin-neuropilin-1 complexes form functional semaphorin-3A receptors. *Cell* **99**, 59-69

6. Wang, Y., He, H., Srivastava, N., Vikarunnessa, S., Chen, Y. B., Jiang, J., Cowan, C. W., and Zhang, X. (2012) Plexins are GTPase-activating proteins for Rap and are activated by induced dimerization. *Sci Signal* **5**, ra6

7. Langosch, D., and Arkin, I. T. (2009) Interaction and conformational dynamics of membrane-spanning protein helices. *Protein Sci* **18**, 1343-1358

8. Cymer, F., and Schneider, D. (2010) Transmembrane helix-helix interactions involved in ErbB receptor signaling. *Cell Adh Migr* **4**, 299-312

9. Bell, C. H., Aricescu, A. R., Jones, E. Y., and Siebold, C. (2011) A dual binding mode for RhoGTPases in plexin signalling. *PLoS Biol* **9**, e1001134

10. Woolfson, D. N. (2005) The design of coiled-coil structures and assemblies. *Adv Protein Chem* **70**, 79-112

11. Grigoryan, G., and Keating, A. E. (2008) Structural specificity in coiled-coil interactions. *Curr Opin Struct Biol* **18**, 477-483

12. Liu, J., Zheng, Q., Deng, Y., Kallenbach, N. R., and Lu, M. (2006) Conformational transition between four and five-stranded phenylalanine zippers determined by a local packing interaction. *J Mol Biol* **361**, 168-179

13. He, H., Yang, T., Terman, J. R., and Zhang, X. (2009) Crystal structure of the plexin A3 intracellular region reveals an autoinhibited conformation through active site sequestration. *Proc Natl Acad Sci U S A* **106**, 15610-15615

14. Takahashi, T., and Strittmatter, S. M. (2001) Plexina1 autoinhibition by the plexin sema domain. *Neuron* **29**, 429-439

15. van Belzen, N., Rijken, P. J., Hage, W. J., de Laat, S. W., Verkleij, A. J., and Boonstra, J. (1988) Direct visualization and quantitative analysis of epidermal growth factor-induced receptor clustering. *J Cell Physiol* **134**, 413-420

16. Hines, K. E. (2013) Inferring subunit stoichiometry from single molecule photobleaching. *J Gen Physiol* **141**, 737-746

17. Courty, S., and Dahan, M. (2013) Tracking individual membrane proteins using quantum dots. *Cold Spring Harb Protoc* **2013**, 925-927

18. Russ, W. P., and Engelman, D. M. (2000) The GxxxG motif: a framework for transmembrane helix-helix association. *J Mol Biol* **296**, 911-919

19. Senes, A., Gerstein, M., and Engelman, D. M. (2000) Statistical analysis of amino acid patterns in transmembrane helices: the GxxxG motif occurs frequently and in association with beta-branched residues at neighboring positions. *J Mol Biol* **296**, 921-936

20. Berger, B. W., Kulp, D. W., Span, L. M., DeGrado, J. L., Billings, P. C., Senes, A., Bennett, J. S., and DeGrado, W. F. (2010) Consensus motif for integrin transmembrane helix association. *Proc Natl Acad Sci U S A* **107**, 703-708

21. Haltia, T., and Freire, E. (1995) Forces and factors that contribute to the structural stability of membrane proteins. *Biochim Biophys Acta* **1241**, 295-322

22. White, S. H. (2005) How hydrogen bonds shape membrane protein structure. *Adv Protein Chem* **72**, 157-172

23. Lopez-Llano, J., Campos, L. A., and Sancho, J. (2006) Alpha-helix stabilization by alanine relative to glycine: roles of polar and apolar solvent exposures and of backbone entropy. *Proteins* **64**, 769-778

24. Javadpour, M. M., Eilers, M., Groesbeek, M., and Smith, S. O. (1999) Helix packing in polytopic membrane proteins: role of glycine in transmembrane helix association. *Biophys J* **77**, 1609-1618

25. Senes, A., Ubarretxena-Belandia, I., and Engelman, D. M. (2001) The Calpha ---H...O hydrogen bond: a determinant of stability and specificity in transmembrane helix interactions. *Proc Natl Acad Sci U S A* **98**, 9056-9061

26. MacKenzie, K. R., Prestegard, J. H., and Engelman, D. M. (1997) A transmembrane helix dimer: structure and implications. *Science* **276**, 131-133

27. Mueller, B. K., Subramaniam, S., and Senes, A. (2014) A frequent, GxxxG-mediated, transmembrane association motif is optimized for the formation of interhelical Calpha-H hydrogen bonds. *Proc Natl Acad Sci U S A* **111**, E888-895

28. Lemmon, M. A., Flanagan, J. M., Treutlein, H. R., Zhang, J., and Engelman, D. M. (1992) Sequence specificity in the dimerization of transmembrane alpha-helices. *Biochemistry* **31**, 12719-12725

29. Roth, L., Nasarre, C., Dirrig-Grosch, S., Aunis, D., Cremel, G., Hubert, P., and Bagnard, D. (2008) Transmembrane domain interactions control biological functions of neuropilin-1. *Mol Biol Cell* **19**, 646-654

30. Su, P. C., Si, W., Baker, D. L., and Berger, B. W. (2012) High-yield membrane protein expression from E. coli using an engineered outer membrane protein F fusion. *Protein Sci* **22**, 434-443

31. Barton, R., Palacio, D., Iovine, M. K., and Berger, B. W. (2015) A cytosolic juxtamembrane interface modulates plexin a3 oligomerization and signal transduction. *PLoS One* **10**, e0116368

32. Giger, R. J., Urquhart, E. R., Gillespie, S. K., Levengood, D. V., Ginty, D. D., and Kolodkin, A. L. (1998) Neuropilin-2 is a receptor for semaphorin IV: insight into the structural basis of receptor function and specificity. *Neuron* **21**, 1079-1092

33. Nakamura, F., Tanaka, M., Takahashi, T., Kalb, R. G., and Strittmatter, S. M. (1998) Neuropilin-1 extracellular domains mediate semaphorin D/III-induced growth cone collapse. *Neuron* **21**, 1093-1100

34. Rollenhagen, M., Buettner, F. F., Reismann, M., Jirmo, A. C., Grove, M., Behrens, G. M., Gerardy-Schahn, R., Hanisch, F. G., and Muhlenhoff, M. (2013) Polysialic acid on neuropilin-2 is exclusively synthesized by the polysialyltransferase ST8SiaIV and attached to mucin-type o-glycans located between the b2 and c domain. *J Biol Chem* **288**, 22880-22892

35. Rey-Gallardo, A., Escribano, C., Delgado-Martin, C., Rodriguez-Fernandez, J. L., Gerardy-Schahn, R., Rutishauser, U., Corbi, A. L., and Vega, M. A. (2010) Polysialylated neuropilin-2 enhances human dendritic cell migration through the basic C-terminal region of CCL21. *Glycobiology* **20**, 1139-1146

36. Rey-Gallardo, A., Delgado-Martin, C., Gerardy-Schahn, R., Rodriguez-Fernandez, J. L., and Vega, M. A. (2011) Polysialic acid is required for neuropilin-2a/b-mediated control of CCL21-driven chemotaxis of mature dendritic cells and for their migration in vivo. *Glycobiology* **21**, 655-662

37. Aricescu, A. R., Siebold, C., Choudhuri, K., Chang, V. T., Lu, W., Davis, S. J., van der Merwe, P. A., and Jones, E. Y. (2007) Structure of a tyrosine phosphatase adhesive interaction reveals a spacer-clamp mechanism. *Science* **317**, 1217-1220

38. Aricescu, A. R., Hon, W. C., Siebold, C., Lu, W., van der Merwe, P. A., and Jones, E. Y. (2006) Molecular analysis of receptor protein tyrosine phosphatase mu-mediated cell adhesion. *EMBO J* **25**, 701-712

39. Su, P. C., and Berger, B. W. (2012) Identifying key juxtamembrane interactions in cell membranes using AraC-based transcriptional reporter assay (AraTM). *J Biol Chem* **287**, 31515-31526

40. Chen, H., He, Z., Bagri, A., and Tessier-Lavigne, M. (1998) Semaphorin-neuropilin interactions underlying sympathetic axon responses to class III semaphorins. *Neuron* **21**, 1283-1290

41. Shi, Q., and Jackowski, G. (1998) One-dimensional polyacrylamide gel electrophoresis. in *Gel Electrophoresis of Proteins: A Practical Approach* (Hames, B. D. ed.), Oxford University Press. pp 1-52

42. Sreerama, N., and Woody, R. W. (2004) Computation and analysis of protein circular dichroism spectra. *Methods Enzymol* **383**, 318-351

43. Arolas, J. L., Broder, C., Jefferson, T., Guevara, T., Sterchi, E. E., Bode, W., Stocker, W., Becker-Pauly, C., and Gomis-Ruth, F. X. (2012) Structural basis for the sheddase function of human meprin beta metalloproteinase at the plasma membrane. *Proc Natl Acad Sci U S A* **109**, 16131-16136

44. Cismasiu, V. B., Denes, S. A., Reilander, H., Michel, H., and Szedlacsek, S. E. (2004) The MAM (meprin/A5-protein/PTPmu) domain is a homophilic binding site promoting the lateral dimerization of receptor-like protein-tyrosine phosphatase mu. *J Biol Chem* **279**, 26922-26931

45. Fiser, A., and Sali, A. (2003) Modeller: generation and refinement of homology-based protein structure models. *Methods Enzymol* **374**, 461-491

46. Schrodinger. (2010) The PyMOL Molecular Graphics System. 1.3 Ed.

47. Fan, C., Rajasekaran, D., Syed, M. A., Leng, L., Loria, J. P., Bhandari, V., Bucala, R., and Lolis, E. J. (2013) MIF intersubunit disulfide mutant antagonist supports activation

of CD74 by endogenous MIF trimer at physiologic concentrations. *Proc Natl Acad Sci U S A* **110**, 10994-10999

48. Lyskov, S., and Gray, J. J. (2008) The RosettaDock server for local protein-protein docking. *Nucleic Acids Res* **36**, W233-238

49. Sambrook, J., and Russell, D. W. (1989) *Molecular Cloning: A Laboratory Manual*, 2 ed., Spring Harbor Laboratory Press, Cold Spring Harbor, NY

50. Rasband, W. (1997-2013) ImageJ. 1.47 Ed., National Institute of Health, Bethesda, Maryland, USA

51. Willard, L., Ranjan, A., Zhang, H., Monzavi, H., Boyko, R. F., Sykes, B. D., and Wishart, D. S. (2003) VADAR: a web server for quantitative evaluation of protein structure quality. *Nucleic Acids Res* **31**, 3316-3319

52. Takahashi, T., Nakamura, F., Jin, Z., Kalb, R. G., and Strittmatter, S. M. (1998) Semaphorins A and E act as antagonists of neuropilin-1 and agonists of neuropilin-2 receptors. *Nat Neurosci* **1**, 487-493

53. Sawma, P., Roth, L., Blanchard, C., Bagnard, D., Cremel, G., Bouveret, E., Duneau, J. P., Sturgis, J. N., and Hubert, P. (2014) Evidence for New Homotypic and Heterotypic Interactions between Transmembrane Helices of Proteins Involved in Receptor Tyrosine Kinase and Neuropilin Signaling. *J Mol Biol* **426**, 4099-4111

54. Su, P. C., and Berger, B. W. (2013) A novel assay for assessing juxtamembrane and transmembrane domain interactions important for receptor heterodimerization. *J Mol Biol* **425**, 4652-4658

Appendix A

Understanding Biosurfactant Sequence and Structural Features for Enhanced Targeted Drug Delivery

Surfactants play an important role in the food, biopharmaceutical, and energy industries, but little is known about their structure-function relationships apart from their amphiphilic nature. Biosurfactants are amphiphilic molecules naturally secreted by a wide range of bacteria and fungi; these molecules offer a 'green' surfactant with potential additional built-in functionalities in their peptide chains. They have applications in bioremediation, as synthetic vaccines, as vaccine adjuvants, and in drug delivery (1-5). Identification of the characteristic regions of biosurfactants responsible for surface activity and the sequence features responsible for stabilizing their surface-active structures may provide insight for novel surfactant production. With this knowledge, we could engineer a biomimetic surfactant that incorporates alternative functionalities to make it a switchable system and responsive material. Such engineered functionalities could provide beneficial drug delivery technology, with engineered side-chain interactions incorporating pH-dependent self-assembly in the biosurfactant as well as ligand recognition triggering drug release and the ability to effectively solubilize hydrophobic drug substance in a micellar drug delivery system while maintaining bioactivity of the drug substance.

The hydrophobin HFBII from *Trichoderma reesei* could serve as a template biosurfactant for structure-function relationship studies (1,2,5,6).

The HFBII protein is a class II hydrophobin and hence considered a hydrophilic biosurfactant (relative to less soluble, class I hydrophobins) (1,5). An α-helix and four β-sheets constitute the HFBII secondary structure, and the tertiary structure of HFBII consists of a hydrophobic patch comprised of side chains from aliphatic residues (Figure A1) (1,5,6). Four disulfide bridges are believed to maintain tertiary structure stability (Figure A1) (1,5,6). Mutations to disrupt disulfide bonds, secondary structure, or the hydrophobic patch may result in a controllable biosurfactant, with amphiphilicity regulated by pH or temperature.

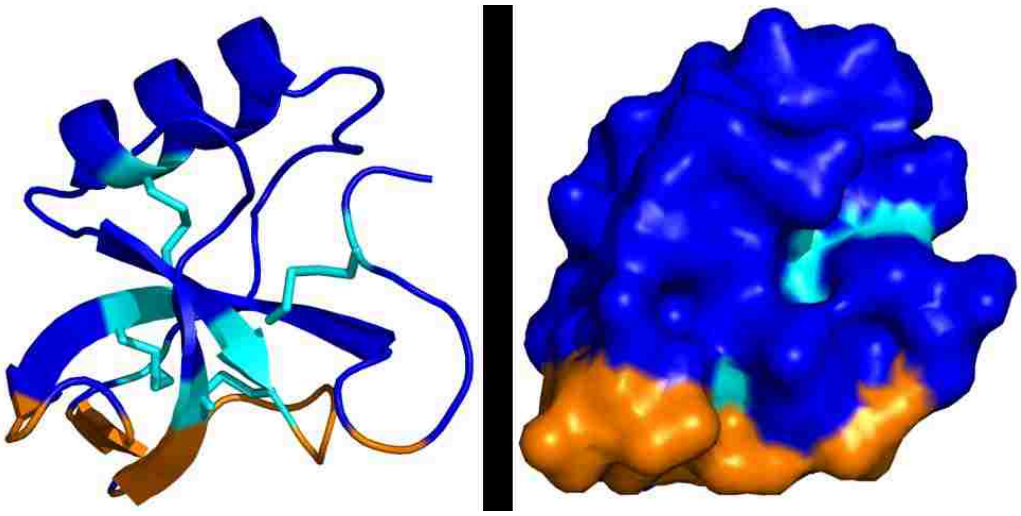

Figure A1. Structure of HFBII, a naturally-occurring peptide biosurfactant (PDB # 1R2M). Tertiary structure is maintained by disulfide bonds (cyan), and amphiphilicity is a result of a patch of aliphatic side chains (orange).

We have successfully expressed a modification of HFBII (HFBII.2) as a thrombin-cleavable ompF-fusion using a bacterial expression system (7). The ompF portion contains a poly-histidine tag, allowing for purification of the fusion via immobilized metal-ion affinity

chromatography (IMAC) (Figure A2). HFBII.2 is dissimilar to HFBII in that one cysteine from each of the four disulfide pairs in the native HFBII protein (four cysteines in total) was removed via truncation or mutation.

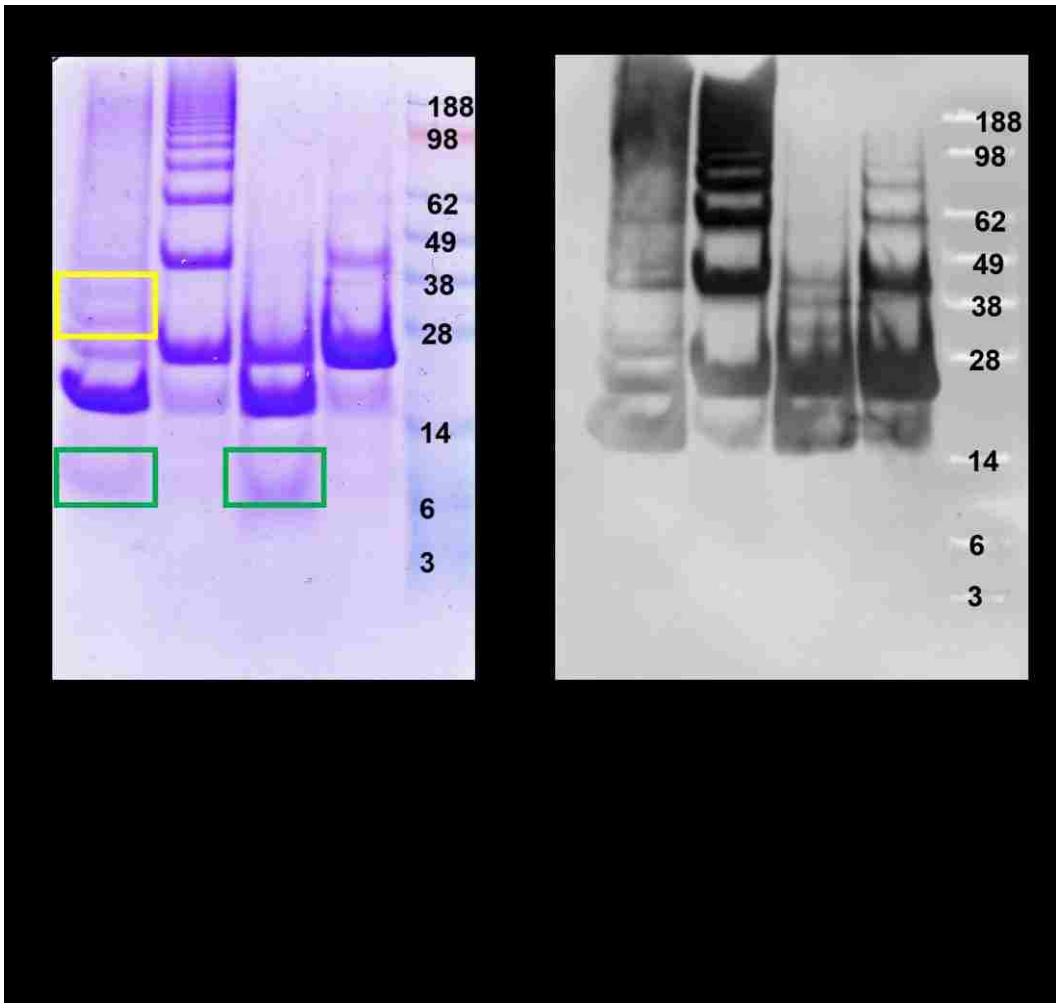

Figure A2. OmpF-HFBII.2 can be expressed using a bacterial expression system. (A) Coomassie-stained SDS-PAGE gel and (B) anti-His (1:1,000, Cell Signaling) western blot confirming expression and cleavage of ompF-HFBII.2. The poly-histidine tag is on the ompF fragment of the the fused protein; bands present on the Coomassie-stained gel and absent on the western blot may be HFBII.2-only (green boxes: monomeric HFBII.2; yellow box: oligomeric HFBII.2 without ompF). The addition of 1% β-mercaptoethanol reduces, but does not eliminate, oligomerization. Expected monomeric molecular weights are 7.4 kDa, 17.4 kDa, and 24.8 kDa for HFBII.2, ompF, and ompF-HFBII.2, respectively.

SDS-PAGE gels provide some insight into the behavior of the ompF-HFBII.2 fusion protein. OmpF-HFBII.2 oligomerization is apparent on SDS-PAGE gels before and after thrombin cleavage (Figure A2). While the oligomers in the thrombin-cut sample may be ompF, uncut ompF-HFBII.2, or complexes of ompF, HFBII.2, and ompF-HFBII.2, at least two are likely due to HFBII.2 only, as the bands (visible via Coomassie-staining) fail to appear in an anti-His western blot (yellow box, Figure A2). Our SDS-PAGE results also suggest the ompF-HFBII.2 protein is capable of forming disulfide-dependent oligomers, as indicated by a reduction to oligomerization upon addition of 1% β-mercaptoethanol (BME) (Figure A2). As the ompF tag lacks cysteines, this disulfide bonding is due to the HFBII.2 peptide. Oligomerization is not eliminated in the presence of BME, however, suggesting ompF-HFBII.2 oligomerizes via disulfide-independent mechanisms. Purification of HFBII.2 from thrombin and ompF may provide additional insight regarding the oligomic potential of the peptide. Preliminary work suggests ompF and HFBII.2 can be separated via reverse-phase chromatography, as indicated by MALDI-TOF results (Figure A3). As this could be due to different ionization potentials of the peptides, a method for confirming HFBII.2 purification (such as SDS-PAGE) is also needed. Upon successful purification, structural analyses of HFBII.2, such as circular dichroism and tryptophan fluorescence mapping of the peptide at variable temperatures and pH's, may help to assess structural stability and switchability.

Preliminary macroscopic emulsification studies suggest the thrombin-cleaved ompF + HFBII.2 solution exhibits surfactant behavior. Direct interpretation of results is convoluted due to the presence of FOS-Choline-15 in the samples (from the IMAC chromatography), and a technique to remove it must be developed for future functional studies. However, our results suggest the thrombin-cleaved ompF-HFBII.2 peptide in FOS-Choline-15 emulsifies nonane better than FOS-Choline-15 alone, as is apparent by a single phase in the presence of thrombin-cleaved

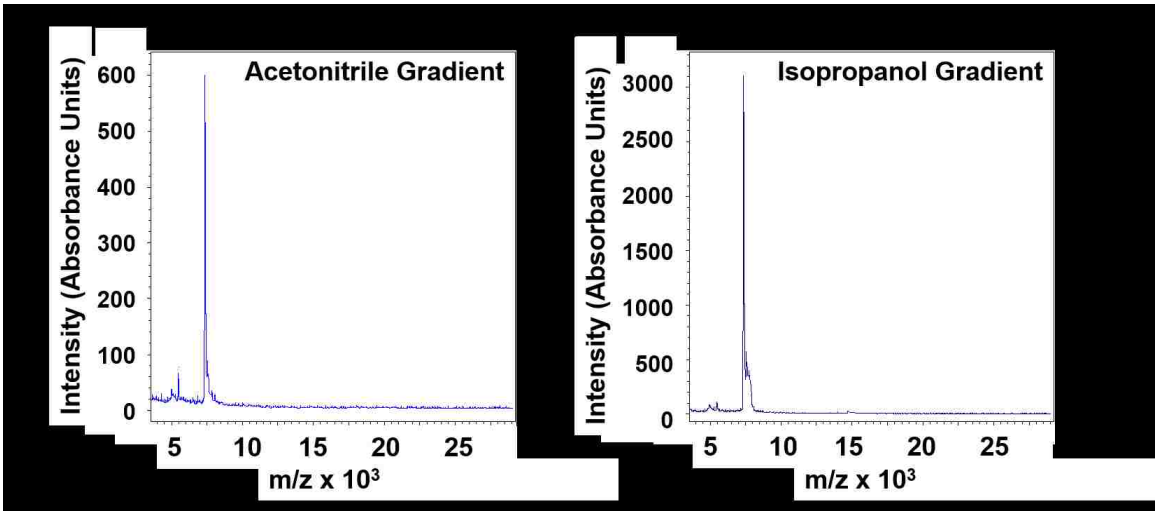

Figure A3. MALDI-TOF spectra of thrombin-cleaved ompF-HFBII.2 subjected to reverse phase chromatography with an (A) acetonitrile or (B) isopropanol gradient. Expected m/z for HFBII.2 is 7.4.

ompF-HFBII.2, but persistence of three phases in its absence. Thrombin-cleaved ompF-HFBII.2 in FOS-Choline-15 poorly emulsifies mineral oil and hexane relative to FOS-Choline-15 alone, as indicated by the decreased depth of the emulsified (white) layer. Additional functional studies on a purified HFBII.2 protein or the ompF-HFBII.2 protein in the absence of detergent should be performed to characterize activity. In addition to emulsion studies, contact angle measurements and solubilization studies of hydrophobic materials, such as Oil Red O or, for drug delivery studies, ketoprofen, could also provide insight into HFBII.2 structure-function relationships.

Changes to the HFBII on its primary structural level could result in a utilizable on-off functionality switch and a responsive system capable of carrying a drug substance until recognition of a specific receptor site. The genetically-engineered biosurfactant could facilitate incorporation of monodispersed hydrophobic drug substances in a micellar drug delivery system. This system could have a high-degree of control over its molecular properties through genetic alteration of the peptide primary sequence, and be easily manipulated for other applications once

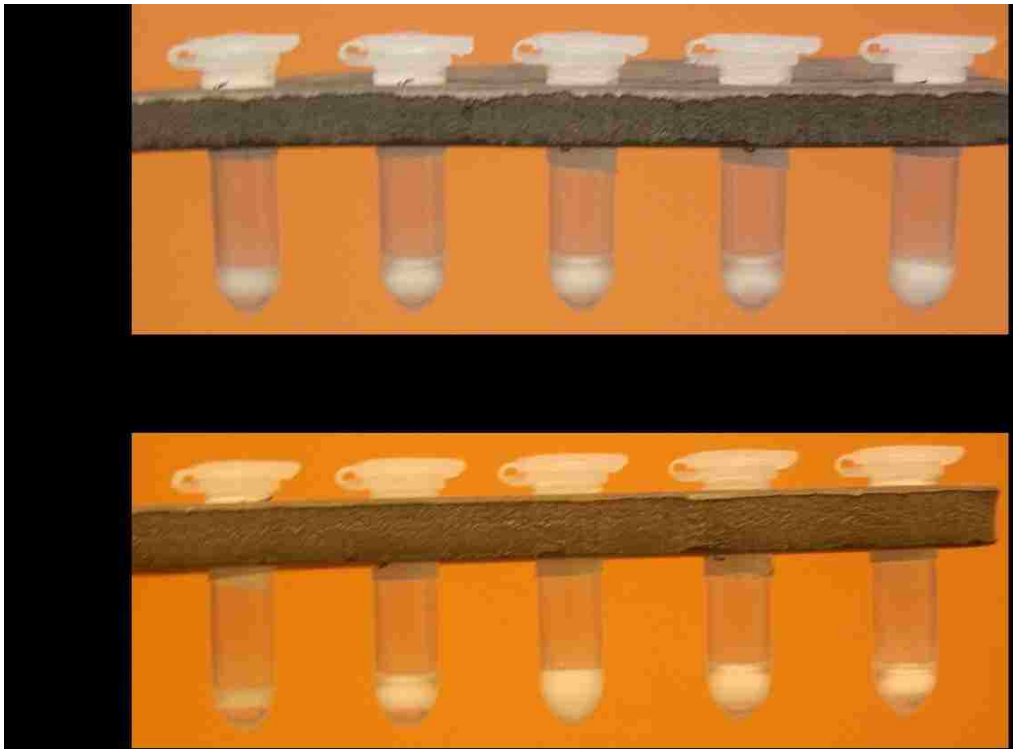

Figure A4. A preliminary macroscopic emulsion study suggests the presence of HFBII.2 affects oil emulsification. Enhanced emulsification is indicated by the persistence of a middle (white) layer, whereas the appearance of three layers (a clear layer on the top and bottom) indicates poor emulsification.

the primary structure is understood. Furthermore, as biosurfactants naturally occur in organisms used for fermentation in the biopharmaceutical industry, the production process would be scalable. The combination of all of these phenomena will result in a novel and efficient targeted drug delivery system.

A1.1 Materials and Methods

A1.1.1 Plasmids

For ompF-HFBII.2, HFBII.2 (residues 20-86 of *Trichoderma reesei* HFBII, NCB Accession # XP_006962048.1, with mutations C29S, C58S, and C67S) was cloned into pOmpF (7) at restriction sites SpeI and XhoI.

A1.1.2 Expression and Purification

Expression, IMAC purification, thrombin-cleavage, and SDS-PAGE were conducted following the methods employed for the *Danio rerio* plexin A3 transmembrane and cytosolic juxtamembrane domains fused to ompF (ompF-TM+JM, Section 5.3). Reverse phase chromatography was conducted using a C4 column on an Agilent 1100 series high performance liquid chromatography system and an acetonitrile or isopropanol concentration gradient (increasing from 10 to 100% solvent over the course of 25 minutes following a 5-minute loading time for the sample and equilibration). MALDI-TOF spectra represent samples collected between 26 and 40 minutes. A sinapinic acid matrix was used for MALD-TOF analyses.

A1.1.3 Emulsion Studies

For emulsion studies, 200µL of oil (hexane, octane, nonane, decane, or mineral oil) were combined with 100µL of 1% FOS-Choline-15 in 20 mM Tris at pH 8 with or without thrombin-cleaved ompF-HFBII.2. Mixtures were subsequently vortexed, bath sonicated for 30 minutes, incubated for 30 minutes with agitation at 37ºC, then centrifuged for 30 minutes. Samples were then incubated overnight in a shaking incubator at 37ºC prior to imaging.

A1.2 References

1. Zhang, X. L., Penfold, J., Thomas, R. K., Tucker, I. M., Petkov, J. T., Bent, J., Cox, A., and Grillo, I. (2011) Self-Assembly of Hydrophobin and Hydrophobin/Surfactant Mixtures in Aqueous Solution. *Langmuir* **27**, 10514-10522
2. Askolin, S., Nakari-Setala, T., and Tenkanen, M. (2001) Overproduction, Purification, and Characterization of the *Trichoderma reesei* Hydrophobin HFBI. *Applied Microbiology and Biotechnology* **57**, 124-130
3. Hubbell, J. A., Thomas, S. N., and Swartz, M. A. (2009) Materials engineering for immunomodulation. *Nature* **462**, 449-460
4. Dexter, A. F., and Middelberg, A. P. J. (2008) Peptides as Functional Surfactants. *Industrial & Engineering Chemistry Research* **47**, 6391-6398
5. Linder, M. B. (2009) Hydrophobins: Proteins that self assemble at interfaces. *Current Opinion in Colloid & Interface Science* **14**, 356-363
6. Hakanpaa, J., Paananen, A., Askolin, S., Nakari-Setala, T., Parkkinen, T., Penttila, M., Linder, M. B., and Rouvinen, J. (2004) Atomic Resolution Structure of the HFBII Hydrophobin, a Self-assembling Amphiphile. *J Biol Chem* **279**, 534-539
7. Su, P. C., Si, W., Baker, D. L., and Berger, B. W. (2012) High-yield membrane protein expression from E. coli using an engineered outer membrane protein F fusion. *Protein Sci* **22**, 434-443

Vita

Rachael Elizabeth Barton was born on April 15, 1986, in Potsdam, NY, to Kelly and Catherine Barton. She is the oldest of their seven children. Upon graduation from Athens Area High School, Pennsylvania, in 2004, Rachael attended Cornell University and subsequently received a Bachelor of Science degree in chemical and biomolecular engineering in 2008. During her time at Cornell, Rachael was an active participant of the Cornell Student Chapter of American Institute of Chemical Engineers as well as the Cornell Engineering Cooperative Education program, through which she participated in two semesters of biopharmaceutical process development research with Merck & Co., West Point, PA. From 2008-2010, Rachael had the wonderful experience of working in the Pre-Clinical Manufacturing and Process Development Department at Regeneron Pharmaceuticals, Tarrytown, NY. Upon receipt of the Lehigh University Presidential Fellowship, she returned to an academic setting to pursue a Doctor of Philosophy degree in chemical and biomolecular engineering under the supervision of Dr. Bryan W. Berger. While at Lehigh University, Rachael had the opportunity to serve as a mentor for undergraduate research courses and the Biosystems Dynamics Summer Institute. She also served as a teaching assistant for select courses including Chemical Engineering Fluid Mechanics, Integrated Biostructural Mechanics Laboratory, and Integrated Biotechnology Laboratory.

Publications

Barton, R., Palacio, D., Iovine, M. K., and Berger, B. W. (2015) "A cytosolic juxtamembrane interface modulates plexin A3 oligomerization and signal transduction." *PLOS ONE* 10(1): e0116368.

Barton, R., Driscoll, A., Flores, S., Mudbhari, D., Collins, T., Iovine, M. K., and Berger, B. W. (2015) "Cysteines in the neuropilin-2 MAM domain modulate receptor homooligomerization and signal transduction." *Biopolymers: Peptide Science.* (accepted)

Presentations

Peer-Reviewed Conference Proceedings

Barton, R., Iovine, M. K., Berger, B. W. (2013) "Identifying a structural basis for plexin A3 homomeric interactions." *39th Annual Northeast Bioengineering Conference*, Syracuse, NY.

Student Seminars

Barton, R., Iovine, M. K., Berger, B. W. (2015) "Specific interfaces in the PlexinA3 transmembrane and juxtamembrane regions influence homodimerization." *BioDesign MegaMeeting,* Piscataway Township, NJ.

Barton, R., Iovine, M. K., Berger, B. W. (2013) "Identifying a structural basis for plexin A3 and neuropilin-2a homomeric interactions." *Lehigh University Chemical Engineering Graduate Student Seminar*, Bethlehem, PA.

Poster Presentations

Barton, R., Palacio, D., Iovine, M. K., Berger, B. W. (2015) "Specific interfaces in the plexin A3 transmembrane and juxtamembrane regions influence homomeric interactions." *Mid-Atlantic Society for Developmental Biology Meeting*, Princeton, NJ.

Barton, R., Palacio, D., Iovine, M. K., Berger, B. W. (2014) "Transmembrane and juxtamembrane regions influence plexin A3 homomeric interactions." *11th International Conference on Zebrafish Development and Genetics*, Madison, WI.

Barton, R., Palacio, D., Iovine, M. K., Berger, B. W. (2014) "Transmembrane and juxtamembrane regions influence plexin A3 homomeric interactions." *Delaware Membrane Protein Symposium*, Newark, DE.

Barton, R., Bhadra, J., Driscoll, A., Collins, T., Flores, S., Mudbhari, D., Iovine, M. K., Berger, B. W. (2013) "A cysteine-rich interface in the neuropilin-2 MAM domain governs homooligomerization." *Mid-Atlantic Regional Zebrafish Meeting*, Baltimore, MD.

Barton, R., Bhadra, J., Driscoll, A., Collins, T., Flores, S., Mudbhari, D., Iovine, M. K., Berger, B. W. (2013) "A cysteine-rich interface in the neuropilin-2 MAM domain governs homooligomerization." *Biophysical Society Pennsylvania Network Meeting*, State College, PA.

Barton, R., Driscoll, A., Bhadra, J., Iovine, M. K., Berger, B. W. (2013) "Understanding the neuropilin-2a homomeric interface: structural characteristics of the transmembrane and MAM domain influence oligomerization." *Delaware Membrane Protein Symposium*, Newark, DE.

Barton, R., Iovine, M. K., Berger, B. W. (2012) "Identifying a structural basis for plexin A3 interactions." *Biophysical Society Pennsylvania Network Meeting*, Bethlehem, PA.

Barton, R., Shieferstein, J., Barton, S., Barnett, G., Berger, B. W. (2012) "Characterization and expression of a class II hydrophobin, a protein-based surfactant." *EPI Annual Review Meeting*, Bethlehem, PA.